Workshop on "Robotic assembly of 3D MEMS".

Michaël Gauthier, Nicolas Chaillet

IROS 2007
Sheraton Hotel and Marina
San Diego, CA, U.S.A.

Robotic Microassembly of 3D Hybrid MEMS

Michaël Gauthier and Nicolas Chaillet

Full Day Workshop, November 2, 2007

www.lab.cnrs.fr/WSmicroassembly

Full-day Workshop IROS 2007

Robotic Microassembly of 3D Hybrid MEMS

November 2, 2007, San Diego, CA, USA

Workshop Contents

Full-day Workshop IROS 2007

Robotic Microassembly of 3D Hybrid MEMS

November 2, 2007, San Diego, CA, USA

Introduction

The increase of MEMS' functionalities often requires the integration of various technologies used for mechanical, optical and electronic subsystems in order to achieve a unique system. These different technologies have usually process incompatibilities and the whole microsystem can not be obtained monolithically and then requires microassembly steps. Microassembly of MEMS based on micrometric components is one of the most promising approaches to achieve high-performance MEMS. Moreover, microassembly also permits to develop suitable MEMS packaging as well as 3D components although microfabrication technologies are usually able to create 2D and "2.5D" components. The study of microassembly methods is consequently a high stake for MEMS technologies growth.

Two approaches are currently developped for microassembly: self-assembly and robotic microassembly. In the first one, the assembly is highly parallel but the efficiency and the flexibility still stay low. The robotic approach has the potential to reach precise and reliable assembly with high flexibility. The proposed workshop focuses on this second approach and will take a bearing of the corresponding microrobotic issues.

Objectives of the workshop are to present a review of current microrobotic approaches for microassembly and to exchange know-how on these different topics to initiate collaborations.

Dr **M. Gauthier** and Pr **N. Chaillet**,
Laboratoire d'Automatique de Besançon,
24 rue Alain Savary,
F-25000 Besançon.
Email:
{michael.gauthier, nicolas.chaillet}@ens2m.fr

High Yield Automated MEMS Assembly: Compliant Snap-Fastener Design, Precision Robotics, and Assembly Evaluation

Dan O. Popa

***Abstract*— Heterogeneous assembly at the microscale has recently emerged as a viable pathway to constructing 3-dimensional microrobots. In contrast to self-assembly, this method is directed and deterministic, and is based on serial or parallel microassembly. Whereas at the meso and macro scales, automation is often undertaken after, and often benchmarked against manual assembly, we demonstrate that deterministic automation at the MEMS scale can be completed with higher yields through the use of engineered compliance and precision robotic cells. One possible application pathway for microassembly exploits modular designs which can be assembled to form a desired micro-machine. Snap fasteners have long been used as a way to exploit the inherent stability of local minima of the deformation energy caused by interference during part mating. In this paper we assume that the building blocks are 2 ½ -dimensional, as is the case with lithographically microfabricated MEMS parts. The assembly of the snap fasteners is done using μ³, a multi-robot microassembly station with unique characteristics located at the ARRI's Texas Microfactory™ lab. Design trade-offs for the assembly and performance of microsnap fasteners are indicated and experimentally evaluated. Several examples of MEMS micro-optical benches and assembled microrobots are presented.**

I. Introduction

A. Microassembly

Microassembly is an enabling technology for constructing heterogeneous (or hybrid) three-dimensional microsystems, in particular microrobots. In many instances, microparts fabricated using different materials and processes need to be assembled and packaged in order to achieve a desired functionality. Progress in lithographic fabrication methods, such as those used for Silicon MEMS, Metal Liga, or Polymer micromolding has enabled the mass production of 2 ½ D microparts. At the same time, in the past 15 years considerable progress has been reported in "top-down" precision assembly, including gripping, handling, positioning and bonding of parts with dimensions between a few and several hundred μm [1-8]. Due to the small size of these parts, specialized microgrippers, fixtures, and positioning systems have been developed. Active microgrippers can be fabricated from a variety of materials, including metals, Silicon, or PZT [6,7]. Other examples are the use of passive microgrippers through the use of mechanical compliance [5,17], or the use of adhesive forces [8]. In addition to serial, single gripper methods, others have pursued parallel manipulation with gripper arrays, for instance Bohringer et. al. [9,13].

Numerous papers describe and classify the architecture and algorithms used in high precision robotic cells for the purpose of directed microscale assembly [1-4]. Classifications can be based on throughput (serial or parallel), deliberate intervention (deterministic or stochastic), type of end-effectors (contact, non-contact) or level of human intervention (manual, teleoperated or automated). Microrobotic assembly cell design is a challenging task, because it requires appropriate precision, throughput and yield across multiple scales of tolerance, part dimension and workspace limitations.

Sequential microassembly requires a high precision micromanipulator and motion control; either by off-line programming with calibration or by on-line sensory feedback control. The later is traditionally accomplished via a microscope or a force sensor integrated with the gripper, or both [3]. However, the price paid in assembly speed is considerable, resulting in low assembly throughputs.

B. Compliant Microassembly

A promising, serial assembly approach that does not require real-time feedback can be envisioned by means of compliant mating. The advantages are fast assembly, disassemblability, self guidance and alignment, and no additional material for joining. The mechanical strength of assembled structures mainly depends on the interaction forces which were generated by the deflections of mating parts.

Bohringer and Prasad were among the first to introduce the concept of snap-fasteners using MEMS as early as 1995 [10]. This approach, however, was limited to "in-plane" assemblies, which today are used in a variety of applications, for instance MEMS inertial guidance and safety switches [11]. Another aspect that limited the use of compliant assembly via snap-fasteners was the limited "out-of-plane" stiffness of surface micromachined parts. An important turning point for the practical feasibility of MEMS snap-assemblies occurred after Metal LIGA and

Manuscript received September 18th, 2007. This work was supported in part by the NIST ATP Program, Office of Naval Research, and the SPRING Texas Annual Fund. The author is with the Automation and Robotics Research Institute (ARRI), at the University of Texas at Arlington, Fort Worth, TX 76118 USA.

Dan O. Popa Ph.D., is currently Assistant Professor of Electrical Engineering (e-mail: popa@arri.uta.edu). His research interests include multiscale robotics, 3D microsystems integration, embedded and distributed sensors and actuators.

Silicon DRIE (Deep Reactive Ion Etching) machining allowed for thicker 2 ½ D part geometries. This enabled the use of automation in serial and parallel MEMS assembly, as pursued by several research groups [12,19,21]. An example of a very well designed fastener allowing 2½ D compliant assembly with SOI MEMS parts is the Zyvex® connector [21]. This connector is easy to assemble, and relative large friction forces generated in grippers and assembly "sockets" firmly hold parts during and after assembly, thus avoiding stiction [5,19,21]. However, the assembly yield was not incorporated in the design phase of this snap-fastener.

C. Focus of this paper

In this paper we use a 3D microassembly station with 3 precision robots named μ³ [19], located at UT Arlington's Texas Microfactory™ to assemble compliant microsnap fasteners. Many other research groups have used microassembly stations since the early 1990's. The kinematics of these systems is often based on available off-the-shelf hardware (for instance by "stacking" precision stages to form a manipulator), and is limited due to tradeoffs between required precision, speed and workspace. We carefully tuned the kinematic configuration of μ³ for high-yield assembly of 2 ½ D MEMS components, rather than trying to provide as much functionality, range of motion, or accuracy as possible. During microassembly, parts are passed between manipulator tools and substrate fixtures so that we never "let go" of the manipulated parts [3]. By using compliant passive or active fixtures, grippers, or microparts we can send end-effector in close proximity to the parts of interest at fairly high speeds, and we complete the assembly without real-time force and vision information [5,15,19].

Here we present past and on-going research at the Automation & Robotics Research Institute (ARRI) at UTA aimed at formulating assembly-related design guidelines and trade-offs for 2 ½ D snap-fastener design and precision robot cell configuration. We use several examples of assemblies evaluated experimentally through tolerance and strength measurements. The paper is organized as follows; in section II we describe general guidelines for achieving high yield assembly of 2 ½ D microparts; in section III we discuss aspects related to the design criteria and tolerance analysis of microsnap fastener; section IV describes the configuration and calibration of the assembly cell for high yield assembly; Section V presents experimental results and characterization of several completed MEMS assemblies; finally section VI concludes the paper.

II. GENERAL GUIDELINES FOR 2 ½ D MICROASSEMBLY

In contrast to macro or meso-scale assembly, the design and precision of a microassembly cell is tightly coupled with the parts to be assembled by means of tolerance analysis and part compliance. Microscale assembly suffers from well-known limitations due to limited robot precision, small field of view for machine vision, and difficulties in sensing small forces. We can compensate for all these difficulties through engineered part compliance and the use of snap-fasteners.

A. Part and end-effector compliance

Microgrippers and microparts are a lot more flexible than the meso and macro scale positioners that they are mounted on. As a result, their compliance needs to be optimized to compensate for position and orientation errors and to prevent damage. Analytic models of compliant insertion can be used to represent the motion and force equations during mating [5,16]. Just as in the case of a conventional peg-in-hole insertion, the deflection and force profiles during chamber crossing, one point contact, and two points contact can be predicted. Design optimization can then be then used to determine the kinematics and characteristics of each flexible joint. This optimization can be based on various optimality indices, or on the mechanism Jacobian [23].

Compliant or non-compliant 2 ½ D micro-parts and micro-grippers are fabricated on a common wafer, such as Silicon on Insulator (SOI). Here we assume that all parts and end-effectors have either engineered compliance or are rigid, however, at least one of them must be compliant. For instance, in a typical operation involving assembling Part A into assembly site B using microgripper C, we assume that at least one of A, B, and C.

End-effectors can be either passive ("jammers") or actuated, and assembly sites are typically snap-fasteners. MEMS grippers are mounted onto robot end-effectors by "flip-chip" bonding. Assembly joints can be strengthened through snap-fastener design to minimize insertion force and maximize retention force, and through the use of bonding agents such as epoxies or solder reflow.

B. Fixtures and micropart transfer

To cut down on the time it takes to "find" MEMS parts in the assembly cell, they should always be presented for assembly in an ordered state either on die – tethered or untethered, but nonetheless in "predictable" spots. Microparts fabricated using lithographic techniques have this property by default, since the wafer is already a fixture.

Microparts which are singulated (for instance micro-optical glass components) must also be presented to the assembly cell in an ordered state. In this case, vibratory energy can be used for sorting, as can typical feeding techniques used in semiconductor industry such as using tapes or gel packs. Fixtures must also contain special compliant or visual markers for end-effector calibration.

During assembly, microparts are transferred from the substrate to the gripper and back into the substrate by means of stable grasps, interference fits and snap-fastening, and at no time are parts "let go" to position themselves due to uncontrolled friction, stiction, gravity, electrostatic or van der Waals forces.

C. Robotic workcell design

The required precision of the robotic cell is dictated by the tolerance budget of the assembly. In turn, this is dictated by the manufacturing tolerances of the parts and the

compliant part interference models. As a result, the maximum allowable part misalignment during assembly depends on the yield strength of the parts and the desired assembly yield. The workcell precision is accomplished via kinematic calibration of end-effector frames from all the robots sharing the workspace.

Microparts are passed between end-effectors and substrate or other assemblies, but because large field of view visual information cannot be obtained at high resolutions, more than one robot is necessary in the assembly cell. To assemble 2 ½ D microparts, the number of DOFs for all robots must add to at least 6 independent joints. This number should exceed 6 if redundancy/increased dexterity or increased workspace is necessary. For our assembly cell, μ³, we use a configuration with 4 DOFs on the gripper carrying manipulators, and 5 DOFs on the substrate carrying manipulator. Furthermore, each robotic chain is composed of at most 3 independent rotational DOFs, and 3 independent translational DOFs so that we can decompose the translational and rotational calibration. Because we will be assembling 2½D microparts, a terminating roll DOF in the robotic chain and a programmable remote center of rotation of the end-effector is required for part rotations of 90 degrees.

Force and visual feedback from the end-effector for close-loop control is not necessary during automation, but it is necessary during calibration. An appropriate approach utilizes weak-calibration by means of vision from multiple microscopes and a "hand-to-eye" configuration (because the microscope FOV is limited). While the configuration of μ³ is not unique, the desired functionality is accomplished with minimal hardware. Finally, high speed MEMS assembly is accomplished through an assembly "script" that must take into account collision and workspace constraints. The assembly yield is guaranteed through analysis of part and robot tolerances.

III. COMPLIANT PART DESIGN

A. General Design Principles

Traditional concepts such as RCC (remote center of compliance), RCR (remote center of rotation), and peg-in-hole insertion models [16] can be used for both part and gripper design. Snap-fastener insertion models can be obtained using full fledged FEA simulation, or reduced order lumped models. These models relate the insertion force along the insertion direction with part misalignment. For instance, the insertion of a 2½D rigid part A into a compliant part B along the X direction, this is usually written as:

$$F_{ABi}(r) = f_{ri}(\Delta x, \Delta y, \Delta\theta, \mu, \bar{a}), \quad (1)$$

where i=x,y are the two components of the insertion force, Δx, Δy are misalignments between the parts in the insertion direction and perpendicular to it, Δθ is angular misalignment around the Z direction, μ is the coefficient of friction, $\bar{a}$ is a parametric vector describing the part geometry, and $r = r_0 \ldots r_f$ is a insertion regime parameter describing the contact (one-point, two point, chamfer crossing, and insertion snap). More complex models are necessary if both parts are compliant, such as in the case of the Zyvex® connector in Figure 1.

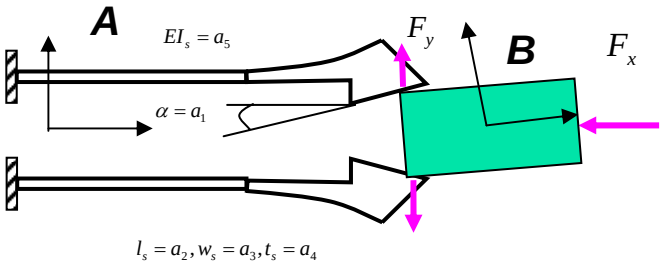

Figure 1: Free body diagram depicting the insertion of rigid part B into compliant Zyvex® snap-fastener A, shown in a two-point crossing state.

To design an appropriate snap-fastener, the geometry design vector $\bar{a}$ is chosen such that for all misalignments in y and θ below a given design threshold $\Delta y \le \sigma_{1y}, \Delta\theta \le \sigma_{1\theta}$, we have:

$$\text{Min}(F_{ABx}(r_j), j < f), \ \text{Max}(F_{ABx}(r_f)) \text{ and } F_{ABy}(r_j) \le F_{yeild}, j \le f, \quad (2)$$

where F_{yeild} is the yield strength of the microstructure. In other words, the snap-fastener design criterion is based on minimizing the insertion force, and maximizing the retention force without breaking the structure.

The misalignment design thresholds σ_1 are chosen in conjunction with the part manufacturing tolerance, part B positioning tolerance prior to assembly with respect to the substrate, and the manipulator positional accuracy holding part B with respect to the substrate. Specifically, a misalignment tolerance below σ_{1y} and $\sigma_{1\theta}$ has over 99% assembly yield (or 3σ spread). For the Zyvex connector in figure 1, $\sigma_{1y} < 5$ μm , and $\sigma_{1\theta} < \pm 6^o$ [17].

B. Example of microsnap fastener design

As an example of fastener design, consider the connector in Figure 2, which is assembled using a lateral insertion operation of a vertical MEMS part into a socket. The part is gripped from the substrate using a microgripper, rotated and laterally forced into the socket. Similarly, the orientation of the snap fastener onto the part can be varied to accommodate vertical, horizontal or any other angular assembly. An example of such assembly is the wheel/axle assembled for a MEMS-based microcar shown in Figure 3. The dominant forces that act upon the microparts during assembly are (1) Insertion force (force along X axis) required to assemble the part and (2) retention force (force along Z axis) with which the MEMS part is retained by the joint after assembly. These forces depend on 1) socket cantilever stiffness 2) parts interference due to design geometry 3) coefficient of friction and 4) positional accuracy during insertion. The aim of our design is to minimize the insertion stiffness and maximize the retention

stiffness.

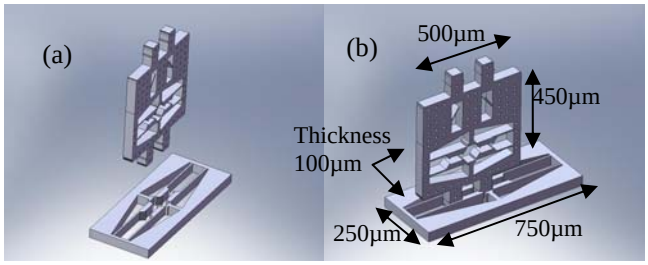

Figure 2: Design of microsnap fastener and micro part (a)Part and microfastener; (b) part placed into the microfastener before snap locking;

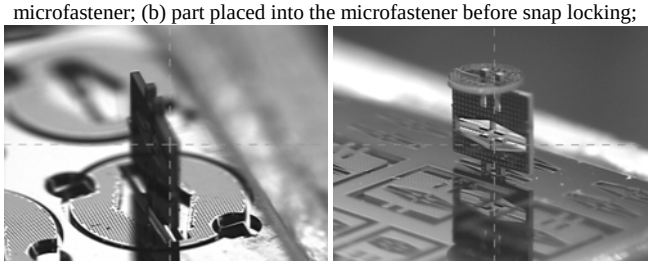

(a) (b)

Figure 3: (a) & (b) Micro part assembled onto the compliant snap fastener, (a) Microassembly with snap fastener on a wheel, (b) Multilayer assembly with snap fastener and modular part.

The snap arm in Figure 4a) can be represented as a cantilever beam with length 'l', width 'b' and height 'h', while δx and δy are the cantilever end deflections during assembly and θ is the guide angle.

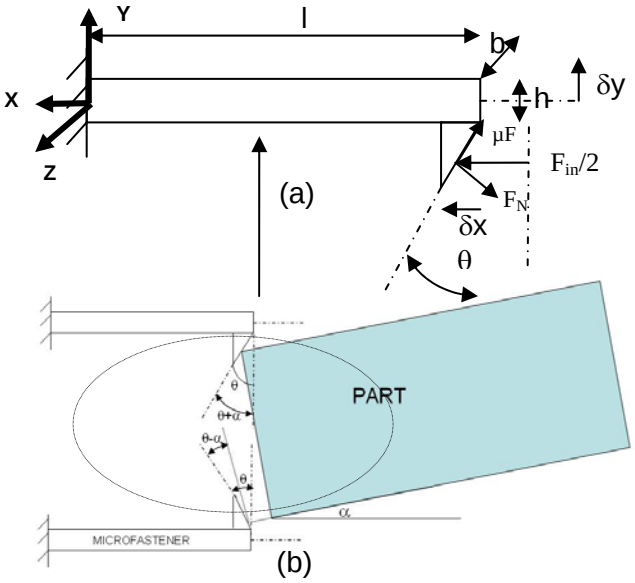

Figure 4: (a) Microfastener modeled as a cantilever (b) -fastener misalignment with part

If F_{in} is the insertion force acting on the socket arms, F_N is the normal force and μF_N is the force due to friction, then:

$$F_{NY} = \frac{-F_{in}}{4}\sin(2\theta), \tag{3}$$

and the force due to friction can be written as:

$$F_{frY} = \mu\frac{F_{in}}{2}\cos^2(\theta), \tag{4}$$

where μ is the coefficient of friction and F_{frY} is the vertical component of the frictional force. Therefore, the net force in Y direction is given by:

$$F_{Yreq} = \frac{F_{in}}{2}(\mu\cos^2\theta - 0.5\sin 2\theta). \tag{5}$$

Using the cantilever bending stiffness equation, we also have that:

$$F_{Yreq} = \frac{3EI\delta y}{(L-\delta x)^3}, \tag{6}$$

Where, 'E' is the Young's modulus of silicon E= 160GPa, 'I' is the moment of inertia about the neutral axis, 'b' = 100 µm is the thickness of the SOI DRIE die on which the microfastener is fabricated, 'h' is the arm height, 'L' the arm length, 'δy' = deflection due to bending, θ is the "snap angle". From equations (5) and (6) we can calculate the insertion force as:

$$F_{in} = F_{ABx}(r_1)\frac{6EI\delta y}{(L-\delta x)^3(\mu\cos^2\theta - 0.5\sin 2\theta)}. \tag{7}$$

Moreover, the stress due to bending is calculated using:

$$\sigma_b = \frac{My}{I} \tag{8}$$

'y' = h/2, 'M' is the moment due to bending force and '*I*' is the moment of inertia about neutral axis.

C. Insertion Simulation

'L', 'h' and 'θ' make up the design vector $\bar{a}$ from equation (1). By varying these parameters, the resulting insertion and retention forces are plotted in Figure 5. The design goal is to reach the highest retention force level while minimizing the insertion force. Thus, the design parameters are varied and an optimal design is chosen. The parameter values associated with this design are 'L'=600µm, 'h'=10 µm and 'θ'=75º with the following insertion force variation, for which we obtain: F_{in}=14.5mN, F_{ret}=13mN. Using equation (8), the maximum bending stress on cantilever arm is found to be 0.17 GPa.

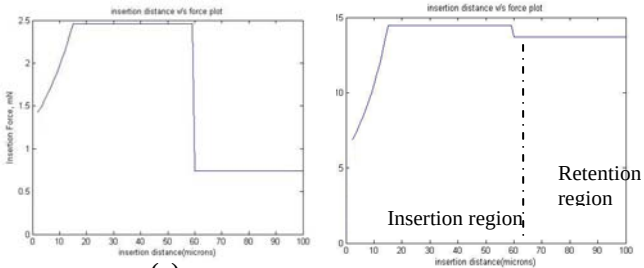

(a) (b)

Figure 5: Insertion force (Y axis) variation for varying cantilever parameters versus insertion distance (X axis):(a) High insertion &low retention forces (b) Lower insertion force with high retention force.

During insertion, a misalignment in the angle between the part and the arm's neutral axis is also a possible cause for variation in forces. This misalignment arises due to the tolerance between the MEMS part width and the socket width between the two cantilever arms. For the current

design, this tolerance was 10 μm. The part has a length of 100 μm. Hence the maximum angular misalignment is α=0.0997 rad. This misalignment angle adds to the 'θ' parameter on one of the arms and subtracts from the same on the opposite arm. This modifies equation (7) as follows:

$$F_{in}^{a,b} = \frac{6EI\delta y}{(L-\delta x)^3(\mu\cos^2(\theta\pm\alpha)-0.5\sin 2(\theta\pm\alpha)}, \quad (9)$$

$$F_{in} = F_{in}^{a} + F_{in}^{b}$$

Figure 6 shows the maximum insertion force for different values of α.

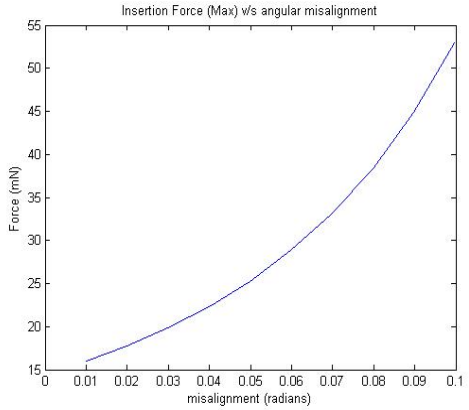

Figure 6: Insertion force (maximum) variation for different values of α.

IV. μ³ MICROASSEMBLY SYSTEM

A. *Kinematics of assembly cell*

To accomplish compliant microassembly, we use the μ³ multi-robot cell configured using 19 DOF discrete stages and arranged into 3 robotic manipulators. Figure 6 shows three μ³ manipulators (M_1, M_2, M_3) sharing a common 25 cm³ workspace. Also depicted are three microscopes that are used for calibration and visual servoing.

M_1 and M_2 are two robotic manipulator arms with 7 degrees of freedom each. They consist of XYZ coarse and fine linear stages, including the PI Nanocube® for nanoscale fine motion. A rotation stage provides a terminating roll DOF (θ) axis which is key for assemblies of 2½D MEMS components. Mounted at the end of the manipulator chains are kinematics mounting pairs that provide for end-effector reconfigurability. The central manipulator M_3 is a high precision 5 DOF robot consisting of a XYθ mechanism placed on a 2 axis tilt stage. This robot carries custom designed fixtures for microparts (the dies/substrate) and a custom designed hotplate for interconnect solder reflow. A schematic diagram and picture of μ³ is shown in Figure 7. Currently, we mount MEMS end-effectors (jammers or active grippers) onto M_1, and end-effectors with rotational symmetry (vacuum nozzles, adhesive-based microgrippers) around the vertical axis onto M_2. Die sites with microparts are placed onto manipulator M_3.

One important aspect in the kinematic configuration of μ³ is that XY scanning with manipulator M_3 (center) is used to "bring" the part to the end-effector, and not the other way around. As a result, the end-effector will always be in focus for the limited field of view.

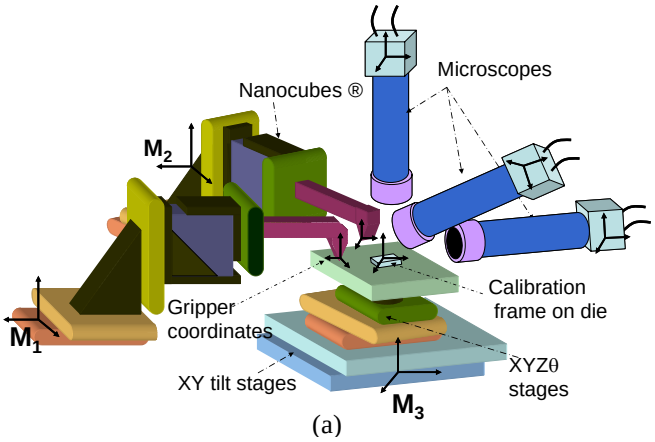

(a)

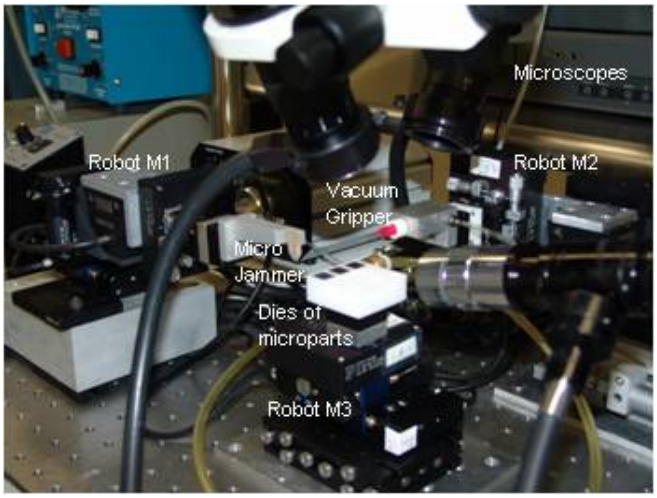

(b)

Figure 7: (a) Schematic diagram of μ³ (meso-micro-nano) platforms with microgrippers; (b) Kinematic representation of the multirobot system

B. *Calibration of assembly cell*

Calibration refers to a set of procedures for locating the robot end-effectors in a global coordinate frame. Calibration of the μ³ system is accomplished by expressing the local coordinate frames attached to robots M_1 and M_3 in a common frame, attached to the end-effector frame of robot M_2. In a typical calibration sequence, each manipulator is commanded to several locations and the actual misalignments are measured using the stereo vision system. From these measurements, a mapping can be derived by doing constrained least-squares fit on the data. The number of data points should be sufficient to bring the variance of the pose estimate below the robot repeatability [18]. Because each of the robots has at most 3 independent rotational DOF's, and 3 translational DOF's, we can decompose the orientation pose calibration from the translation pose calibration. The calibration steps are as follows:

Step 1: M_1 end-effector calibration of the remote center of rotation.

Manipulator M_1 is primarily used as a pick and place tool for 2 ½ D microparts, with an additional 90 degrees rotation

for vertical part orientation for snapping into the substrate. As a result, it is important that parts that are rotated 90 degrees be situated in close vicinity to their original orientation. In μ³, we use machine vision with a microscope to program the RCR of microgrippers. Due to variability in gripper designs and fabrication, it is currently necessary to repeat this step every time a new MEMS gripper is mounted on M_1. Future improvements should provide a manipulator with RCR ability, or a way of mounting microgrippers through a tool changer that does not need to be recalibrated. A summary of techniques for mounting MEMS grippers and program the RCR can be found in [19, 20].

Step 2: M_3 Angular pose alignment to M_1 end-effector through vision.

Now that the gripper is mounted on M_1, and the die containing 2½D MEMS parts is mounted on M_3, it is necessary to calibrate the relative pose misalignment between the M_1 and M_3 end-effector coordinate frames. We accomplish this via the tilt DOF's of manipulator M_3, through the use of machine vision. The terminating roll DOF of M_3 is also mapped with respect to the M_1 end-effector frame. Because we servo based on a line detection algorithm, we estimate an angular calibration tolerance σ_θ = 0.0108º.

Step 3: M_3 to M_1 Translational pose alignment through taught fiducials.

After the alignment poses of M_1 and M_3 coincide, we must calibrate the remaining translational DOF's of manipulators M_1 and M_3. Assembly operations will now involve translations, rotations by 90 degrees via the terminating roll of manipulator M_1 with RCR property, and arbitrary rotations via the terminating roll of manipulator M_3. Note that we do not utilize M_1 DOF's X, Y translations but only the Z translation, in order to remain in the limited field of view of the microscopes. As a result, we produce calibration maps based on translation by pointing with the end-effector to features (fiducials or microparts) located on the MEMS die. A detailed description of this calibration procedure and experimental results can be found in [19].

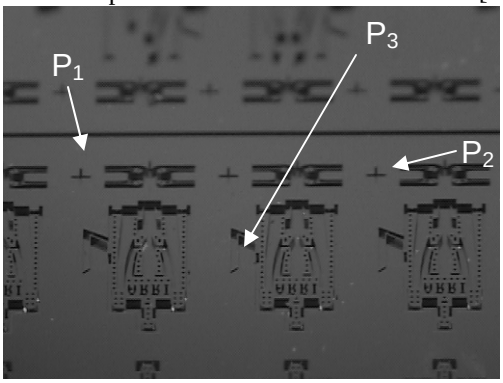

Figure 8: MEMS Layout containing arrays of Zyvex jammers and calibration sites P_1,P_2,P_3 where the end-effector must be pointed to.

Figure 8 depicts a MEMS layout populated with Zyvex jammers and corresponding calibration fiducials (P_1, P_2) as well as assembly sites (P_3). P_1, P_2, and P_3 can be used for calibration. As an alternative to pointing to fiducials, we can actually physically place the gripper tip inside a compliant feature on the die, and visually observe that it does not cause part shift along x, y, and z. The parts themselves are thus used for both calibration and assembly. In [19] we showed experimental results that indicate a calibration accuracy better than $\sigma_{3x,y} \le 7$ μm, and $\sigma_{3z} \le 1$ μm using the three point teaching method and 5x zoom microscope objectives.

C. Tolerance analysis to predict assembly yield

Tolerance analysis has popularly been used not only to predict the variations generated during assembly, but to improve the assemblability [16,17]. In addition to the uncertainty of part location, the positional uncertainty of a robotic manipulator is also needed to estimate an overall uncertainty. Tolerances are represented using Gaussian models with a mean and a covariance, and the position and orientation of a feature are statistically propagated from part to part [17].

As an example, we use the Zyvex connector shown in Figure 1. Prior to assembly, the standing part of the assembly must be released from the substrate by breaking of tethers that hold them in place after DRIE. The analysis of part positioning tolerance after the tethers are broken can be done experimentally using a microscope as the parts were presented to the jammer gripper.

In this case, the variances obtained experimentally were σ_{2y}= 2.89μm, and $\sigma_{2\theta}$= 4° [22]. This means that if an end-effector is positioned with repeatability σ_{3y} and $\sigma_{3\theta}$ relative to the substrate, the assembly yield will be over 90% if the following **high yield condition is satisfied:**

$$\sigma_{1y}^2 \ge \sigma_{2y}^2 + \sigma_{3y}^2, \text{ and } \sigma_{1\theta}^2 \ge \sigma_{2\theta}^2 + \sigma_{3\theta}^2 \quad , \qquad (10)$$

where σ_{1y} and $\sigma_{1\theta}$ are tolerances obtained by design through the compliant insertion model. In the case of the Zyvex connector shown in Figure 4, these design criteria, and the robot calibration accuracy result in a predicted 99% (3σ) assembly yield as previously reported in [19, 22].

V. EXPERIMENTAL RESULTS

A. Repeated assemblies

With knowledge of the calibration map, we now can simply servo the joint axes of robots M_1 and M_3 to position the end-effector of M_1 to pick up a part on the MEMS die at die coordinates P. We accomplish this task at fairly high speed (1 assembly operation per second or higher) with our manipulators, and without any force and vision feedback. Because we have experimentally verified that the connector design tolerance σ_1, the part misalignment tolerance σ_2, and the manipulator positional accuracy σ_3 are:

$$\sigma_{1x,z,y,z} \le 5\mu m, \sigma_{2x,y,z} \le 2.89\mu m, \sigma_{3x,y,z} \le 7\mu m \quad , \qquad (11)$$
$$\sigma_{1\theta} \le 6, \sigma_{2\theta} \le 4, \sigma_{3\theta} \le 0.75^\circ$$

we now satisfy the high yield (over 99%) assemblability condition (10). Figure 9(b) shows an array of 12 Zyvex jammers assembled in sequence using automation scripting

after appropriate calibration. To strengthen the snap-fastener joints after assembly, epoxy was also applied using a dispensing nozzle mounted on manipulator M_2. The total assembly time for this array was a few minutes and the assembly yield was 100%.

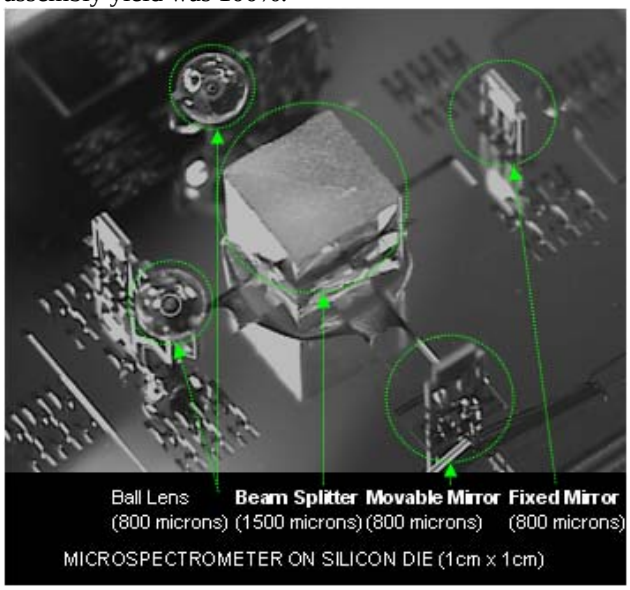

(a)

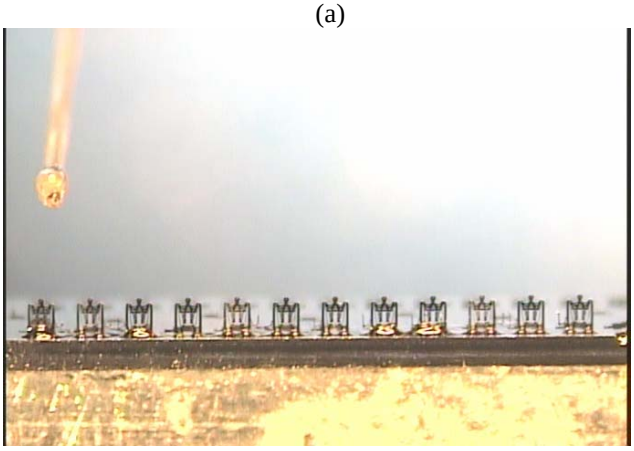

(b)

Figure 9: (a) A micro spectrometer assembled on a 1x1 cm^2 silicon die; (b) Array of 12 Zyvex jammers assembled in sequence and epoxy cured in place.

B. *Assembly of a microspectrometer*

Figure 9(a) shows a micro spectrometer assembled on a 1x1 cm^2 Silicon die. It consists of two vertically assembled micro mirrors, two vertically assembled ball lens holders, two glass micro ball lenses, and a glass beam splitter. Each of the ball lens assemblies consists of a rigid part (ball) inserted into a compliant holder. The microspectrometer was tested using fiber coupled laser light and a detector assembled onto the substrate. After successful assembly of part into the compliant microsnap fastener we tested the angular misalignment in the assembly with respect to the substrate, using the setup in Figure 10. By measuring the deviation in laser spot between calibrated prism and the assembled part on the die, the angle between assembled parts is measured and is found to be 0.776º.

C. *Assembly force and friction measurement*

To experimentally determine the force required for micro part insertion into the snap fastener and the force required to knock the part off the substrate, we used a SensorOne® beam element - a single crystal silicon beam with one ion implanted resistor on each side mounted in a special miniature header. A deflection of the beam gives a resistance change fed into a Wheatstone bridge. This sensor is mounted onto the M_1 robot, and pushed against a snap-fastener assembly to obtain force measurements as shown in the Figure 11(a). Figure 11(b) shows the insertion force vs. displacement obtained. The experimentally determined insertion force is 40mN and the retention force is 22mN.

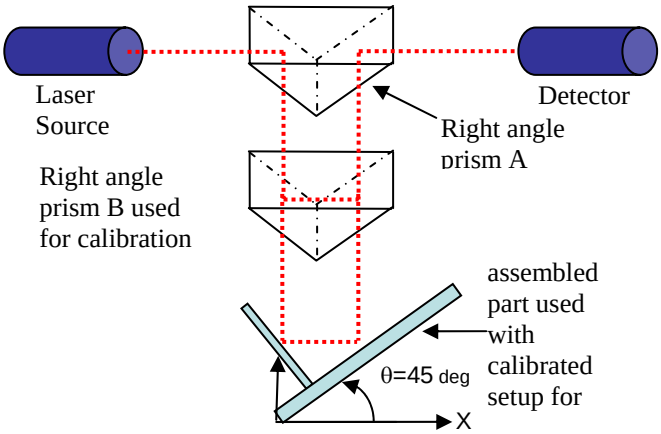

Figure10: Calibration and assembly angle measurement using laser setup.

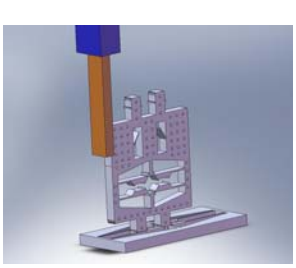

(a)

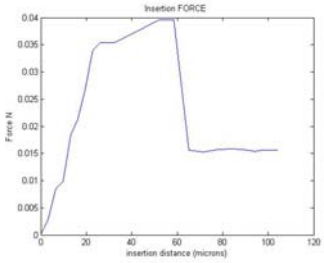

(b)

Figure 11: Microforce sensor with μ^3 station acting on assembly, and the resulting force.

The coefficient of friction 'μ' was estimated using a line fit from equation (7) with experimentally determined force values and x displacement values. This results in an estimate μ=0.31, which is used in the force simulation. Comparing this to the simulation results in section III, we can infer that during assembly, the part was misaligned to the socket arm by 0.07 radians. Therefore, the experimentally determined retention force which is 14.9 mN matches closely with the simulation result.

D. *ARRIpede Microcrawler*

The ARRIpede microrobot consists of an array of prismatic joints on a 1cm x 1cm area Silicon on Insulator (SOI) die. Currently, we prototyped 1D prismatic joints, however, in-plane 2D (X, Y) or 3D (X,Y, θ) designs are straightforward extensions. The prismatic joints consist of Chevron electro-thermal actuators with a microsnap

fastener. The first ARRIpede prototypes consist of 4, 6 and 8 actuated legs, as shown in Figure 12. The principle of motion is based on stick-and-slip. The ARRIpede joint actuators are powered using a custom designed electronic backpack. A payload measuring 1cm x 1cm x 0.05cm and weighing 1g (made of Au-Sn alloy) was placed on the inverted robot and 2mm/s velocities were obtained with 50Hz square-wave gait motions. We are currently testing the ARRIpede payload and speed capabilities.

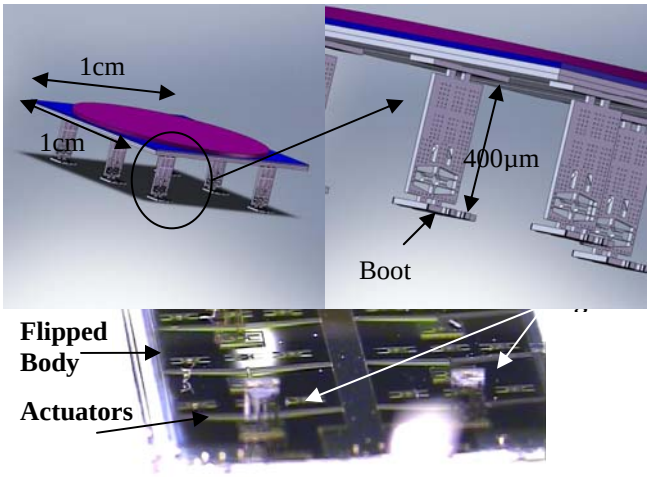

Figure 12: (top) Solid model of ARRIpede with payload; (bottom) Inverted ARRIpede conveyor showing four assembled legs.

VI. CONCLUSION AND FUTURE WORK

In this paper we presented a systematic approach to address precision and throughput issues in compliant MEMS assembly. This approach includes snap-fastener designs, tolerance analysis, and appropriate robot calibration to accomplish a desired target yield. We presented several microsnap fastener designs, and their assembly yield prediction and evaluation. Micro-fasteners can be used as an interconnects to construct more complex 3D micro-structures, such as microrobots. Through proper force simulation modeling and experimental data of assembly force, it has been demonstrated that the design offers good compliance during assembly as well as good retention after assembly. The µ³ multirobot cell was used to assemble hybrid on-die MEMS devices such as microoptical benches or the ARRIpede microcrawler. Future work includes improvements to our connector designs, tolerance analysis for cascaded assemblies, and their use in prototyping other miniaturized instruments and robots.

ACKNOWLEDGEMENT

The author wishes to thank Texas Microfactory™ graduate students Rakesh Murthy, Aditya N. Das, and Dr. Woo Ho Lee for their contributions to the design, simulation and experimental work presented in this tutorial paper.

REFERENCES

[1] Y. Zhou, B.J. Nelson, and B. Vikramaditya, "Fusing force and vision feedback for micromanipulation," in Proc Of IEEE ICRA, Leuven, Belgium, May 1998.

[2] A. M. Hoover, S. Avadhanula, R. Groff, Ronald S. Fearing, "A Rapidly Prototyped 2-Axis Positioning Stage for Microassembly Using Large Displacement Compliant Mechanisms" in Proc of IEEE ICRA, Orlando, Florida, May 2006.

[3] D.O. Popa, H.E. Stephanou, "Micro and meso scale robotic assembly", in SME Journal of Manufacturing Processes, Vol. 6, No.1, 2004, 52-71.

[4] A. Rizzi, J. Gowdy, R.L. Hollis, "Agile assembly architecture: an agent based approach to modular precision assembly systems," in Proc of IEEE ICRA, Volume: 2, 20-25 April 1997, pp 1511 – 1516.

[5] W.H. Lee, B.H. Kang, et al., "Micropeg Manipulation with a Compliant Microgripper," in Proc of. IEEE ICRA, Taiwan, Page(s): 3213-3218, 2003.

[6] G. Greitmann, R.A. Buser, "Tactile microgripper for automated handling of microparts," Sensors and Actuators, A.53, pp.410- 415, 1996.

[7] M. Shimada, J.A. Tompson, J. Yan, R.J. Wood, R.S. Fearing, "Prototyping millirobots using dextrous microassembly and folding," in Proc of ASME IMECE/DSCD, vol.69-2, pp.933-940, 2000.

[8] F. Arai, T. Fukuda, "Adhesion-type micron-endeffector for micromanipulation," in Proc of IEEE ICRA, pp.1472-1477, 1997.

[9] K.F. Bohringer, et. al., "Sensorless manipulation using massively parallel microfabricated actuator arrays," in Proc of IEEE ICRA, pp.826-833, 1998.

[10] R. Prasad, K..F. Bohringer, N.C. MacDonald, "Design, Fabrication, and Characterization of Single Crystal Silicon Latching Snap Fastners for Micro Assembly," in Proc of ASME International Mechanical Engineering Congress and Exposition (IMECE '95), San Francisco, CA, Nov. 1995.

[11] M.B. Cohn, K.F. Böhringer, et. al., "Microassembly technologies for MEMS", International Society for Optical Engineering Proc, vol. 3513, Page(s):. 2-16, 1998.

[12] N. Dechev, W.L. Cleghorn, J.K. Mills, "Microassembly of 3-D microstructures using a compliant, passive microgripper", Journal of Microelectromechanical Systems, Volume 13, Issue 2, April 2004 Page(s): 176 – 189.

[13] J Fang, K. F. Böhringer, "Parallel micro component-to-substrate assembly with controlled poses and high surface coverage", Journal of. Micromechanics and. Microengineering, Issue 4 , Vol 16, Page(s): 721-730, 2006.

[14]Kazuhiro Saitou, Mark J. Jakiela, "Design of a self-closing compliant mouse trap for micro assembly" Proc. of ASME International Mechanical Engineering Congress and Exposition November 17-22, 1996, Atlanta, Georgia.

[15] Ping Zhang, Mohammad Mayyas, et. al., "An active locking mechanism for assembling 3D micro structures", Proc of SPIE - Volume 6414, Smart Structures, Devices, and Systems III, 2006.

[16] D. Whitney, "Quasi-Static Assembly of Compliantly Supported Rigid Parts," ASME Journal of Dynamic Systems, Measurement, and Control, pp. 65-77, Vol. 104, March, 1982.

[17] W. H. Lee, M. Dafflon, H.E. Stephanou, Y.S. Oh, J. Hochberg, and G. D. Skidmore, "Tolerance analysis of placement distributions in tethered micro-electro-mechanical systems components," in Proc of IEEE ICRA, May 2004.

[18] D.O. Popa, R. Murthy, et al., "M3-Modular multi-scale assembly system for MEMS packaging", in Proc of IEEE/RSJ IROS Beijing, China, October 2006.

[19] A.N. Das, P. Zhang, W. H. Lee, D. O. Popa, and H. E, Stephanou, "µ³: Multiscale, Deterministic Micro-Nano Assembly System for Construction of On-Wafer Microrobots," in Proc of IEEE ICRA, Rome, Italy, April 2007.

[20] M. Mayyas, P. Zang et al, "Design Tradeoffs for Electrothermal Microgrippers", in Proc of IEEE ICRA, Rome, Italy, April 2007.

[21] K. Tsui, A.A. Geisberger, M. Ellis, G. D. Skidmore, "Micromachined end-effector and techniques for directed MEMS assembly," Journal of Micromechanics and Microengineering. Vol. 14, pp. 542-549, 2004.

[22] R. Murthy, A. Das, D. O. Popa, "ARRIpede: A Microcrawler Robot Constructed via 2 ½ D MEMS Assembly," under review for IEEE ICRA' 08, Pasadena, CA, 2008.

[23] B.H. Kang, J.T.-Y. Wen, N.G. Dagalakis, J.J. Gorman, "Analysis and design of parallel mechanisms with flexure joints," in Proc of IEEE ICRA, Volume 21, Issue 6, Dec. 2005 Page(s):1179 – 1185.

Robotic Microassembly of 3D MEMS Structures

Nikolai Dechev[1], and Mohamed Basha[2]

Abstract—**This paper describes ongoing development of a general microassembly system used to construct sub-millimeter, 3D Micro Electromechanical Systems (MEMS) from a collection surface micromachined micro-parts. An overview of our robotic-based method is presented, which includes: (a) the overall grasping, manipulation and joining strategy, (b) the use of passive (non-powered) microgrippers, and (c) the use of various micro-mechanical joints to create 3D microstructures. Current work using modified microgrippers and a 6 DOF (degree of freedom) robot to construct advanced 3D microstructures, is discussed. Examples of 3D MEMS applications that have been successfully assembled using this system include: micro-coils, and motorized micro-mirrors for optical cross-connect switches. The present advantages and challenges with this system are discussed, along with avenues for future development.**

I. Introduction

THE purpose of microassembly is to create useful microsystems by assembling together a set of various micro-parts. When designing any microsystem that will require assembly, careful design of the individual micro-parts is required to ensure they are compatible with the assembly process. Specifically, the design of the micro-parts must take into account: (i) the function/role of each micro-part within the microsystem, (ii) the joining method to fasten the micro-parts together to create a functioning whole microsystem, and (iii) ensuring that the micro-parts can be handled appropriately by the microassembly process. Note that these three considerations are ranked in relative order of importance. In other words, the functionality of the micro-part is more important than the joining method, which is in turn more important than the compatibility with the microassembly process. Generally, there would be no point to assemble micro-parts with good microassembly compatibility, if this compatibility reduces the functionality of the microsystem, or inhibits the joining process. In a sense, a balance must be reached between these three considerations.

The goal of this work is to develop a general microassembly process that can be used to construct a wide variety of 3D microsystems. In working towards this goal, four major objectives have been identified. The first major objective is to develop the microassembly process so that it minimizes the impact on the function/role of the micro-parts, and hence the finished microsystem. The second objective is to maximize the number of possible assembly configurations, by allowing the micro-parts to be moved and oriented to any possible position in space. The third objective is to develop a joining system that can mechanically and electrically join together micro-parts at any orientation or position in 3D space. The final objective is to develop the microassembly process so that it is capable of rapid automatic assembly. This paper will describe work involving the first three objectives, and provide examples of achievements. Recently, we have applied our microassembly system to the development of a novel micro-electrostatic-motor/mirror combination used for micro-optical switching.

This work makes extensive use of MUMPs [1] surface micromachined micro-parts, since that process provides a reliable fabrication method for prototyping micro-parts with good consistency between fabrication runs. The micro-parts used to demonstrate the principles of this work are generally 60 to 300 μm in length or width, and are 5 μm in thickness. Regardless of their shape or function, all micro-parts are designed to incorporate three 'specific features'. These three features ensure that the micro-parts are compatible with the microassembly process, and minimize their impact on the function/role of the micro-parts. Firstly, all micro-parts are designed with *tether features* [2] protruding from their sides, which allow them to be securely held and accurately located on the surface of a silicon chip. Secondly, they have a built-in *joint feature* [3] used for joining them to other micro-parts during assembly. Thirdly, and most importantly, they have an *interface feature*, which allows them to be grasped by a handling system. The handling system used in this work consists of a microgripper attached to a robotic micromanipulator. The microgripper tips are specifically designed to grasp a micro-part by an *interface feature*. A novel aspect of this work is that all microgrippers or micro-tools used for the microassembly process, are fabricated alongside the micro-parts on the same chip. Prior to performing a microassembly task, the microgripper is first removed from the chip by bonding it to the end effector of the robotic micromanipulator [4]. Next, the microgripper is used to grasp the micro-parts and remove them from the chip, from their original fabricated locations. The micromanipulator translates and rotates the micro-parts to the target assembly site, and joins them at that site [5].

A number of other robotic based, serial microassembly strategies are being developed. Serial microassembly is a sequential process, in which individual assembly tasks are performed one after the other. Some examples of other

Manuscript was submitted September 18, 2007. This work was supported in part by the Natural Sciences and Engineering Research Council of Canada (NSERC), and by the Canadian Microelectronics Corporation.

1. Nikolai Dechev is with the Department of Mechanical Engineering, University of Victoria, PO Box 3055, STN CSC, Victoria, BC, Canada, V8W 3P6; (Contact: phone: 250-721-8933; e-mail: dechev@me.uvic.ca).

2. Mohamed Basha is with the Department of Electrical & Computer Engineering, University of Waterloo, 200 University Ave. West, Waterloo, Ontario, Canada, N2L 3G1 (e-mail: mbasha@maxwell.uwaterloo.ca).

groups making use of robotic, serial microassembly include those systems equipped with microgrippers [6,7,8,9] or systems equipped with micro-tweezers [10,11].

II. Grasping Interface

Ideally, a microgripper used for robotic-based microassembly should be designed to handle a wide assortment of micro-parts, of various shapes and sizes. However, designing such a versatile microgripper is challenging. Often, the design of micro-parts must be altered and standardized in some way, to allow the microgripper to grasp them. In this work a single, standard microgripper [5] was initially developed. It can handle various micro-parts, which are equipped with a corresponding standard *interface feature* [5]. Fig. 1(a) shows a SEM (scanning electron microscope) image of the grasping tips of the original, standard microgripper. This microgripper is a 'passive' design, in that it requires no 'active' actuation of the microgripper tips. Rather, the microgripper tips passively open and grasp a micro-part, as they are inserted into a micro-part *interface feature*. Similarly, they passively open and release micro-parts, after those micro-parts are joined to a microstructure. Fig. 1(b) illustrates the cross-sectional view of the microgripper tips along Section A. Note that the microgripper tips have a split-level design consisting of an '*upper level*' and a '*lower level*'. This split-level design assists in providing a secure grasp of micro-parts.

Fig. 1(c) shows an SEM image of the original, standard *interface feature* located in the center/back of micro-parts. Fig. 1(d) illustrates the cross-sectional view of the *interface feature* along Section B. Note that the *interface feature* is comprised of two layers of polysilicon, denoted Poly 1 and Poly 2. The Poly 2 layer has been intentionally fabricated to create the 'raised Poly 2' structure shown in Fig. 1(d-2). This allows the split-level microgripper tips to 'inter-lock' with the *interface feature*, to create the secure grasp. This *interface feature* design has been applied to a wide variety of micro-parts. Fig. 2 shows some video microscope images of various micro-parts used in this research, which are about to be grasped by the standard microgripper tips. Note that the micro-parts have different shapes, sizes, and different joint features, yet all are equipped with an identical, standard *interface feature*, located on the center/back of the micro-parts.

The passive microgrippers used in this work have a number of advantages. They do not require complex and bulky actuator designs, and do not require electrical power. Since they do not require power, they have a single bonding pad, which makes them easy to bond to the robot end effector, and makes them smaller in size than active microgripper designs. As passive designs, they employ a grasping and releasing strategy [5] that overcomes the problems of stiction, which can occur when attempting to release micro-objects with active microgrippers. As such, passive microgrippers are ideally suited for this microassembly work.

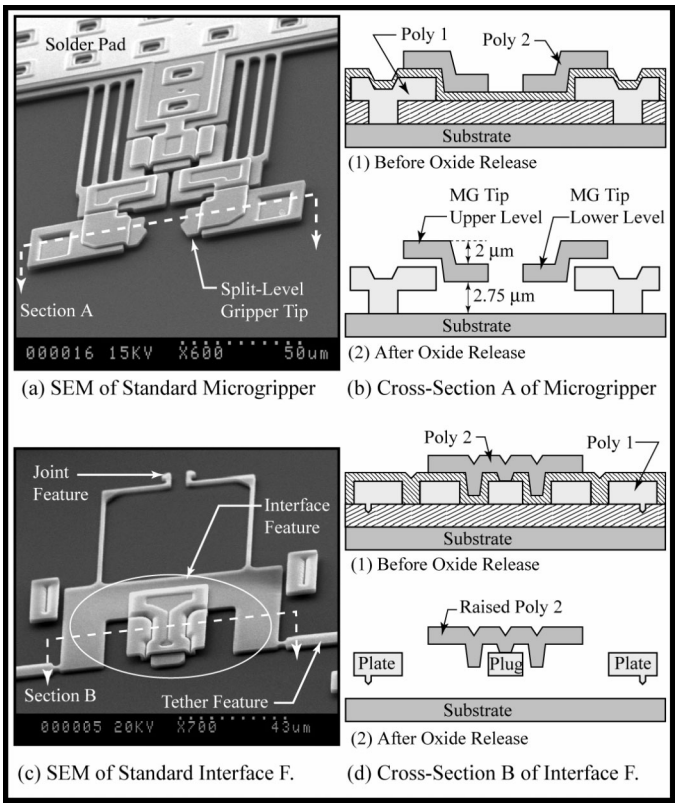

Fig. 1 SEM Image of Microgripper Tips and Micro-Part Interface Feature With Cross-Sections of Both.

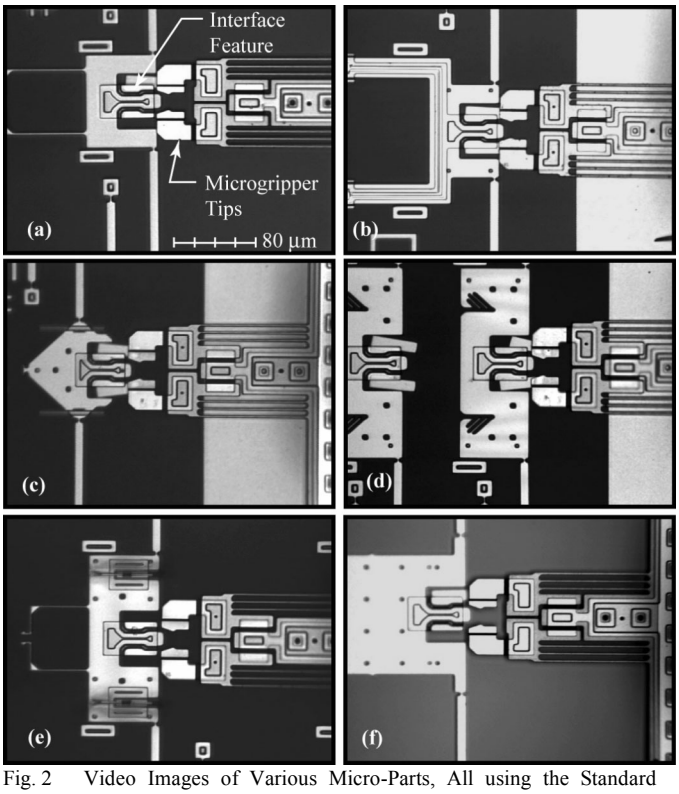

Fig. 2 Video Images of Various Micro-Parts, All using the Standard *Interface Feature* Design.

However, passive microgrippers also have a number of limitations. Passive microgrippers can only grasp and release objects that are adequately restrained, and that have specific *interface feature* geometries. These are reasonable pre-conditions for microassembly purposes, however, these requirements are not reasonable for general micromanipulation of non-standard, unrestrained, or irregular micro-objects, which can be better handled by active microgrippers. Additionally, the 'grasping interface' design between the microgripper and the micro-part is more complex, due to the passive grasping and release process. In comparison, active microgrippers generally have a simpler grasping interface such as a hole, or two parallel external sides on a micro-part.

III. Robotic Micromanipulator System

The robotic micromanipulator used in this work is shown in Fig. 3. This micromanipulator has been designed to accomplish two of the objectives of this work, which are to maximize the number of possible assembly configurations, and also to implement automatic microassembly tasks. Details of the design and development of the micro-manipulator are described in [4]. The micromanipulator is a 6-DOF robot, that is capable of translating and rotating micro-parts with respect to the MEMS chip in 3 translational DOF (x, y and z), and rotating in 3 rotational DOF (α, β and γ), as shown in Fig. 3(a). More importantly, the micromanipulator is able to actuate all 6-DOF simultaneously, within a relatively large operational workspace. The useable rotational workspace is: 360˚ about α, 180˚ about β, and 110˚ about γ, (although larger rotational ranges are possible for certain configurations of the axes [4]) and 25 mm of translation in the x, y and z directions.

The interface point (end effector) between the micromanipulator and the MEMS chip is a tungsten probe, illustrated in Fig. 3(b). Prior to commencing microassembly operations an appropriate microgripper is bonded to the tip of the probe using a UV (ultra violet) light curable adhesive. All microgrippers are initially located on the substrate of the MEMS chip, alongside the micro-parts to be assembled. Fig. 4(a) shows an SEM image of a microgripper on the chip substrate. Note that the microgripper is attached via *tethers*. Fig. 4(b) shows the microgripper after it is bonded to the tip of the probe. Since the adhesive bond is very strong, the *tethers* are easily broken when the probe is retracted from the substrate using the micromanipulator. Once bonded, a microgripper can be used for many grasping and joining cycles. Should a microgripper no longer be needed for a particular size of micro-part, the UV-adhesive is dissolved using a solvent and the unnecessary microgripper is brushed off. Next, fresh (un-cured) UV-adhesive is applied to the tip, the tip is pressed against a new microgripper, and becomes bonded to the probe tip when UV light is applied. The microgripper shown in Fig. 4 is a new 'modular design' [12] that can be fabricated with various widths between the tips, to accommodate larger micro-parts.

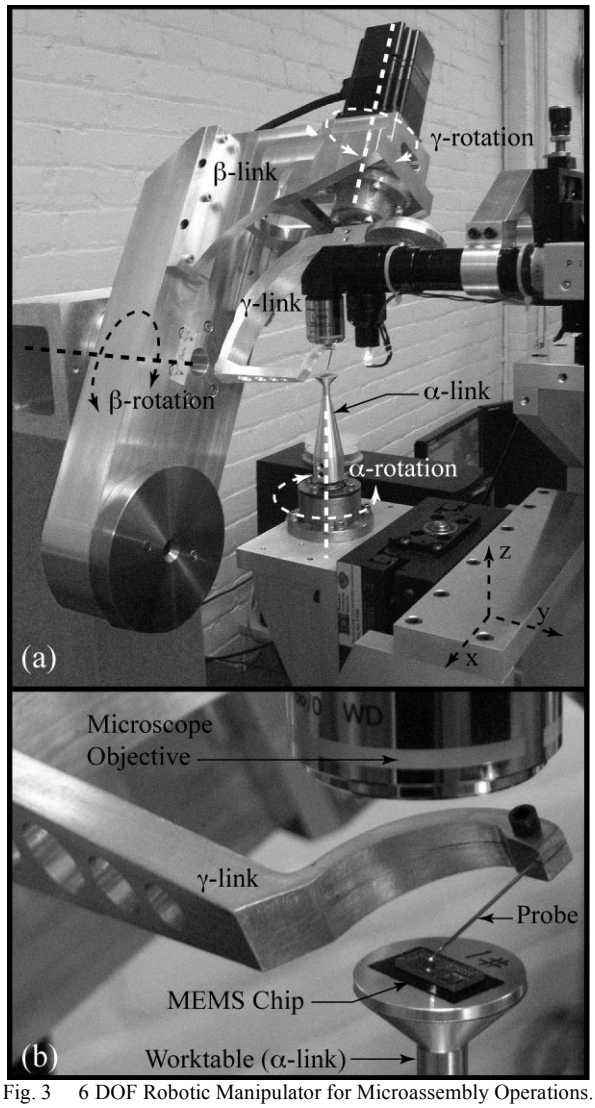

Fig. 3 6 DOF Robotic Manipulator for Microassembly Operations.

IV. Microassembly Process

The process of assembling a microsystem is now described. One of the more recent and novel microsystems constructed using this microassembly process is a 3D micro-electrostatic-motor/mirror [13], with applications for micro-optical switching. This 3D micro-mirror assembly is shown in Fig. 5. In creating this microsystem, a number of new techniques were developed and build upon the general microassembly method. Therefore, the microassembly process will be described in the context of constructing this 3D micro-mirror, and will describe some of the novel aspects. The process to construct the micro-mirror involves the sequential addition of micro-parts, to first assemble the micro-parts onto the electro-static *motor rotor*, and subsequently, to assemble more micro-parts into those previously assembled. To do this, each micro-part assembled must go through five tasks. These tasks are: (A) the micro-part is grasped with the microgripper, (B) the micro-part is removed from the chip substrate, (C) the micro-part is rotated and translated through space, (D) the

micro-part is joined to other micro-part(s), and (E) the micro-part is released by the microgripper. Currently, these five operations are performed by tele-robotic control, using a human operator. Work to automate these operations is ongoing, in order to maximize the assembly rate.

Fig. 6 shows SEM images of the micro-parts used to construct the 3D micro-mirror, as they lay in their fabricated positions on the chip substrate. Fig. 6(a) shows the *mirror-micro-parts* and Fig. 6(b) shows the *mirror support posts*. Note that all these micro-parts are attached to the chip substrate via *tethers*. These *tethers* are specially designed [2] to securely hold the micro-parts onto the chip during transportation, but are also designed to break away during the grasping operation. Also note the built-in *interface feature* on each micro-part, that is specifically designed to mate with the microgripper tips shown in Fig. 4. These microgripper tips and *interface features* have been re-designed, in comparison to those shown in Fig. 1. This new 'wider' configuration is better suited for grasping and holding these relatively wide micro-parts that comprise the 3D micro-mirrors.

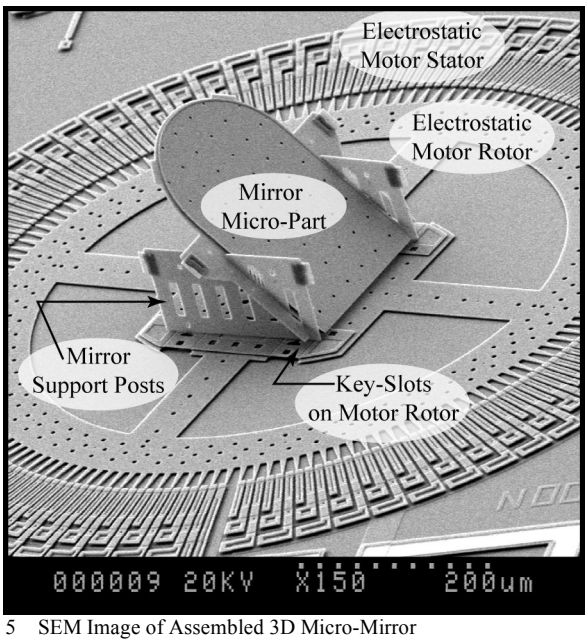

Fig. 5 SEM Image of Assembled 3D Micro-Mirror

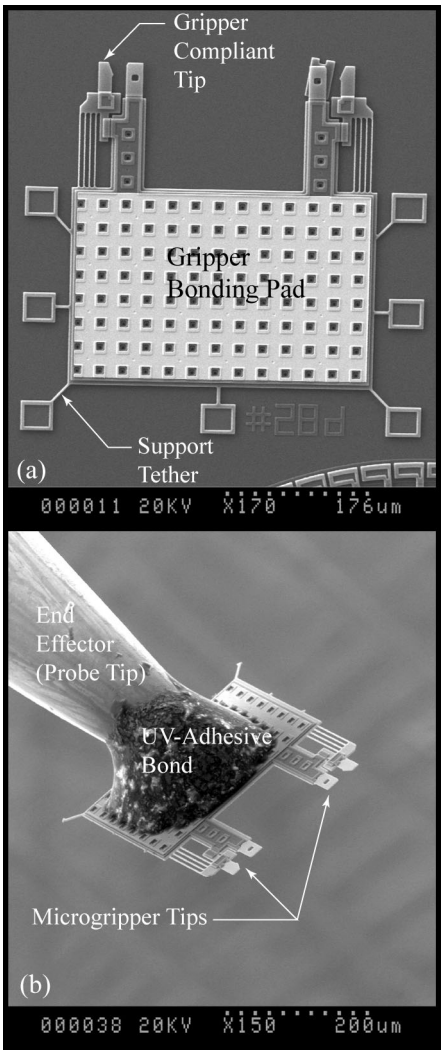

Fig. 4 SEM Image of Microgripper. (a) Microgripper on the Chip Substrate held by Tethers. (b) Microgripper Bonded with UV-Adhesive to the End Effector (Probe Pin) of the Micromanipulator.

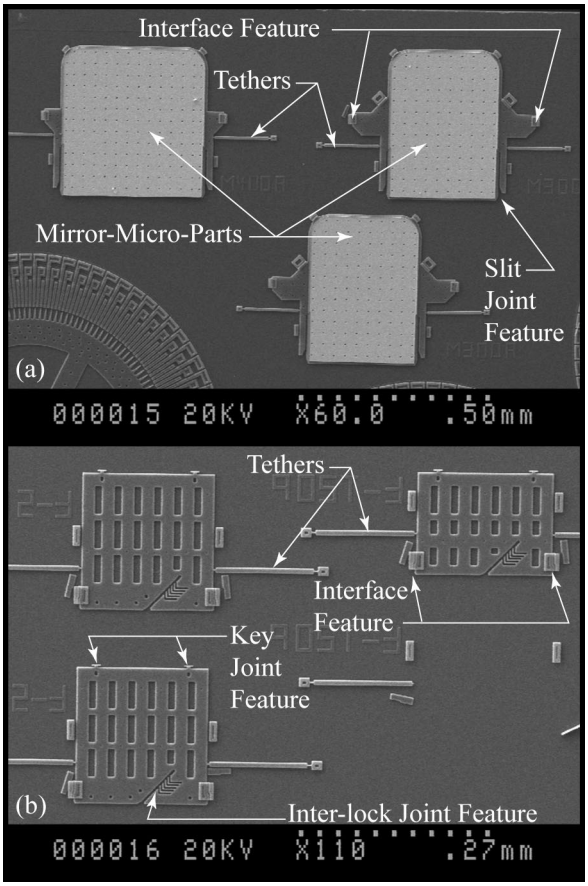

Fig. 6 SEM Image of Micro-Parts Secured to Substrate via Tether Features. (a) Micro-Mirror-Parts (b) Mirror Support Posts. Note the Interface Features to which the Microgripper Tips Mate with.

A. Grasping a Micro-Part

The first step in the assembly process is to grasp a micro-part by aligning the microgripper tips with the *interface feature* on the micro-part. Fig. 7(a) shows the microgripper tips positioned approximately 30 μm above the *interface feature* of the micro-part to be grasped. The depth of focus of the microscope system is only 1.5 μm, and the microscope remains in-focus with the microgripper tips at all times. Therefore, all other objects either closer to, or further from the focal plane will appear out-of-focus. The field of view of these images is 320 μm horizontally by 240 μm vertically. Fig. 7(b) shows the initial insertion of the microgripper tips into the *interface feature*. As the tips are inserted into the *interface feature* in the *x*-direction, they passively open outwards (*y*-direction). Fig. 7(c) shows the completed grasp. Note that although the micro-part is now grasped, it still remains tethered to the chip substrate.

B. Removing the Micro-Part from Chip

To remove the micro-part from the chip, force is applied in the *x*-direction, as shown in Fig. 7(d), to break the *tethers*. The deflection of the *tethers* can be observed in the image. The *tethers* have a narrow '*notch*' at each end to create a stress concentration point. The *tethers* are designed to break at these *notches* when 100 μN or more, is applied at the *interface feature* in the *x*-direction. Fig. 7(e) shows the micro-part after the first *tether* is broken. Continued motion in the *x*-direction will result in the break away of the second *tether*. Fig. 7(f) shows the released micro-part held by the microgripper approximately 30 μm above the chip substrate.

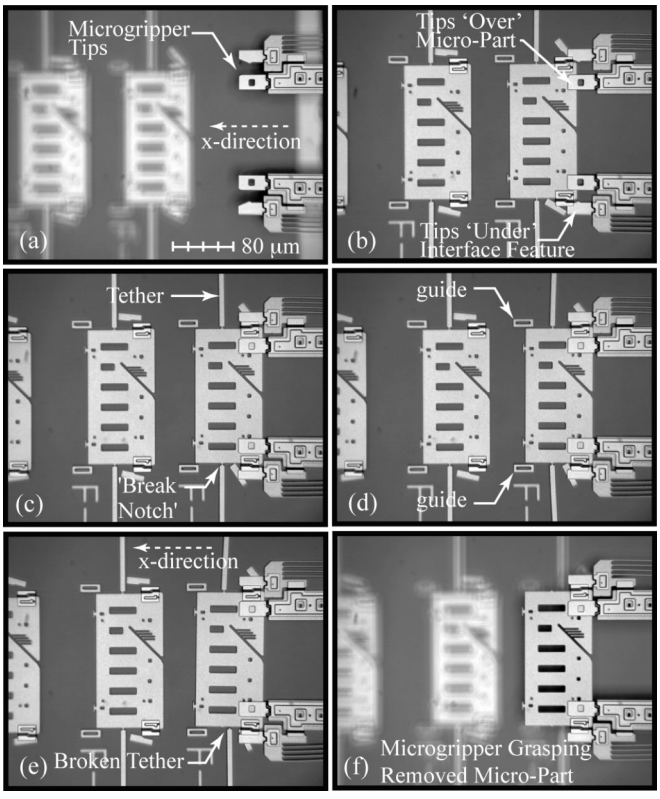

Fig. 7 Sequence of Video Images Showing the Grasp of a Micro-Part Equipped with a Standard *Interface Feature*, Using a Passive Microgripper.

C. Translating and Rotating the Micro-Part

The microgripper exerts a 'holding' force upon the micro-part it grasps, to keep it from shifting during manipulation. When the microgripper is in the rest position, as shown in Fig. 4(b), it has a space of 298 μm between the compliant (flexible) tips. The space between the 'grasp edges' of the *interface feature* on a micro-part is 302 μm wide, therefore, the microgripper tips are elastically deflected by 2 μm each, during a grasp. When designing the microgripper and the micro-parts, different interference values can be selected, allowing for suitable 'holding' forces for a particular application.

It can be seen from Fig. 7 that the micro-parts are grasped planar with the microgripper and with the chip substrate. In order to build the 3D micro-mirror, the micro-parts must be re-oriented and translated in various ways, to ensure that they are lined up with the joint feature they must be jointed with. For the *support posts*, they must be perpendicular to the *motor rotor* on the substrate (i.e. 90˚ to the substrate). For the *mirror-micro-part*, it must be perpendicular with respect to the interlock-joint axis on the *support post*, which is 45˚ to the substrate.

D. Joining Micro-Parts to other Micro-Parts

This work has developed a number of different mechanical joining strategies. These joint methods involve an interference fit between *joint features* on mating micro-parts, causing the joints to elastically deflect and push against each other. In combination with the effects of stiction, the resulting joints become very secure. For the 3D micro-mirror assembly, two different micro-joint systems are used. One is the 'key-lock' joint system and the other is the 'inter-lock' joint system, and both are illustrated in Fig. 8. The design details of these joint systems are provided in [3, 13]. The 3D micro-mirror shown in Fig. 5 consists of three micro-parts, which are two *support-posts* and one *mirror-micro-part*. Fig. 9 shows a sequence of video images showing the final assembly step to construct the 3D micro-mirror. This involves inserting the *mirror-micro-part* into the two *support posts*. Prior to this operation, the two *support posts* are key-lock joined into the *motor rotor* (this operation is not shown). The pre-assembled *support-posts* can be seen in Fig. 9(a) where the microscope is focused on their top edges. Fig. 9(a) also shows the microgripper grasping the *mirror-micro-part*, and holding it in an orientation parallel to the chip substrate, at about 90 μm above the substrate. This orientation is not suitable for the joint operation, and *mirror-micro-part* must be rotated so that it's plane is at 45˚ to the substrate.

Fig. 9(b) shows the *mirror-micro-part* re-oriented at 45˚ to the substrate. Due to the limited depth of focus of the microscopy system, the *mirror-micro-part* is out of focus, and appears as a dark blur, since the co-axial light from the microscope is not reflected back into the microscope. As a result, it can become difficult for the human operator controlling the micromanipulator to clearly see the *mirror-micro-part*.

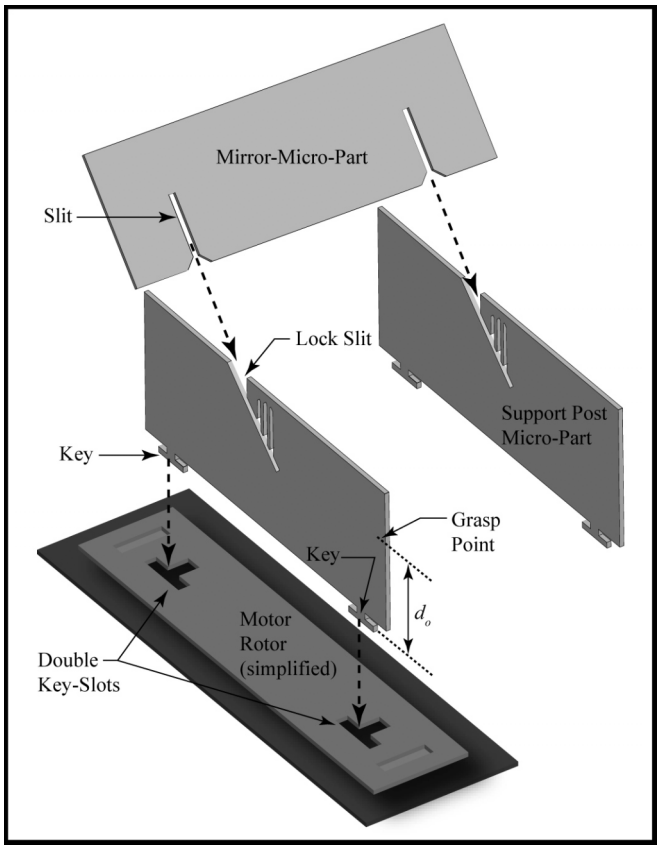

Fig. 8 Illustration of Key-Lock Joint and Inter-Lock Joint Operation

In order to properly insert the *mirror-micro-part* into the *support posts*, its position with respect to those *support posts* must be accurately localized. This is done with a touch-based and visual target-based calibration procedure, which relies on the digital encoders and high repeatability of the micromanipulator. After the localization procedure, the *mirror-micro-part* and the *support posts* are brought into alignment, as shown in Fig. 9(c), based entirely on the numerical localization data. The insertion trajectory vector is programmed into the robot (in this case a simple vector at 45˚ to the substrate), and the microgripper (holding the mirror-micro-part) is commanded to move along that vector. This joining procedure relies heavily on the initial calibration, and on the robot to maintain the insertion vector. Interestingly, it relies very little on the operator skill. The operator is indeed in the 'control loop', but only to the extent as to permit the robot to either 'advance' along the insertion trajectory, or to 'retract' along it. The operator visually watches for anything unusual during the joint attempt, that may indicate something is wrong. If that is the case, the joint attempt is aborted, the calibration procedure is performed again, and the micro-parts are re-aligned for another joint attempt. Fig. 9(d) shows the *mirror-micro-part* successfully inserted into the *support posts*, to form a double inter-lock joint.

E. Releasing the Assembled Micro-Part

Releasing a micro-part from the grasp of the microgripper is straightforward, as long as that micro-part has been joined to another object. After an inter-lock joint has been achieved, as shown in Fig. 9(d), the microgripper is retracted along a vector opposite to the initial insertion vector. This retraction causes the inter-lock joint to 'lock in' thereby securing the micro-parts together [13]. As a result, when the microgripper is retracted further from the *mirror-micro-part*, the microgripper tips 'self-open' and release the *interface feature* of the *mirror-micro-part*. At this stage, the 3D micro-mirror is complete.

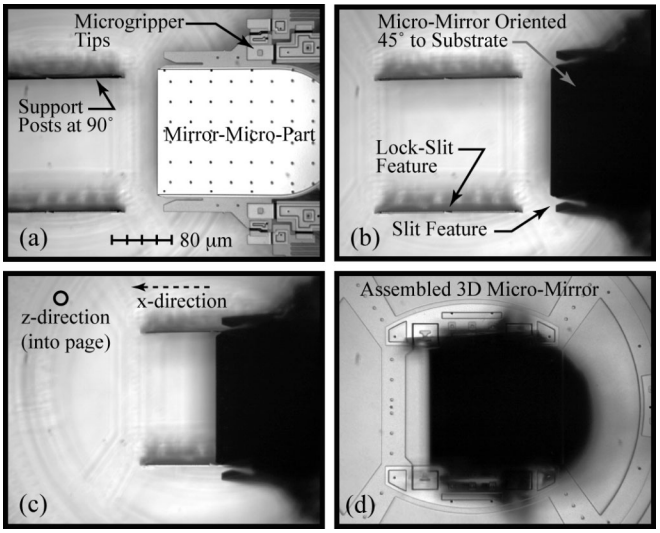

Fig. 9 Sequence of Video Microscope Images Showing the Process of Joining the Mirror-Micro-Part into Two Support-Post Micro-Parts

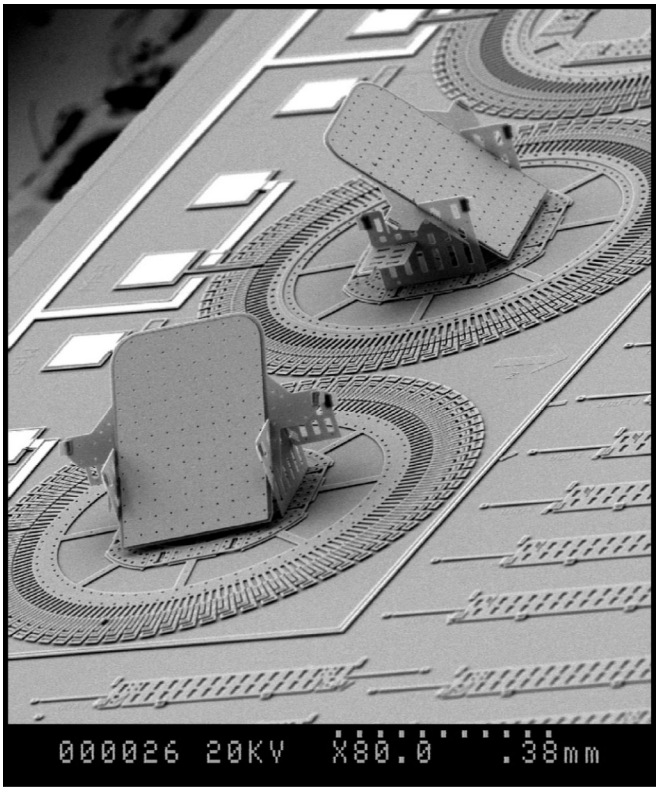

Fig. 10 SEM Image of Two Different 3D Micro-Mirrors, Assembled Side-by-Side in a Configuration Suitable for Optical Switching.

V. Experimental Results and Discussion

The microassembly process was applied to construct a working prototype of a 3D micro-mirror mounted onto an electrostatic micro-motor. In this regard, the experiment was a success in that 4 different mirror/motor devices were assembled [13]. Two of these designs are shown in Fig. 10, in a configuration suitable for optical switching. The more fundamental goal of the experimental microassembly work, was the development of new assembly techniques that could achieve the major objectives of this research, and expand the capabilities of the PMKIL (Passive Microgripper with Key and Inter Lock) microassembly system.

Prior to this work, the PMKIL microassembly system typically handled micro-parts from 60 x 60 μm to 200 x 300 μm in size. Since some of the micro-parts used for the 3D micro-mirror construction were larger than this, the microassembly system required the development of a few new assembly methods and a re-design of the *interface features*. This allows it to handle the bigger micro-parts and to account for some of the unique aspects of the 3D micro-mirror construction. However, the majority of the assembly steps, such as bonding the microgrippers, grasping the micro-parts or breaking the *tethers*, remained the same as those used to assemble other devices in the past.

The microassembly proceeded smoothly for most steps, however, a number of unique challenges were encountered when dealing with the 3D micro-mirror. These include (in order of importance): (a) limited depth of focus when joining micro-parts at oblique angles, (b) difficulty in creating key-lock joints with large micro-parts, (c) limited visual field of view when handling and joining large micro-parts, and (d) joining micro-parts onto a rotatable base (*motor rotor*) that can rotate slightly during assembly. These four challenges are specifically mentioned, since they will require future work to resolve/minimize them.

As can be observed in Fig. 9., any micro-part whose plane is at an angle of more than 2˚ to the substrate appears out of focus on the video images. As the angle of its plane approaches 90˚ to the substrate, the ability to discern features on the micro-parts becomes increasingly difficult with the video microscopy system. For this reason, when attempting to create an inter-lock joint, identification of the joint features, such as the *slit* and *lock slit* (compare Fig. 8 and Fig. 9(d)) was difficult. This in turn caused a difficulty in correctly aligning two micro-parts, prior to an inter-lock joint insertion attempt. In order to resolve this problem, a more effective video imaging system is required. A proposed system for future work involves the use of multiple microscopy cameras, to obtain images at different angles. Such a system will also require a interconnected software reference system, so that common reference points, with x, y and z position information, will appear on each video image. This will significantly help to achieve the correct alignment between micro-parts prior to a joining operation. This system will also aid in the development of automated visual identification techniques that can assist the human operator in target recognition.

Due to the increased size of the surface micromachined micro-parts for the 3D micro-mirror, the location of the *interface feature* (where the micro-part is grasped) on the micro-part becomes important. In the case of the key-lock joint system, it is important to keep the microgripper tips (which grasp the micro-part) as close as possible to the bottom edge of the micro-part where the key features are located. This is necessary for a smooth insertion of the *keys* into the *double key-slots*, in a single sliding motion, as illustrated in Fig. 8. The reason for this can be explained by observing the 'grasp point' indicated on Fig. 8. The microgripper holds onto the micro-part (via the *interface feature)* at the grasp point. The distance, d_o, indicates the distance from the grasp point, to a line that passes through both *key* features. In order to create a key-lock joint, after the *keys* are inserted into the wide region of the *key-slot*, the micro-part must be translated parallel to the substrate, so that the *keys* can slide into the narrow region of the *key-slot.* However, stiction and friction make it difficult for the *keys* to slide smoothly into the narrow region of the *key-slot*. In order to drive the *keys* into the narrow region of the *key-slot*, force is applied by the microgripper. When distance d_o is small (< 20 μm), this force is easily transferred, and the *keys* overcome stiction and friction, and slide into position. However, when d_o is large (> 30 μm), a moment is developed on the microgripper. Since the microgripper tips have some flexibility, they start to bend, rather than to drive the *keys* to slide into the narrow region. When dealing with the *support posts* used in the 3D micro-mirror, d_o is often 80 to 130 μm, or more. This makes it impossible to 'fully slide' the *keys* into the *key-slot*. As a result, an inefficient and time consuming two-step process had to be used during the assembly experiments, to assemble the *support posts* into the *motor rotor*. To prevent this problem in the future, the microgrippers tips must be re-designed to be (a) more rigid along the direction in which they apply the sliding force for key-lock joints, and (b) be designed to grasp micro-parts such that the distance d_o is at a minimum.

The field of view of the video microscope system is 427 μm horizontal × 320 μm vertical, with an optical resolution of 0.8 μm. However, the largest micro-parts handled and joined are over 400 μm wide. Since they are held in the vertical direction, both edges of the micro-parts cannot be viewed simultaneously. This complicates the grasping and joining procedures, since the camera must be moved back and forth (on its manual translation stage) to allow the operator to monitor the grasping and joining of large micro-parts. The solution is not as simple as using a microscope system with a larger field of view, because this can only be achieved at the cost of having a lower resolution. The resolution required for the joint features of this work must be at least sub-micron. Therefore, a suitable system to view large micro-parts, must be developed in future work.

One of the interesting and unique challenges of assembling the 3D micro-mirror is that the base micro-part (the *motor rotor*) is free to rotate. This means that during the assembly operation, if any forces are applied such that there is a net imbalance about the motor axis of rotation, the

motor rotor will rotate. Since the key-lock and inter-lock joints require translation with a direction component along the plane of the *motor rotor*, they needed to be designed to ensure that the net force created during assembly, would pass through the center of rotation, and thereby not rotate the motor. This is the ideal case, and would usually work in practice. However, there were a few cases were an initially small imbalance, due to an insertion that was not sufficiently aligned, or became out of alignment, would cause a small rotation, leading to a greater imbalance of force, leading to more rotation, etc… This situation could be corrected by aborting the joint attempt, re-aligning the micro-part by rotating the robot α axis, and trying again. However, for future work, it is worth investigating ways to restrain the rotating *motor rotors* during the assembly operation. Methods under consideration could be the use of *tethers*, that can be broken-away after assembly, or a temporary layer of material that could be deposited to secure the rotors, and could then be rinsed away after assembly.

VI. Conclusion

This work described the on-going development of a general microassembly system for constructing micro-systems. In particular, the assembly of a novel 3D micro-mirror has been described. A micromanipulator equipped with a microgripper was used to grasp micro-parts from the substrate of the chip. The micro-parts were then oriented at various angles to the chip, and joined together. By inserting the key features of the *support posts* into the *motor rotor*, key-lock joints were created. By lining up and inserting the slits of the *mirror-micro-part* into the lock-slits on the *support posts*, inter-lock joints were created. Together, these joints allowed for the construction of the 3D micro-mirror. Preliminary testing of the assembled mirror/motor MEMS device has shown good results [13]. It is important to note that since assembly is used, it is possible for the electrostatic motor, and the various micro-parts of the 3D micro-mirror, to be fabricated on different chips, by different fabrication methods. The robotic workstation would then be able to assemble all these components together. This creates various possibilities such as assembling bulk micro-machined mirror elements with gold coatings, onto surface micromachined devices. This would be useful in creating a flatter and more reflective mirror. The use of this microassembly system allows for many possibilities.

Acknowledgment

The authors wish to thank Prof. J. K. Mills and Prof. W. L. Cleghorn of the Department of Mechanical Engineering, University of Toronto, for providing access to the 6-DOF Robotic Workstation used to perform the assembly experiments described in this paper.

References

[1] D. Koester, A. Cowen, R. Mahadevan, and B. Hardy, "PolyMUMPs Design Handbook Revision 9.0", *MEMSCAP, MEMS Business Unit (CRONOS),* Research Triangle Park, N.C., USA, 2001.

[2] N. Dechev, W. L. Cleghorn, and J. K. Mills, "Tether and Joint Design for Micro-Components used in Microassembly of 3D Microstructures", *Proceedings SPIE Micromachining and Microfabrication, Photonics West 2004*, San Jose, CA, Jan 25-29, 2004.

[3] N. Dechev, J. K. Mills, and W. L. Cleghorn, "Mechanical Fastener Designs for use in the Microassembly of 3D Microstructures", *Proceedings ASME International Mechanical Engineering Congress and R&D Expo 2004*, Anaheim, California, Nov 13-19, 2004.

[4] N. Dechev, L. Ren, W. Liu, W. L. Cleghorn, and J. K. Mills, "Development of a 6 Degree of Freedom Robotic Micromanipulator for use in 3D MEMS Microassembly," *Proceeding of the IEEE International Conference on Robotics and Automation, (ICRA 2006),* Orlando, FL, May 2006, pp. 15–19.

[5] N. Dechev, W. L. Cleghorn, and James K. Mills, "Microassembly of 3D Microstructures Using a Compliant, Passive Microgripper", *Journal of Microelectromechanical Systems,* vol. 13, no. 2, Apr. 2004, pp. 176-189.

[6] G. Yang, J. A. Gaines, and B. J. Nelson, "A Supervisory Wafer-Level 3D Microassembly System for Hybrid MEMS Fabrications", *Journal of Intelligent and Robotic Systems*, vol. 37, 2003, pp. 43-68.

[7] M. A. Greminger, A. S. Sezen, and B. J. Nelson, "A four degree of freedom MEMS microgripper with novel bi-directional thermal actuators", *Proceedings of IEEE/RSJ International Conference on Intelligent Robots and Systems, (IROS 2005),* Edmonton, Canada, Aug 2-6, 2005

[8] K. Tsui, A. A. Geisberger, M. Ellis, and G. D. Skidmore, "Micromachined End-effector and Techniques for Directed MEMS Assembly", *Journal Micromechanics and Microengineering*, vol. 4, pp. 542–549, Jan 2004.

[9] D. H. Kim, K. Y. Kim, K. Kim, J. O. Park, "Micro Manipulation System based on Teleoperation Techniques" *Proceedings of the 32nd International Symposium on Robotics (ISR 2001)*, July 4-7, 2001.

[10] E. Shimada, J. A. Thompson, J. Yan, R. Wood, and R. S. Fearing, "Prototyping MilliRobots Using Dextrous Microassembly and Folding", *Proceedings of ASME International Mechanical Engineering Congress and Expo (IMECE / DSCD)*, Orlando, Florida, Nov. 5-10, 2000.

[11] M. Last, V. Subramaniam, and K. S. J. Pister, "Out-of-Plane Motion of Assembled Microstructures using a Single-Mask SOI Process", *International Conf. Transducers 2005*, Seoul, Korea, June, 2005.

[12] N. Dechev, W. L. Cleghorn and James K. Mills, "Design of Grasping Interface for Microgrippers and Micro-Parts Used in the Microassembly of MEMS," *Proceedings of the IEEE International Conference on Image Acquisition*, Chinese University of Hong Kong, Hong Kong and Macau, China, June 27–July 3, 2005.

[13] M. A. Basha, N. Dechev, S. Safavi-Naeini, and S. Chadhuri, "A Scalable 1xN Optical MEMS Switch Architecture Utilizing A Microassembled Rotating Micromirror", *IEEE Journal of Selected Topics in Quantum Electronics,* Vol. 13, No. 2, pp. 336-347, March/April 2007.

Robotic Self-Assembly at Small Spatial Scales

Ari Requicha

Gordon Marshall Professor of CS and EE
Director, Laboratory for Molecular Robotics
University of Southern California

http://www-lmr.usc.edu/~lmr

Supported in part by NSF Grants EIA-98-71775, IIS-99-87977, EIA-01-21141, DMI-02-09678 and Cooperative Agreement CCR-01-20778; and the Okawa Foundation

Advertisement

Submit high-quality nanorobotics papers to the

IEEE Transactions on Nanotechnology

http://www-lmr.usc.edu/~requicha/tnano

Ari Requicha, Editor in Chief

Dan Arbuckle

Outline

A New Manufacturing Paradigm

- Self assembly by a robot swarm
- Robot-constructed structures for direct use or as scaffolds or templates
- Identical robots, identically programmed, re-usable
- Fully distributed process, robust, tolerant to malfunctions
- Independent of spatial scale, but most attractive at micro and nano scales

- Issues addressed here:
  - What can be built?
  - Algorithms
  - Self-Repair, Self-Reproduction, Learning

Why Bother?

- Intellectually interesting
  - Emergence
  - Global vs. local behavior
  - Robustness
  - Adaptability in a dynamic environment
  - Distributed control
- Potential applications
  - Parallel process for manufacturing at the nanoscale
  - Establishing connections – building wires
  - Making scaffolds for electronics, bones, organs (program attachment sites for components of various types)

Related Work

- Robotic self-assembly: Nagpal; Klavins; Jones & Mataric; Arbuckle & Requicha
- Biological swarms: Bonabeau; Deneubourg; Dorigo…
- Passive self-assembly, esp. DNA
- Swarm robotics
- Reconfigurable robotics
- Networked robotics
- Distibuted robotics
- Cellular automata
- Self-replication

Could spend your life reading and get nothing whatsoever done…

Self-Assembly (A Massively Parallel Process)

- Passive
  - Driven by the environment: thermal agitation, surface tension, …
  - Symmetric structures, typically
  - For asymmetry may need patterning at the nanoscale (difficult)
  - Programmed in hardware
- Active
  - Use swarm of programmable agents (robots) to form a shape
  - Use robot-formed shape as the desired structure
  - Or as a template (e.g., for stamping)

Expected Limitations of Nanorobots

- One nanorobot will not achieve much – swarms are needed
- Small size
- Small computing power
- Small memory
- Low energy
- Short messages
- Communication only on contact or very close (chemical?)
- Collisions with environment objects

Assembly Agent Model

- Perform a random walk (environment)
- Grab and release neighbors
- Exchange messages with neighbors
- Store, look-up and execute reactive rules
- Increment and decrement a hop counter

Outline

- Introduction
- Finite-State Machine (FSM) Robots
- Reactive Robots
- Learning Robotic Self-Assembly Rules
- Conclusions

Active Self-Assembly

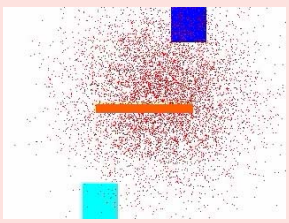

Arbuckle & Requicha (2004) *Proc. ICRA*, 896

Path Planning (1)

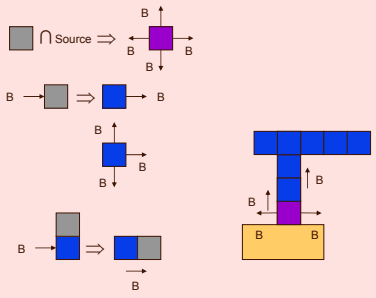

Path Planning (2)

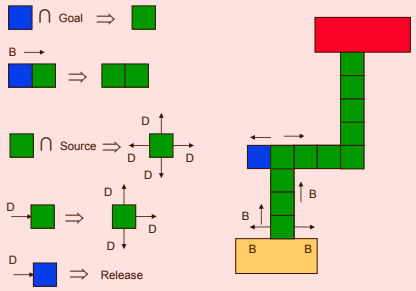

Building a Square (1)

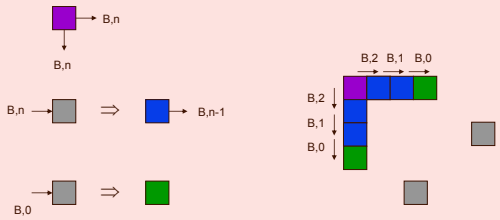

Building a Square (2)

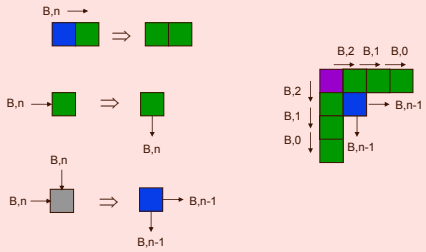

Making and Connecting Primitives

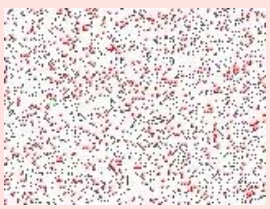

Building a Polygon Boundary

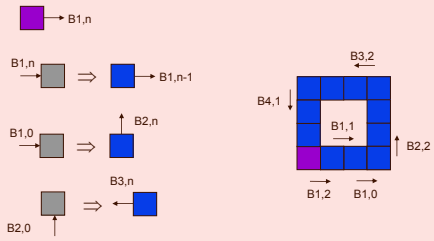

Building a Polygon Interior

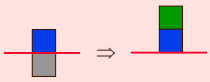

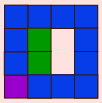

Random: Release and wander

Guided: Push boundary and interior agents

Building Polygons

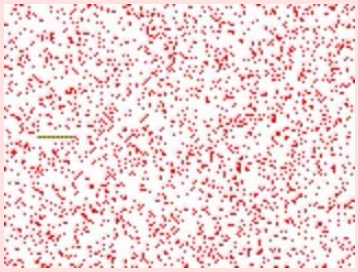

Arbuckle & Requicha (2004) *Proc. ISRA*, 173

Shape Restoration

- S_i is the unknown initial shape
- S_g is the desired goal shape
- S_i is a subset of S_g
- Build S_g by active self-assembly

Shape Restoration Example

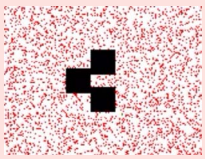

State Considered Harmful – An Example

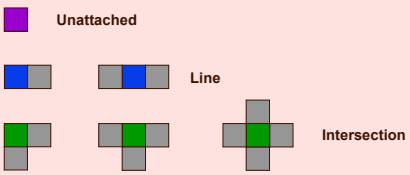

FSM

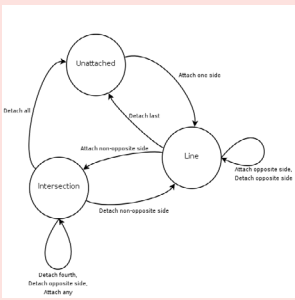

A Simple Construction

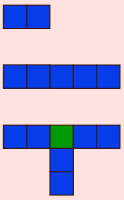

Attach Opposite Side * 3

Attach Non-Opposite Side
Attach Opposite Side

The Perils of State

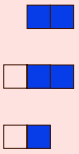

Faulty Sensor Info

Detach Opposite Side

Inconsistent State

Outline

- Introduction
- Finite-State Machine (FSM) Robots
- Reactive Robots
- Learning Robotic Self-Assembly Rules
- Conclusions

Reactive Self-Assembly (1)

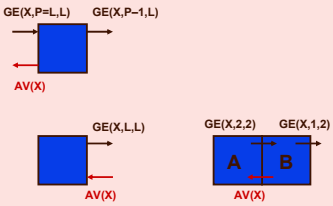

Reactive Self-Assembly (2)

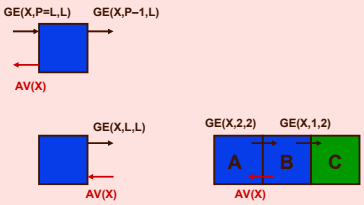

Reactive Self-Assembly (3)

Reactive Self-Assembly (4)

Reactive Self-Assembly (5)

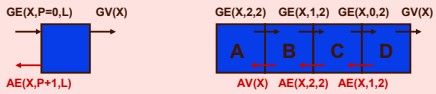

Reactive Self-Assembly (6)

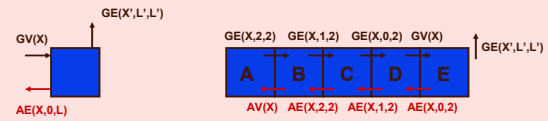

Reactive Self-Assembly (7)

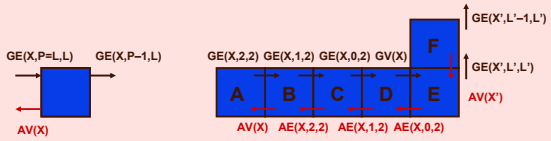

Reactive Self-Repair (1)

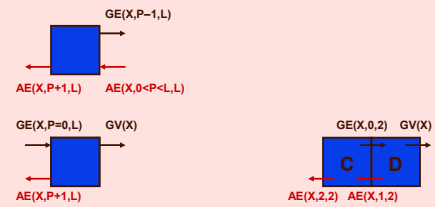

Reactive Self-Repair (2)

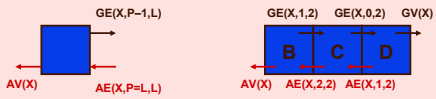

Self-Repair and "Reproduction"

Self-Assembly and Self-Repair of Structures

Partial growth of a structure, followed by it's being broken into three parts and the growth of each part into a complete version of the original target structure

Daniel Arbuckle
Aristides A. G. Requicha

Outline

- Introduction
- Finite-State Machine (FSM) Robots
- Reactive Robots
- Learning Robotic Self-Assembly Rules
- Conclusions

Copying a Structure- Learning

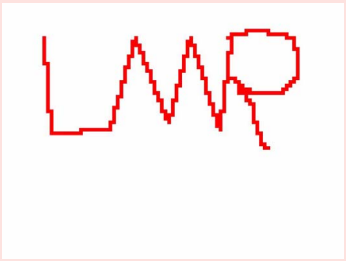

Copying a Structure - Building

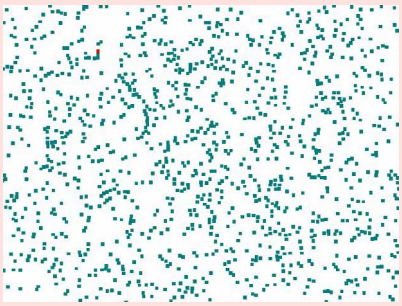

Outline

- Introduction
- Finite-State Machine (FSM) Robots
- Reactive Robots
- Learning Robotic Self-Assembly Rules
- Conclusions

Summary of Active Self-Assembly Results

- Very simple robots: small memory, simple execution mechanisms, few message types exchanged only when in contact, …
- Build various primitives: squares, rectangles, triangles
- Connect primitives in a simple manner
- Build wires (collision-free path planning)
- Restore shapes when the current shape is unknown
- Build arbitrary polygons
- Self-repairing structures
- Self-replicating structures (to a limited extent)
- Programs built automatically by "compiler"
- Reverse engineering built structures

Issues

- Theory?
- Physics-based simulation?
- Physical implementation
  - Nanoscale
  - Macroscale, with small numbers of robots and different Physics?
- Completion rates
- Positional uncertainties
- How characterize self-repair?
- How measure performance in a dynamic environment (robustness, adaptability, …)

Design of desktop micro-assembly machine and its industrial applications

Akihiro Matsumoto, *Member, IEEE*, and Kunio Yoshida

***Abstract*— We have been developing desktop micro-assembly machines for handling/assembling MEMS/optical components such as HDD head parts that are very small and fragile. We have achieved placement (positioning) accuracy of the micro-assembly machine up to 1 μm on the desktop with keeping relatively large working space, not by using rigid surface plate nor constant temperature room; the key to the solution is to introduce ideas and technologies of robotics. First, we introduce design considerations of the machine with careful mechanical design and fine vision measurement system, and we show the results of experimental evaluation of the machine. Next we explain several industrial applications of the micro-assembly machine, including solder ball handling. Last, we show our efforts on yet further improvement for the better placement accuracy.**

I. Introduction

The development of micro electronic/optical components such as micro sensor components, micro semiconductor devices, micro fiber optical components, micro laser diode components, or flying head components of HDD is becoming more and more active these days. Thanks to the MEMS technology, these products are made in good quality and in mass quantity. Nevertheless, the assembly of them are time consuming and thus expensive in the viewpoint of production cost. Historically, assembly has been always bottleneck to the progress of automation because of the complexity of the task. And micro assembly is not the exception.

We focused on the positioning accuracy around 1μm, where traditional mechanical engineering and micro/nano electrical engineering did not cover, but the very required accuracy for MEMS component assembly. In other words, the area between several 0.1μm to 1μm has been left undeveloped. In this view, we have been developing micro assembly machines that meet this demand [1]-[5]. One of the features of our machines is the target of positioning accuracy is achieved, yet keeping the large working space. One example is that accuracy is less than 1μm and the working stroke is 150mm. Moreover, this feature is obtained on normal desktop, by NOT using constant temperature room or heavy rigid plates. This is one step toward desktop factory [6]. Thanks to this feature, initial cost for the installation of the assembly facilities becomes very cheap, comparing to the traditional micro assembly machines.

Research on micro-assembly is increasing these days, and we are in the direction of sysnthesis side rather than the analysis side of the micro-assembly research. Researches in the similar direction have been done actively, for example [7]-[10].

In this paper, first we explain the design considerations of the desktop assembly machines, especially how we achieved the fine positioning accuracy. Next, we show one example of industrial application of micro solder ball handling. Last, we show our efforts on the further improvement for the better placement accuracy.

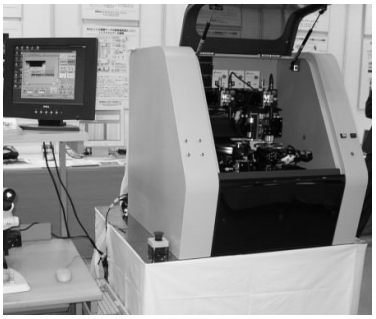

Fig. 1 Largest model of our assembly machines for bonding application

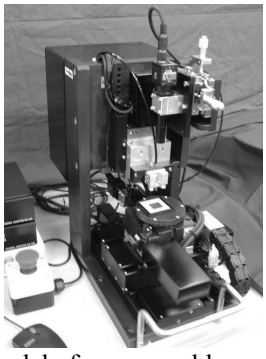

Fig. 2 Smallest model of our assembly machines (the size of the base area is about A4 paper size)

II. Outline of the Machine Design to Achieve Fine Accuracy

A. Design considerations

The first requirement is to realize desk top factory [6]. We

Manuscript received September 18, 2007. This work was supported in part by the city of Yokohama, the prefecture of Kanagawa, and The Electro-Mechanic Technology Advancing Foundation (EMTAF), Japan.

Akihiro Matsumoto is with the Department of System Robotics, Toyo University, Kawagoe, Saitama, 350-8585 Japan (corresponding author to provide phone: (+81) 49-239-1344; fax: (+81) 49-231-5026; e-mail: akihiro@eng.toyo.ac.jp).

Kunio Yoshida is with AJI Co. Ltd. (former name was Adept Japan), Yokohama, Kanagawa, 231-0001 Japan (e-mail: yoshida@ajisso.com).

want to use micro assembly machine in normal factory environment; in other words, without using big and heavy granite plate or air dumper, or without special room for constant temperature. Compact size yet high rigidity of the machine is the most important requirement.

Next requirement is to achieve fine positioning accuracy (target : 1μm) with keeping wide working space. 10nm positioning is really achieved by using Piezo actuators, but the working space (stroke) is very small, and use of Piezo is not suitable for this application. Vision technology and force control technology, which are normally used for industrial robots, could be used for this purpose.

The degrees of freedom (DoF) of the assembly machine are illustrated in Fig. 3. Basically, it has X-Y-θ table at the lower part of the machine, and X-Z axis motion in the upper part for traveling micro component to be assembled. The working space of this mechanism is relatively large (from 50mm to 150mm depending on the model) comparing to the size of the target parts (around 0.2mm × 0.3mm). The measuring resolution of linear encoder for each axis is 50nm, but of course, positioning accuracy is bigger than the resolution of encoders because of the stick-slip phenomena in this area of the size.

Consider the positioning accuracy of three dimensional measuring machines, for example. The values are generally ranging from 5μm to 10μm, and using constant temperature room with rigid base. The positioning accuracy of Industrial robots is worse than three dimensional machines or NC machining centers because of their structure. The positioning accuracy of industrial robots is ranging from roughly 10μm to 100μm depending on the structure. In this sense, the target accuracy 1μm by using the normal industrial machines seems to be difficult to achieve.

Thanks to our experiences of designing/installing industrial robot, we adopted to use relative accuracy instead of absolute accuracy. The relative accuracy of industrial robots, for example, is better than absolute accuracy; usually five to ten times better. Relative accuracy is usually called repeatability.

By the careful machining and good encoders, the absolute accuracy of the most positioning machines can usually be up to 20μm order. Of course, stress analysis by using CAE in the mechanical design stage is indispensable. Then, the repeatability can be, say, 1~5μm (of course, depending on the structure). But the further improvement is an unknown world in the common sense of traditional mechanical engineering. Nevertheless, if the size of the machine becomes smaller, the deformations of the machine are also small. This means that miniaturization of the machine itself is one key to the fine positioning accuracy.

Additionally, we decided to use vision system to improve positioning accuracy. If the both the target position and the current position are seen in the same area in the vision system, the positional error could be compensated by the sake of the repeatability of the machine. This idea is really effective after many evaluation experiments. Next point, which is also important, is the position of the measuring system, i.e. camera in our case. As shown in Fig.1 and Fig. 2, the camera is installed in the same framework of the machine, thus, the measuring system and positioning system do vibrate in the same frequency and phase, canceling the effect of the vibration of the whole of the assembly machine.

Plus, we adopted force control in placing the target parts to the substrate, since MEMS components are very fragile against external force.

In result, the key to the success of the fine positioning accuracy can be realized by

- the fine mechanical design and machining in order to miniaturize the size, yet to keep rigidity,
- use of vision measurement,
- use of force control.

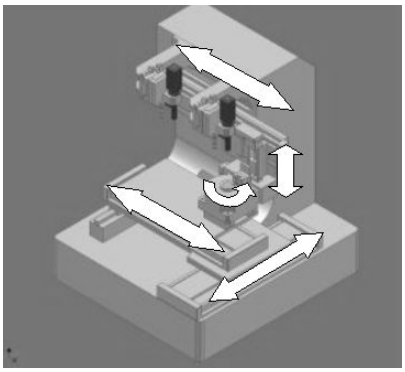

Fig. 3 Allocation of degrees of freedom (DoF)

B. The vision measurement subsystem

By seeing the working space by a camera, the positioning of the machine can be improved as long as both the current position and the target position are seen within the same camera area. This is called “vision servo” in our group as shown in Fig. 4. From the difference of the current position and the target position, the offset to be moved is calculated. Note that this process is done before the placement of the target part, and the part should be slightly over the submount that is position-controlled by X-Y-θ stage.

The image processing of the vision measurement is done by the special software HexSight® by Adept Technology (USA) and AJI (formerly adept japan), that uses special interpolation technique to improve sub-pixel resolution (theoretical maximum is 1/16 pixel). Normally the visible area is 1.6mm by 1.2mm, and the image memory size is 640 by 480 pixels (8bit greyscale) as shown in Fig. 5 and Fig. 6. Then 1 pixel is equivalent to about 3μm, but it becomes less than 0.1μm (theoretically) for the measuring accuracy by using the special interpolation technique in the HexSight®. The actual measurement accuracy is experimentally evaluated as to 0.1μm [1][2].

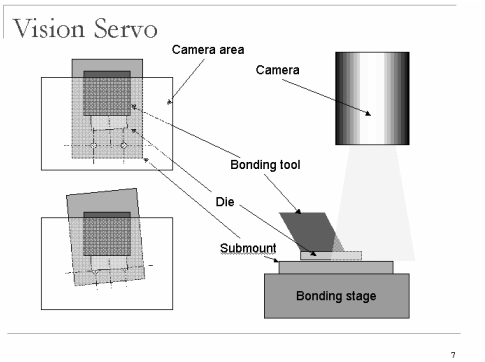

Fig. 4 Use of image processing for vision measurement in order to compensate positional error

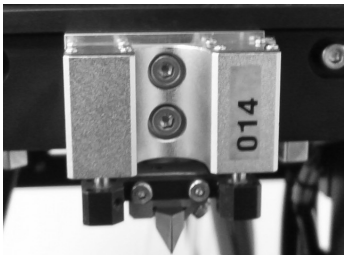

Fig. 5 Collet (lower part) suspended by force control unit (upper part) composed by air cylinder inside
(Target part is picked up by the edge of the collet in pneumatic way)

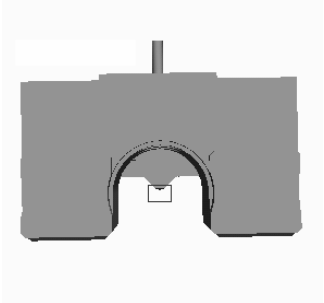

Fig. 6 Top view of the force controlling unit
(Note that the camera is mounted above the control unit, and the target view area of the camera is shown in rectangle)

C. *Force control*

The target micro parts are handled not by grasping but by picking by negative air pressure. Fig. 5 shows the handling device that is placed as the end effector of the assembly machine. This part can be replaced for other applications. The lower part of the collet is pushed or pulled by controlling the air pressure of the cylinders that are placed in the upper part of the force control unit (Fig. 5). The target micro parts are picked by the small hole that is placed on the edge of the lowest part of the collet. After the positioning improvement by vision processing, the target part is pushed on the submount using the positive air pressure control. Note that MEMS components or optical components are very fragile, so the pushing force for the placement is carefully designed.

III. SOLDER BALL HANDLING APPLICATION

Reflow soldering for joining electric components may replace wire bonding in industry, mainly because MEMS components are weak to vibration by wire bonding. For this purpose, we used this micro assembly machine, and adopted to use micro solder balls for joining. The diameter of the solder ball is 100μm at first, then 80μm.

Since handling only one solder ball for each circuit is not efficient, we decided to pick multiple solder balls at the same time. For this purpose, solder ball sheets are specially prepared [3][4]. Fig. 7 shows top view and side view of the solder ball sheet. Each solder ball is placed in the circular hole and stuck on the adhesive layer.

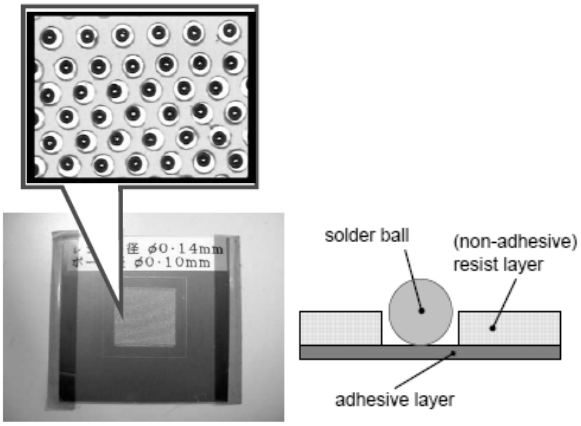

Fig. 7 Solder ball sheet (top view and side view)

As shown in the left side of Fig. 8, the position of each solder ball in the hole is random, aligning multiple solder balls is necessary for picking them up simultaneously. Since they are picked by "collet" using negative air pressure through nozzle of collet, we move this collet by the assembly machine in order to softly push solder balls for alignment. As shown in Fig. 6, the balls roll to the end of the hole, thus alignment is done. This motion is realized thanks to the fine positioning accuracy of the micro assembly machine. Fig. 9 is the photograph during alignment. The left of Fig. 9 is the situation before alignment, and the right of Fig. 9 is after alignment, which shows the good result of alignment experiment. We have experimentally evaluated the performance of this idea and reported in [3][4].

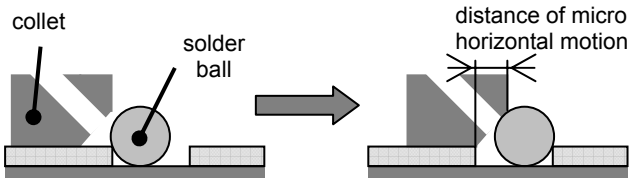

Fig. 8 Alignment of solder balls

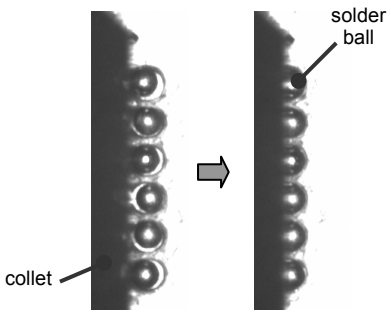

Fig. 9 The photograph of alignment of multiple solder balls

Since MEMS parts are often very weak on heat, the heating of solder must be carefully done. We used optical fiber and laser (suitable wavelength must be selected depending of the application) In one case, we used blue velvet laser (wavelength is 405nm which is suitable for heating gold) and target position where solder ball placed is heated upto 230°C, then the heat temperature distribution is shown in Fig. 10. This shows that the only the solder ball is heated and other area is not so heated. An example of the final quality of reflow soldering is shown in Fig. 11. Solder balls are well placed on the target positions. Fig. 12 is the cross section of solder in such case, and it shows quite good uniform condition.

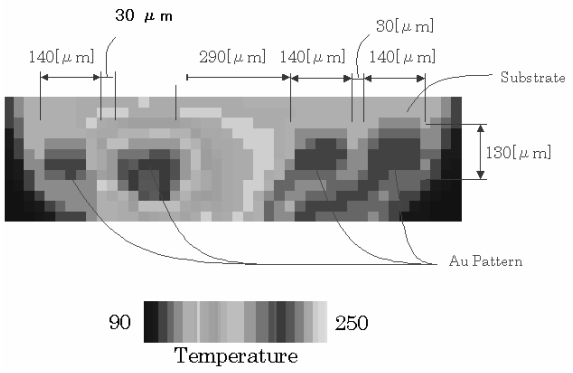

Fig. 10 Temperature distribution on substrate (temperature is expressed in °C)

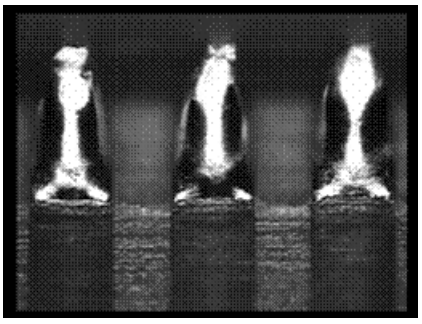

Fig. 11 Good result of reflow soldering

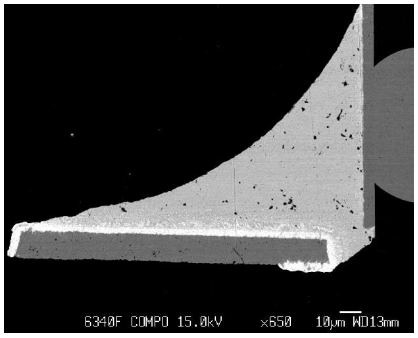

Fig. 12 The cross section of solder

IV. Efforts on Pursuing Better Accuracy

A. Positioning accuracy and placement accuracy

In the current industrial applications such as assembly (mounting) of HDD head parts, the accuracy around 1μm is enough. Nevertheless, from the manufacturers' point of view, we should continue to pursue better accuracy.

After the first installation of the machine to the factory floor, we realized that the positioning result is worse than the anticipated positioning accuracy. The differences are measured by using the vision measurement system on this machine and the result is shown in Fig. 13. This shows that the there are some phenomena that makes accuracy worse during pushing parts to submount, which must be analyzed. Currently we assume that the difference comes from the machine itself, non-linearlity of the force control unit, the assembly process, or others.

Thus, we call this accuracy as "placement accuracy" instead of positioning accuracy from now on. Note that placement accuracy is the result of the assembly (placement).

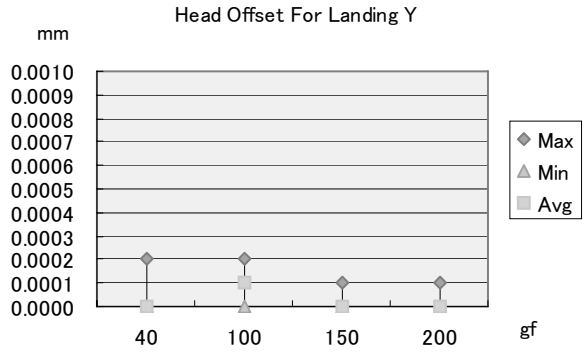

Fig. 13 Head offset in landing

B. Verification of vision measurement

Fig. 14 shows the experimental results of the vision measurement of the stable object after 100 times trial. The value should be zero in theory, but the result data are stochastic. In this case, the standard deviation is 0.04μm for X axis, 0.03μm for Y axis, and 0.03 milli-radian for θ axis.

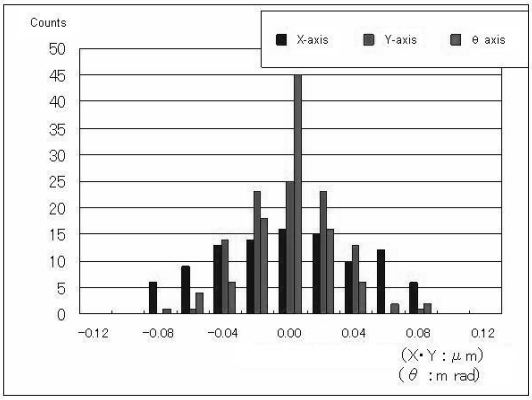

Fig. 14 Result of the vision measurement of the stable object (the deviation must be zero, but σ is 0.03μm (30nm))

If we use this kind of barrier/shield, we expect that the vision measurement accuracy improves, and this result shows that air flow fluctuation between camera and the target affects the vision measurement. Then, we made experiments on whether the air flow fluctuation can affect the result of the vision measurement. Fig. 15 shows the experimental result when the workspace is covered with a fence. This result shows that vision measurement and positioning accuracy is much better than before, and the air flow turbulence can not be neglected any more.

Note that the theoretical measurement accuracy is less than 0.1μm, which is smaller than the wavelength of the visible light. It seems that we have come to the extreme of the vision measurement and the result is affected by inflection of light.

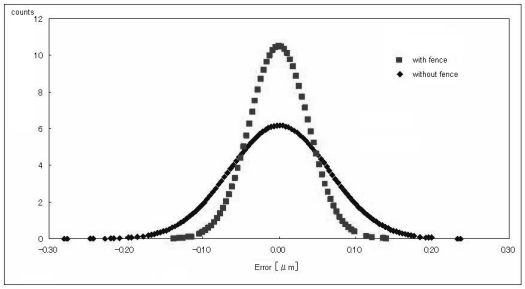

Fig. 15 The effect of fence around the workspace (air flow affects the vision measurement accuracy)

Next, instead of fence surrounding the machine, we put different sizes of transparent shield (5mm, 20mm), and/or paper tube (barrier) in order to avoid the effect of air turbulence (even if it is small) to the vision measurement, i.e.

1. normal FCU (force control unit) only
2. FCU + 5mm shield
3. FCU + 20mm shield
4. FCU + 20mm shield + paper tube

Transparent shield is a kind of fence and is used in order to that the target part is seen from the camera. Then heater is placed below the working space up to 400°C.

The outline of the experiment is shown in Fig. 16. The effect of such barrier against air turbulence between camera and working space is experimented, and the result is shown in Fig. 17.

As the 'barrier' for the air flow becomes bigger, the standard deviation of vision measurement becomes small. This effect is much remarkable when the heating temperature rises. These experiments show that protecting 'the way of light' between camera and the working space from external air flow is very effective for this fine vision measurement.

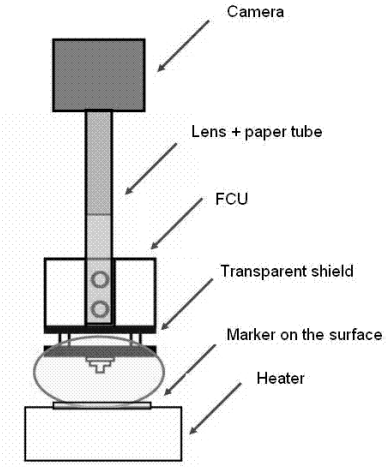

Fig. 16 Experiment to exclude air turbulence (several types of shield/barrier is placed and tested)

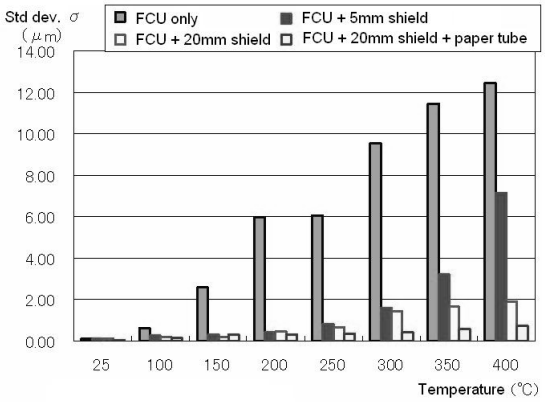

Fig. 17 The effect of different shields/barrier to the vision measurement (the effect of shield/barrier becomes bigger when the heating temperature rises)

C. Verification of mechanical structures

Next we checked whether mechanical alignment of the assembly machine itself can affect the positioning accuracy. By some adjustment of the orientation of end effector, around X-axis and Y-axis as shown in Fig.18, the result of the positioning errors are measured by using different FCU (force controlling unit).

By using the vision measurement system, the positions of the collet are measured when it is pushed onto the glass plate in 400gf of force (the air pressure of the force control unit is 0.1MPa). This is assumed that some target part is pushed onto the base where glue is inserted between the base and the part.

This experiment is repeated by changing the value of force to 200gf and 50gf.

Fig. 19 (a) and (b) shows the result for different FCU. Both shows the nice repeatability (relative accuracy) for the same force values, but shows different absolute accuracy for different force values. The is the normal results of absolute accuracy and relative accuracy. The result also shows the different performance for different force control unit. This experiment shows that the careful calibration is necessary and effective. But, as a whole, the results show that mechanical alignment of the assembly machine itself does not so much affects the final placement accuracy. Thus, although the careful adjustment of the machine alignment is necessary, it affects little to the placement accuracy.

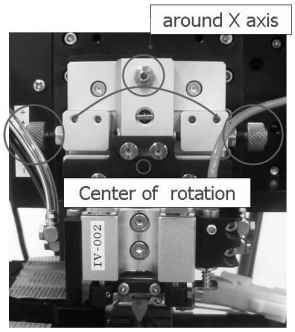

Fig. 18 Adjustment of mechanical alignment

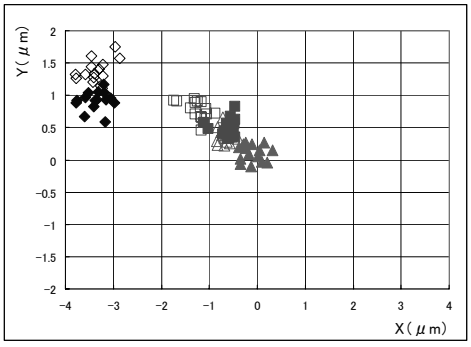

(a) FCU-A

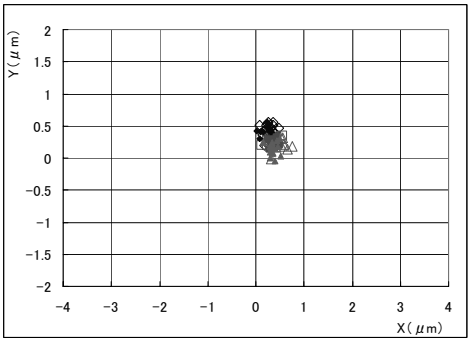

(b) FCU-B

◇ 50g □ 200g △ 400g adjustment for 400gf only

◆ 50g ■ 200g ▲ 400g adjustment for all forces

Fig. 19 Check of placement accuracy for different FCU (Force Control Unit) showing the nice repeatability

V. Conclusion

We showed the design considerations on micro-assembly machine how the fine positioning is achieved. Many ideas including repeatability, vision and force control is applied for assembly machine for the better accuracy. Next we explained the experiment on the multiple solder ball handling application. Last we showed our efforts on the better accuracy. As a whole, we have feeling that the placement accuracy can be a little better, say 0.7μm, but area beyond 0.5μm is another world where knowledge of micro-physics must be incorporated and experimentally evaluated.

Acknowledgment

The authors would like to thank Prof. Yusuke Maeda, Mr. Satoshi Makita, and Mr. Tatsuya Kobayashi at Yokohama National University, Japan, for their advices and efforts on experiments. Also, they would like to thank all AJI members who joined in this activity.

References

[1] K. Yoshida, H. Inoue, K. Kamijo, A. Matsumoto, T. Akimoto: "Design of microchip bonder to meet accurate MEMS-component assembly", Proc. of 6th Japan-France Congress on Mechatronics, pp.613-618, Hatoyama, Sep. 2003.

[2] A. Matsumoto, T. Akimoto, K. Yoshida, H. Inoue, K. Kamijo: "Development of MEMS component assembly machine - application of robotics technology to micromechatronics", Proc. of International Symposium on Micro-Mechanical Engineering, pp.83-88, Tsuchiura, Dec. 2003.

[3] T. Kobayashi, Y. Maeda, S. Makita, S. Miura, I. Kunioka, K. Yoshida: "Manipulation of micro solder balls for joining electric components", Proc. of 2006 Int. Symposium on Flexible Automation (IFSA), pp.408-411, Osaka, Jul. 2006.

[4] A. Matsumoto, K. Yoshida, I. Kunioka, Y. Ozawa, S. Miura, Y. Maeda, T. Kobayashi: "Handling and heating problems of micro solder balls for micro assembly", Proc. 5th International Workshop on Microfactoris, Besançon, S3-2, Oct. 2006.

[5] A. Matsumoto, K. Tsuiki, S. Miura, K. Yoshida: "Experimental study of improving the positioning accuracy of micro assembly", Proc. of the 1st CIRP-International Seminar on Assembly Systems (ISAS), pp.55-60, Stuttgart, Nov. 2006.

[6] Y. Okazaki, N. Mishima, K. Ashida: "Microfactory – concept, history and developments", Journal of Manufacturing Science and Engineering, Vol. 126, No. 4, pp. 837-844, 2004

[7] T. Eriksson, H. N. Hansen, A. Gegeckaite: "Automated assembly of micro mechanical parts in a microfactory setup", Proc. 5th International Workshop on Microfactoris, Besançon, S2-2, Oct. 2006.

[8] Q. Zhou: "More confident microhandling", Proc. 5th International Workshop on Microfactoris, Besançon, S3-1, Oct. 2006.

[9] S. Perroud, A. Codourey, Y. Mussard: "PocketDelta: a miniature robot for micro-assembly", Proc. 5th International Workshop on Microfactoris, Besançon, S2-2, P3-5, Oct. 2006.

[10] J. Bert, S. Dembélé, N. Lefort-Piat: "Toward the vision based supervision of microfactories through images mosaicing", Precision Assembly Technologies for Mini and Micro Products, Springer 2006.

A Microassembly System with Microfabricated Endeffectors for Automated Assembly Tasks

F. Beyeler, M. Probst and Bradley J. Nelson

***Abstract*— For the fabrication of complex sensor and actuator systems, hybrid MEMS devices are gaining importance. While the manufacturing of the 2.5D building blocks are performed by standard microfabrication processes, microassembly techniques are required for building hybrid devices. This work presents the mechanical design and the vision system of a six-degrees-of-freedom microassembly station. Additionally, two types of microfabricated end-effectors are presented. The first is a force sensing micro probe and the second a microgripper with force sensing capabilities.**

I. Introduction

There is a growing interest in MEMS devices that are built by assembling individual microcomponents. A strong motive for microassembly is the demand for hybrid MEMS that can combine incompatible materials or manufacturing processes (e.g. CMOS, MEMS). Microassembly can also overcome the planar, 2.5D shape limitations of standard MEMS manufacturing processes and create complex 3D geometries [1]. In addition, microassembly can increase the overall yield as the number of layers and manufacturing steps grow for a complex device.

The majority of robotic assembly operations in the macroworld rely on accurate robots that play back recorded motions. However, this form of open-loop manipulation is not suitable at the microscale due to the increased precision requirements and the vastly different mechanics of manipulation. While gravity is the dominant force in the macro domain, electrostatic forces, surface tension effects due to humidity and intermolecular Van der Waals forces become dominant at the microscale and act as external disturbances to the microassembly process. Closed-loop control through computer vision feedback has been applied to overcome some of these problems. A large number of microassembly systems for various applications have been developed over the past few years. They can be classified as parallel microassembly, self–assembly and serial microassembly systems [2] [3]. The aid of computer vision has proven to be a robust method for coping with high precision requirements and vastly different physics governing part interactions at the microscale and some interesting work can be found in [1] [4] [5] [6].

Micromanipulation of micron-sized parts requires the use of miniaturized end-effectors on the size-scale of the manipulated objects. Another requirement is that they allow the controlled application of a force during the assembly process.

Reliable force sensing is an important objective in microrobotics [7, 8]. Most of the time micromanipulations are performed under control of cameras or an optical microscope. Often sensor feedback is only given by the means of optical measurement, thus leading to a lack of information about the interaction forces between the endeffector and the micro-components [9]. In order to avoid breaking or damaging objects during the manipulation processes, force feedback is important for a proper functionality. The forces dominating micro-manipulations are in the range of tens of nano-Newton (10^{-9}N) up to several micro-Newton (10^{-6}N) [10, 11].

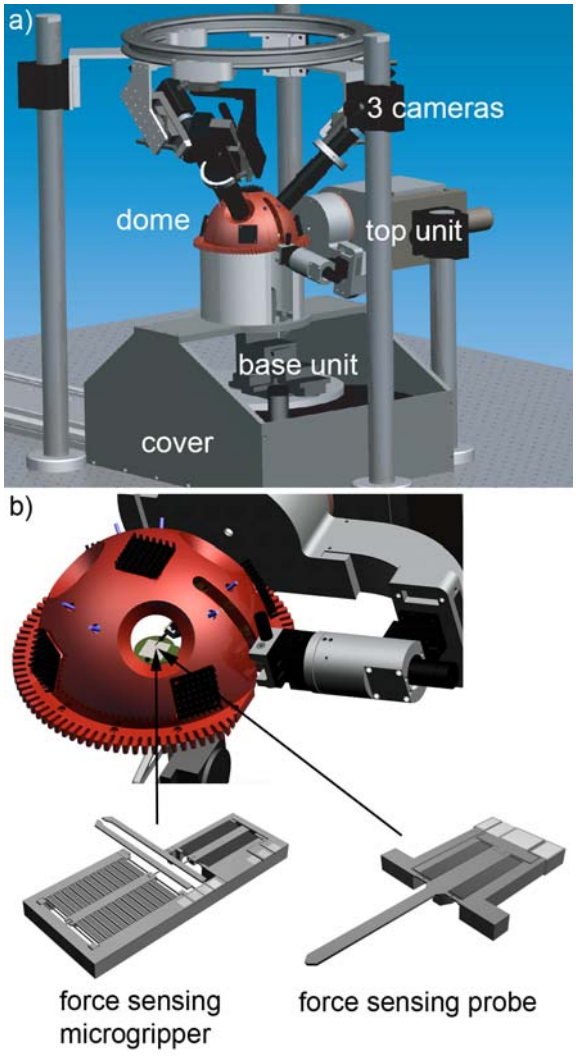

Figure 1: CAD model of the microassembly system with microfabricated end-effectors

This work demonstrates the conceptual design of a six-axis microassembly station. A short description of the mechanical system and the vision system is given. Two types of microfabricated end-effectors are presented. The first is a force sensing probe for electro-mechanical measurements and the second a force sensing microgripper. Both tools can easily be mounted on the micro assembly station. We believe that force feedback will significantly increase the reliability of automated microassembly processes.

II. Mechanical Microassembly System Design

The microssembly system presented here is based on a previous system also built at IRIS three years ago [12]. A large number of experiments and input from different users lead to the final design shown in Figure 1. The current system consists of a base unit, a top unit, three camera units as well as a cover that holds the illumination dome. The kinematic setup can be seen in Figure 2. The base unit consists of a robust and precise rotation table (θ-axis) with an integrated slip ring that transmits 36 electrical wires and 2 pneumatic/vacuum lines and therefore allows full 360° rotation in both directions. On top of the rotation table there is an xyz-stage (Sutter MP-285) with the working table attached to its end. The working platform has a diameter of 28mm and a square microfabricated insert with a side length of 15mm with fixtures in the shape of holes where microparts of different sizes can be docked. A vacuum applied on the lower side of the insert ensures constant airflow through the holes and helps releasing parts from the gripper (see Figure 3).

The top unit defines a kinematic chain of two rotational axes η and ζ at a 90° angle which are both driven by a combination of DC motors and Harmonic Drives in order to minimize backlash. The end-effector at the end of the upper arm is of a modular design and allows changing tools with minimal effort. The base as well as the top unit are each mounted on additional translation stages which allow movements in the x-direction and the y-direction respectively. Both axes are used for calibration, i.e. to create a remote center of motion (RCM) at the tool center point (TCP). For that reason, two lasers are mounted creating a focused laser beam intersecting at the desired RCM point.

Table I: System Performance

Axis	Range	Type	Resolution	Speed
xyz	+-12.5mm	Stepper	40nm	2.9mm/s
θ	360°	DC	0.010°	80°/s
η	-45°- +60°	DC	7.8E-5°	47°/s
ζ	+-90°	DC	0.002°	540°/s
c_x	25mm	manual	10µm	-
c_y	656mm	DC	1.66µm	231mm/s
d_x, d_y	6.3mm	manual	0.8µm	-
e_x, e_y	6.3mm	manual	0.8µm	-

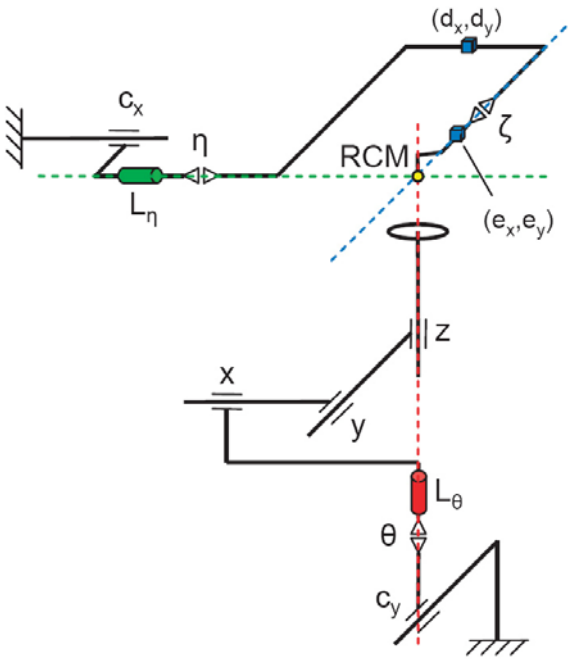

Figure 2: Kinematic chain

Table I shows a complete list of the performance of all axes. The present microassembly system requires a space volume of 1220x620x670mm and as mounted on a vibration isolated optical table. The absolute workspace has the shape of a cube with a side length of 25 mm.

III. Lighting and Vision System

The precision of microassembly is strongly dependent on the performance of the vision system that provides a clear image for the user as well as for the auxiliary computer vision modules. Three IEEE 1394 cameras (Basler A602fc) with variable zoom microscope lenses (Edmund Scientific VZM-300i) are equally spaced around the center at a 45° angle to the horizontal plane. This configuration maximizes the visual resolvability [13] and guarantees that for any given position of the gripper there are always two non occluded views. Depending on the magnification requirements, the lenses can be easily replaced by a different model

The illumination system (Figure 4) has been completely redesigned and consists of three modules. The central part is the aluminum dome with a coated inner side to provide a diffuse ambience on the working platform. The section plane of the dome contains a circuit board with 12 high power LEDs facing upwards to the inside of the dome and thus creating a strong diffuse illumination. The dome itself is equipped with a spotlight perpendicularly facing down to the center of the hemisphere and 4 spotlights equally spaced around the center axis. All LEDs are triggered in sync with the camera shutter (30Hz) which allows operating them at higher intensity at minimal heating.

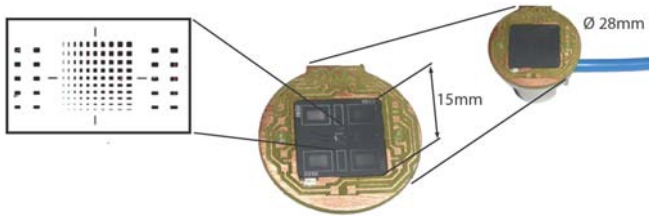

Figure 3: Workbench

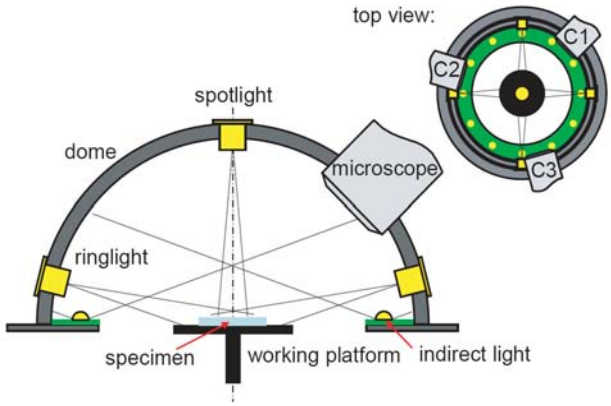

Figure 4: The illumination system inside the dome

The LEDs can also be controlled and dimmed individually which is a convenient feature when working with microparts of various reflections. Capturing one image at each light cycle yields four images each showing different shadows of the parts. The combination of those images results in a depth image [9] that provides a much more intuitive view of the scene and is also used as a basis for image processing tasks. The illumination dome also contains holes for 6 UV LEDs that are used for curing UV activated glue. This setup provides extremely bright illumination and allows closing the apertures of the lenses to a minimum which increases depth of field.

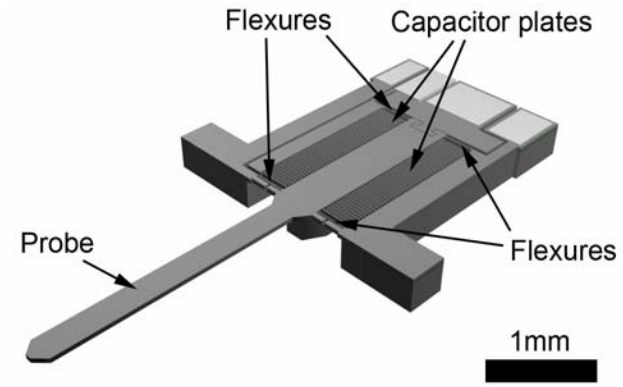

Figure 5: Microfabricated MEMS force sensing probe

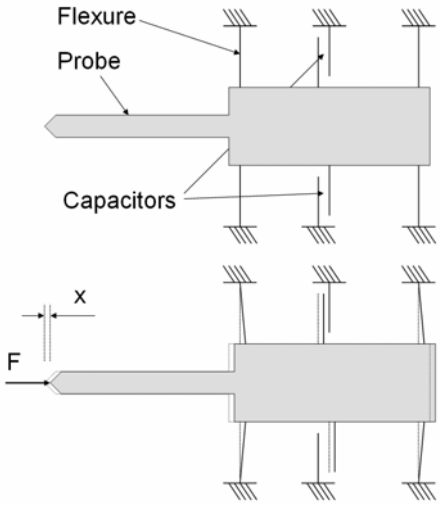

Figure 6: Force sensing principle

IV. Force Sensing Probe

Figure 5 shows a solid model of the force sensing probe. The force sensor dimensions are 8.5mm x 2.6mm x 0.45mm. The device is based on the capacitive force sensing principle. This type of sensor has successfully applied in micromanipulation and biological research [14, 15]. The sensor basically consists of three parts:

- a 3mm long probe on which the force is applied
- a set of flexures which convert the force into a deflection
- an array parallel plate capacitors which convert the deflection into a change of capacitance

The range of the sensor is chosen by the stiffness of the sensor. For an applied force F the deflection x is given by

$$x = \frac{F}{k} \tag{1}$$

where k is the stiffness of the flexures. Four flexures are used in this sensor design having a total stiffness of about 600N/m. The capacitance C of the parallel plate capacitors is given by

$$C = n \cdot \varepsilon \frac{A}{d + x} \tag{2}$$

where n is the number of capacitor electrode pairs, ε is the permittivity of air, A the area of the capacitors and d the initial gap of the capacitor plates. For the given design the zero-load capacitance is 2.0 pF. A differential configuration of two capacitors on a single force sensor has been realized as shown in figure 6. This design creates a linear relationship between the applied load F and the capacitance difference *as* shown in [15].

The force sensing probes are fabricated by micromachining of silicon wafers. This highly parallel wafer level process allows the cost efficient fabrication of a large number of devices. The fabrication sequence is illustrated in figure 9.

A) A silicon-on-insulator wafer with a device layer of 50µm, a handle layer of 400µm and a buried SiO_2 layer of 2µm is used for the process.
B) A 1.5µm layer of SiO2 is deposited on the wafer backside and patterned using reactive ion etching (RIE).
C) The backside silicon is etched using deep reactive ion etching (DRIE). After etching 200µm, the SiO_2 patterned in step B is removed. Then the remaining 200µm of silicon is etched. The buried SiO_2 acts as an etch stop. This procedure creates the step of the thickness of the handle layer. The buried SiO2 is etched using RIE.
D) 250nm of aluminum is evaporated and patterned by etching the metal to create the pads for wire-bonding.
E) The SOI wafer is mounted on a silicon support wafer. The device layer, including the flexures, comb drives and gripper arms are etched using DRIE dry etching. By etching a border around the device it is released onto the support wafer below the SOI wafer.

To make electrical contacts to the capacitor electrodes and to mount the device on the microassembly system, the device is glued directly onto a printed circuit board (PCB). Right next to the sensor a capacitance-to-voltage converter is located which generates an analog output signal (0-5V). Figure 7 shows the PCB with the wire-bonded micro force sensing probe. The size of the PCB is 36mm x 12.5mm.

The specifications of the force sensing probe are given in table II. The individual force sensing probes are calibrated with a reference force sensor. A good linearity can be observed for the full range of +-2mN as shown in figure 8.

The probe is electrically conductive and electrically insulated from the rest of the sensor. The probe can therefore be used as an electrical probe as well. This is useful for electro-mechanical characterization or making electrical contact to the object to be manipulated.

TABLE II: FORCE SENSING PROBE PERFORMANCE

Full range:	+-2500µN
Sensitivity:	1000µN/V
Full range output:	0-5V
Resonance frequency:	3200Hz
Resolution @ 3000Hz:	5.0uN
Resolution @ 30 Hz:	0.3uN

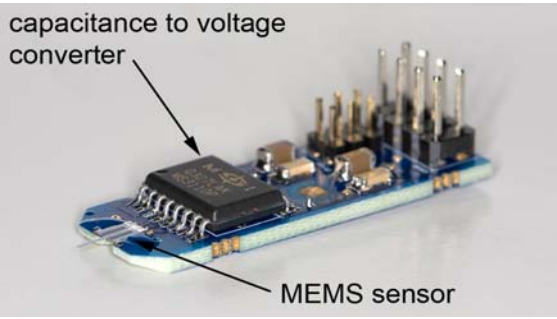

Figure 7: MEMS sensor mounted on printed circuit board

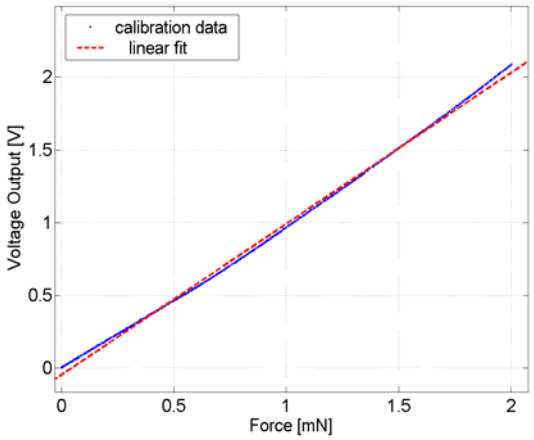

Figure 8: Sensor calibration curve

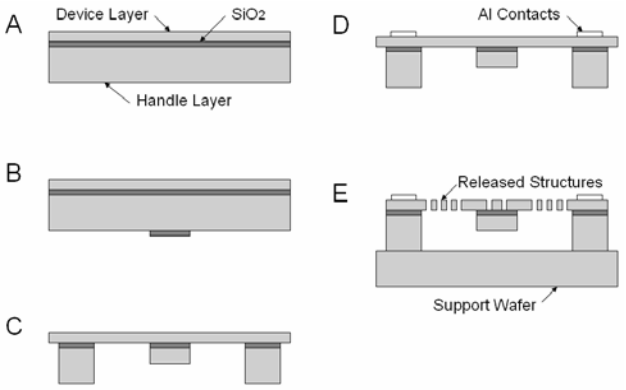

Figure 9: MEMS fabrication sequence

V. FORCE SENSING MICROGRIPPER

For the manipulation of parts with a size up to 200µm a microgripper has been developed as shown in figure 9, based on the design presented in [16]. Different types of gripper arms have been designed with an initial opening ranging from 30µm up to 200µm as shown in the insets a)-d) of figure 9. The gripper size is 7.7mm x 5.6mm x 0.45mm.

The gripper consists of two main parts. First is an electrostatic actuator for actuating the left gripper arm (figure 10). The second part is a capacitive force sensor similar to the force sensing probe described in the foregoing chapter. When gripping an object, the right gripper arm is moved to the right. This deflection is sensed by the capacitive force feedback sensor.

A lateral comb drive is used which is described in more detail in [9] is used for electrostatic actuation. The force F_a generated by the lateral actuator comb drive is

$$F_a = n_a \cdot \varepsilon \cdot \frac{t \cdot V_a^{\,2}}{d_a} \qquad (3)$$

where n_a is the number of electrodes in the comb drive, t the thickness of the comb drive arms and V_a the actuation

voltage. The actuation force is proportional to V_a^2. The restoring force for opening the gripper arms is generated by four elastic flexures.

Different flexure designs (straight and folded) are used as shown in figure 9e) and 9f). The folded flexure design results in larger deformations but smaller restoring forces of the gripper arm. A maximum of 200V can be applied to the gripper arms. The deflection by the comb drive (25µm) is amplified by a factor of four by the gripper arm geometry which results in a stroke of 100µm.

The same fabrication process which has been used for the force sensing probe is also used for manufacturing microgrippers. Table III gives an overview of the microgripper performance.

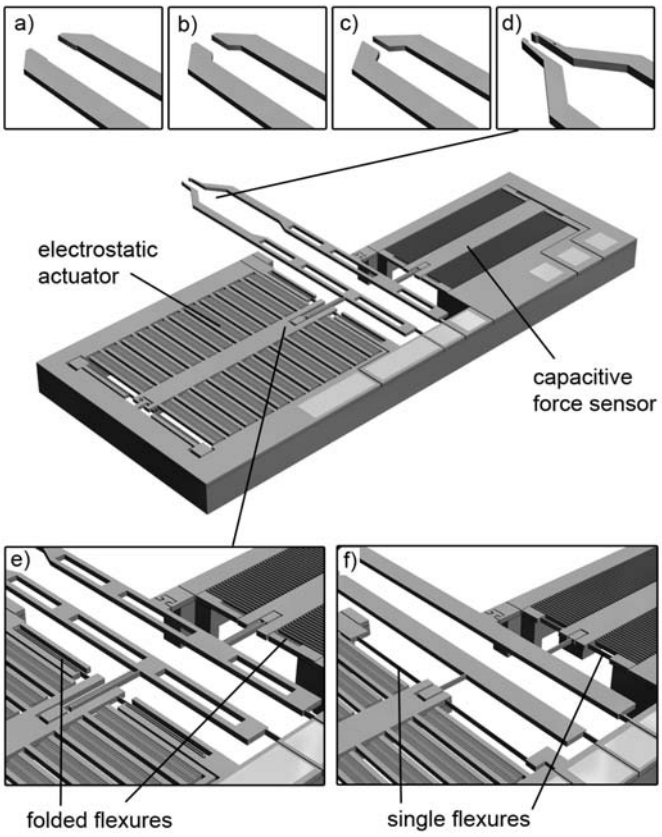

Figure 10: Solid model of the microgripper

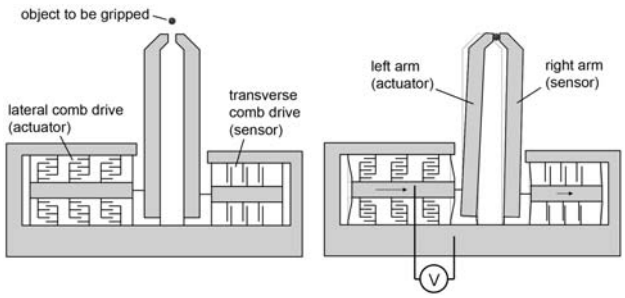

Figure 11: Force sensing microgripper working principle

TABLE III: FORCE SENSING GRIPPER PERFORMANCE

Stroke:	100µm
Actuation voltage (max):	200V
Sensitivity:	2000µN/V
Full range output:	0-5V
Resolution @ 3000Hz:	2.5uN
Resolution @ 30 Hz:	0.15uN

For testing the force sensing gripper, glass spheres ranging from 20µm to 90µm (Duke Scientific) have been manipulated. Figure 12 shows the gripping force profile during picking up and releasing of a 35µm glass sphere. First pick-and-place experiments have been performed with electroplated nickel parts for microassembly. The microgripper has been mounted on a three-axis micromanipulator. Pick-and-place experiments have been successfully performed with high precision. Figure 13 illustrates the manipulation sequence.

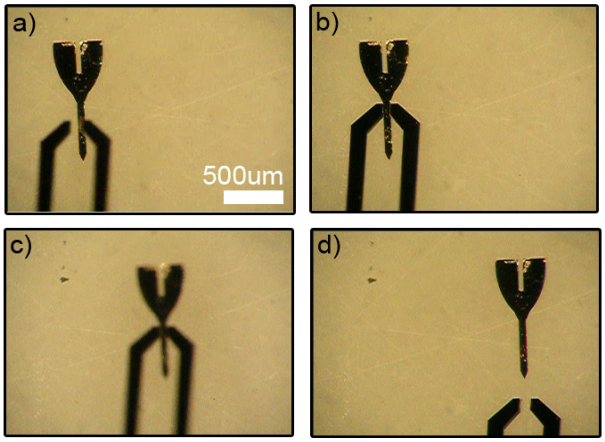

Figure 13: Handling of an electroplated nickel part using the force sensing microgripper

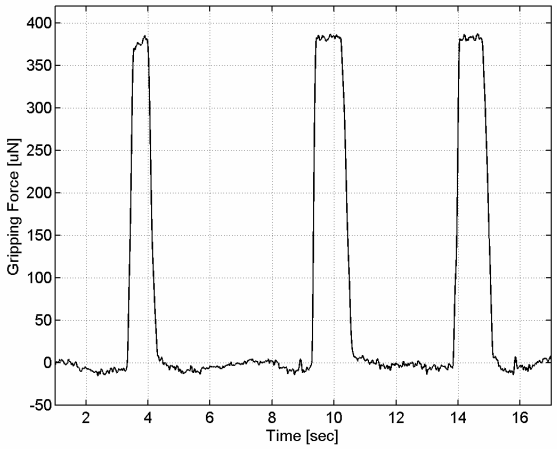

Figure 12: Force reading during the manipulation of during the manipulation of 35µm glass spheres.

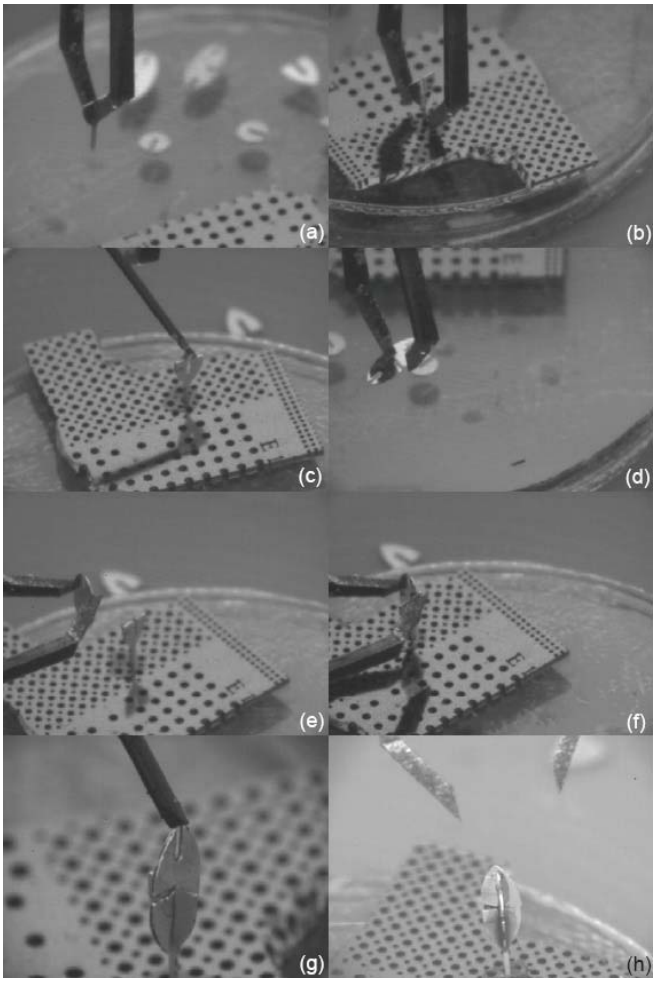

Figure 14: Assembly of electroplated microobjects

Once the microassembly station is fully operational, the microgripper will be integrated into the system. Using the six-axis positioning capabilities will allow the assembly of the nickel parts to build magnetically propelled microrobots for drug delivery [17].

VI. Conclusion

The design of a six degrees-of-freedom microassembly system is presented. The mechanical setup as well as the vision system is explained. Current work is focused on the final assembly of the system followed by an intensive test phase. Also, the design and working principle of two microfabricated end-effectors is presented. First is a force sensing probe and the second is a force sensing microgripper Once the final assembly and the integration of the end-effectors has been accomplished the system is ready for taking a further step towards the automated assembly of microsystems. It is expected that force feedback will greatly enhance the performance and the reliability of automated assembly system.

References

[1] K. B. Yesin, “CAD model based tracking for visually guided microassembly, ”Ph.D. thesis, University of Minnesota, Minneapolis, Minnesota, USA, June 2003.

[2] K. F. B¨ohringer, R. S. Fearing, and K. Y. Goldberg, The Handbook of Industrial Robotics (chapter Microassembly), S. Y. Nof, Ed. Wiley & Sons, 1999.

[3] M. B. Cohn, K. F. Boehringer, J. M. Noworolski, A. Singh, C. G. Keller, K. A. Goldberg, and R. T. Howe, “Microassembly technologies for MEMS,” in Proceedings of the SPIE Conference on Micromachined Devices and Components IV, A. B. Frazier and C. H. Ahn, Eds., vol. 3515, no. 1. SPIE, 1998, pp. 2–16.

[4] B. Nelson, Y. Zhou, and B. Vikramaditya, “Sensor-based microassembly of hybrid mems devices,” Control Systems Magazine, IEEE, vol. 18, no. 6, pp. 35–45, 1998.

[5] J. T. Feddema and R. W. Simon, “Visual servoing and cad-driven microassembly,” in IEEE International Conference on Robotics and Automation (ICRA), vol. 2, 1998, pp. 1212–1219.

[6] A. Ferreira, C. Cassier, and S. Hirai, “Automatic microassembly system assisted by vision servoing and virtual reality,” IEEE/ASME Transactions on Mechatronics, vol. 9, no. 2, pp. 321–333, 2004.

[7] N. Dechev, W. L. Cleghorn, and J. K. Mills, “Construction of 3D MEMS microstructures using robotic microassembly,” in Sensing and Manipulation of Micro and Nano Entities: Science, Engineering, and Applications, Workshop, International Conference on Robots and Intelligent Systems (IEEE/RSJ IROS 2003), 2003.

[8] N. Dechev, J. K. Mills, and W. L. Cleghorn, “Mechanical fastener designs for use in the microassembly of 3d microstructures,” in Proceedings of the ASME International Mechanical Engineering Congress IMECE, 2004.

[9] F. Beyeler, A. P. Neild, S. Oberti, D. J. Bell, Y. Sun, J. Dual, B. J. Nelson, “Monolithically Fabricated Micro-Gripper with Integrated Force Sensor for Manipulating Micro-Objects and Biological Cells Aligned in an Ultrasonic Field” IEEE/ASME Journal of Microelectromechanical Systems (JMEMS), Vol. 16, No. 1, February 2007, pp. 7--15.

[10] F. Arai, D. Ando, T. Fukuda, Y. Nonoda, T. Oota., Micro manipulation based on micro physics - strategy Based on Attractive Force Reduction and Stress Measurement., Proceedings of the 1995 IEEE/RSJ International Conference on Intelligent Robots and Systems, IROS'95, Vol.2, pp.263-241,1995.

[11] Y. Zhou and B.J. Nelson, Adhesion force modeling and measurement for micromanipulation, Proc. of SPIE Intl. Symp. on Intelligent Systems and Advanced Manufacturing, V3519, pp. 169-180, 1998.

[12] B. E. Kratochvil, K. B. Yes¸in, V. Hess, and B. J. Nelson, “Design of a visually guided 6 DOF micromanipulator system for 3D assembly of hybrid MEMS,” in Proceedings of the 4th International Workshop on Microfactories, October 2004.

[13] Q. Zhou, A. Aurelian, B. Chang, C. del Corral, and H. N. Koivo, “Microassembly system with controlled environment,” Journal of Micromechatronics, vol. 2, pp. 227–248, 2002.

[14] Sun, Y., Nelson B.J., Potasek D.P. and Enikov E., A bulk microfabricated multi-axis capacitive cellular force sensor using transverse comb drives. Journal of Micromechanics and Microengineering, 12(6): pp. 832-840, 2002.

[15] Sun, Y., Fry S.N., Potasek D.P., Bell, D.J. and Nelson, B.J., Characterizing fruit fly flight behavior using a microforce sensor with a new comb drive configuration. J. Microelectromech. Syst., 14(1): pp. 4-11, 2005.

[16] F. Beyeler, D.J. Bell, Y. Sun, A. Neild, S. Oberti, J. Dual, B.J. Nelson, “Design of a Micro-Gripper and an Ultrasonic Manipulator for Handling Micron Sized Objects” IEEE/RSJ International Conference on Intelligent Robots and Systems

[17] M. Probst, K. Vollmers, B. E. Kratochvil, B. J. Nelson, "Design of an Advanced Microassembly System for the Automated Assembly of Bio-Microrobots", Proc. 5th International Workshop on Microfactories, October 2006.

Microhandling Strategies for Automation

Quan Zhou, Veikko Sariola and Heikki N. Koivo

***Abstract*—This paper reviews two important physical principles in microhandling, namely the scaling effect and the principle of minimum potential energy. Microforces involved in microhandling are also analyzed from the point of view of the previous principles. A number of deterministic microhandling strategies and self-assembly methods are discussed. By analyzing the similarities of different microhandling strategies including self-assembly, we generate a unified understanding of different methods that can be used to enhance their suitability for automation.**

***Index Terms*—Microhandling, microgripper, self-assembly, potential well, microforces**

I. Introduction

Microhandling technology has advanced mainly in two branches. The first one is based on deterministic microhandling, including robotic contact microhandling and non-contact methods. The main feature of this type of microhandling is flexibility, or the capability of the system, including dexterity of operations, capability of working with different objects in a large work space. The second one is self-alignment/assembly based on the principle of minimum potential energy (using e.g. gravity, capillary forces or electric fields). The advantage of self-alignment techniques is that the final positioning of the objects is automatic (due to physical law) which makes massively parallel operation possible. The *potential wells* or *traps* determine the final desired location of micro objects.

Both branches have their limitations. For robotic contact microhandling, the releasing process is severely hindered by adhesion forces. Without properly designed releasing strategies or fixing strategies (e.g. form-closure, bonding, adhesive), the placing process can be very tedious and time-costly due to the adhesion between the tool and the object. Robotic contact microhandling may also damage the manipulated object. Moreover, these manipulation methods are not easily parallelizable.

To overcome these limitations, new physical principles for gripping micro objects have been researched. These include capillary, electrostatic, phase-changing and adhesion grippers. The main motivation in those researches is to solve the tool-part adhesion and part damage problem. They still suffer from tedious placing problem and not being easily parallelizable.

Manuscript received September 18, 2007.

Q. Zhou is with the School of Mechatronics, Northwestern Polytechnic University, China and the Control Engineering Laboratory, Helsinki University of Technology, Finland. (e-mail: quan@ieee.org).

V. Sariola and H.N. Koivo are with the Control Engineering Laboratory, Helsinki University of Technology, Finland.

Despite the weakness of this technology, deterministic microhandling has been extensively pursued due to its flexibility and good adaptability. It has been applied in many complicated handling tasks such as MEMS assembly, quality control and many biological applications.

So far, self-assembly processes have been developed mainly at mass production of simple micro structures. Even though it is possible to use multi-batch process to extend the complicity of the target structure, it is not competitive with the flexibility and dexterities of deterministic microhandling. Also, because of its stochastic nature, there is always possibility of an error, when the system gets stuck in a local minimum.

Because self-assembly process utilizes the principle of minimum potential energy, positioning of objects is driven by potential energy where no tool is needed. The absence of mechanical tool means that there is no tool-part adhesion or part damaging due to the tool. They are inherently parallel processes and thus have high throughput. Furthermore, if the locations of the potential wells are accurate and system disturbances can be controlled, the final locations of the micro objects will be accurate.

Automation is a key driving factor for wider application and deeper penetration of microhandling technologies. For a microhandling technology to be competent in automation, the technology should be *capable*, *efficient*, *precise* and *reliable*. Firstly, the technology should have the capability to carry out the desired task – e.g. picking-positioning-placing of microparts with simple or dexterous motion, or tasks such as penetration, injection, aspiration. Secondly, the technology should be efficient – often means how fast a full operation cycle can be carried out, which is an important measure in automation. Thirdly, the technology should be able to achieve desired precision and accuracy of operations. This could be a part of the capability of a micromanipulation or microhandling technology, we take it as a standalone measure to ease the discussion. The last measure – reliability – refers to how reliable and certain the process is, which is crucial for a micromanipulation or microhandling technology to be automated.

Indeed, it is obvious that if we could combine only the advantages of robotic microhandling and self-alignment, the resulting microhandling process would be more capable, more efficient, more reliable, and still precise, which is necessary to achieve automatic microhandling systems. The question is how to achieve that.

In this paper, we try to discuss deterministic microhandling and self-assembly in a unified framework of potential energy, attempting to create a general understanding of microhandling strategies, which will eventually lead into high level of automation. The discussion of microhandling is focused on the

positioning of microscopic objects. Other handling is excluded, such as penetration, injection and aspiration.

In Section II, the two general concepts in micro physics are briefly discussed; namely, the scaling effect and the principle of minimum potential energy.

Section III reviews important physical phenomena in microhandling. The nature of different forces is explained and their potential energy functions described, if possible. Especially interesting are forces that can be represented as the gradient of potential energy with well-defined minimum, so that it can be used to aid in the positioning of a micro object.

In Section IV, microgripping technologies based on different physical principles is introduced. The main focus is to study how the physical phenomena from Section III are taken into account in the gripper design (or not) and which parameters affect the gripper suitability for automation.

In Section V, self-assembly technologies are discussed. The qualities of the processes are detailed in comparison to the microgripping technologies.

In Section VI, the discussion from two previous sections is unified by introducing general handling strategies. With handling strategy we understand general actions that can be taken to make a microhandling more competent. The discussion includes creation of local potential trap, choosing surface properties, environment control, etc.

Section VII concludes the paper.

II. General phenomena in microhandling

A. Scaling effect

When manipulating micro objects or designing microsystems, we have not only smaller instruments and different actuation principles, but also different behavior of the tool/part interaction and other phenomena special in the microworld. The physics of the micro world is the same as that of the macro world. However, the dominant physical quantities are different due to the down scaling. We can use the term *scaling effect* to describe the change of dominant physical quantities in the microworld compared to those in the macro world [1].

The most important difference is that volume forces, most notably gravity, are much smaller, while surface forces, especially adhesion, dominate. The different scaling laws have been discussed in detail in many different research papers e.g. ref. [2]. The scaling laws are usually expressed by how the physical quantities depend proportionally to the characteristic dimension L. Typically they are proportional to a power of L, which can be derived from the governing physical equations. For example, area has a scaling law of L^2 and volume has a scaling law of L^3.

Furthermore, as the characteristic dimensions decrease to nanoscopic size, the continuum approximation become invalid and quantum effects start to dominate. However, the quantum effects can be accounted for, to some extent, by adding corrective factors into equations.

B. Principle of minimum potential energy

The principle of minimum potential energy states that any system will evolve towards a state with minimal potential energy by dissipating energy. In microhandling, the state of the system is the position of micro objects and energy is usually dissipated as heat. Examples of different potential energies include gravity [4], electrostatic potential [5] or energy associated with the surface tension.

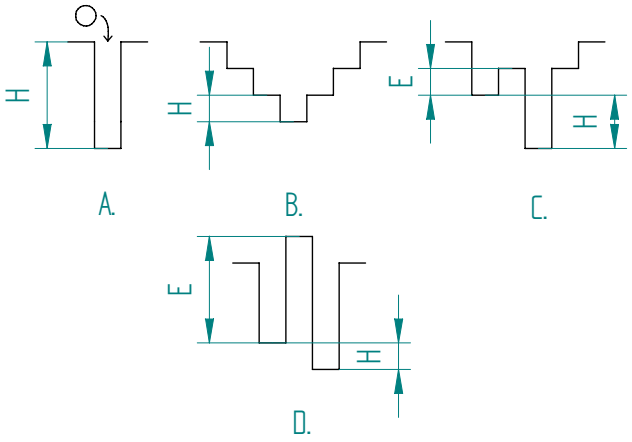

Fig. 1. Comparison of favorable and unfavorable potential energy functions for self-assembling systems. A. B. & C. Favorable potential wells. D. Unfavorable potential well. Adapted from Cohn et al. [3]

For self-assembly three criteria must be met [3]: 1) The desired configuration must represent the minimum of potential energy. 2) Any energy barriers E must be small compared to the driving potential H. The latter is the difference between the ground and the next lowest state. 3) A source of random kinetic energy must be provided. Fig. 1 shows favorable and unfavorable potential wells.

But even without 2) and 3), the system will go to a local minimum. In this case, the self-assembly process must start with the micro object close enough to the local minimum. So, even if the manipulation is done by a serial type manipulator, the final positioning may be helped by the creation of a local potential trap that corresponds with the desired final location of the microchip [6].

Real-life potential wells are often rather smooth. The preferred shape for them would be as in Fig. 2A. However, many real-life potentials are as shown in Fig. 2B. They have a well shape, but with flat bottom, so that there are multiple local minima close to the desired position. Thus, the accuracy of the process depends how narrow can the potential well be made, and how quickly the energy can dissipate.

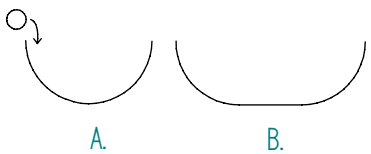

Fig. 2. A. Favorable potential well B. Unfavorable potential well, because of multiple minima. [7]

III. Physical phenomena

In the following sections, different forces and their potential functions are discussed, if possible. The discussion is limited to the most commonly applied forces in microhandling.

A. Gravity

Gravity force is the gradient of the potential energy $E = mgh$, where E is the potential energy, m is the mass of the object and h is the height of the center of mass of the object.

Because mass is proportional to the volume of object (by $m = \rho V$, where ρ is the density of the material), which has a scaling law of L^3, and height has a scaling law of L^1, the potential has a scaling law of L^4. Thus the gravity scales very unfavorably when the system is miniaturized.

However, gravity, even if weak, is not negligible in sub millimeter scale. It has been successfully demonstrated as the driving potential in many self-assembly applications [4], [8]. The releasing of micro grippers in this scale is also aided by gravity, but sometimes not sufficiently enough [9].

Gravity is comparably easy to take into account in microhandling, because for each micro object, only one gravity potential needs to be considered; namely, that of earth.

B. Electrostatic force

The electrostatic force is the gradient of an electrostatic potential energy. Electrostatic forces arise from electrostatic charges and contact/tribo electrification. For microhandling, often it is more relevant to describe the electrostatic potential by capacitors, instead of deriving the potential from Coulomb's law. A simplified model of plate capacitor can be applied and the energy is approximated with $E = \varepsilon A V^2/(2d)$ where E is the energy stored in the capacitor, ε is the permittivity of the medium, A is area of the plates, V is the voltage and d is the distance of the plates. The approximation is valid if $A << d^2$.

If the voltage is kept constant, the capacitor energy scales very favorably with a scaling law L^1. However, if the charge density Q/A is kept constant, the capacitor energy has the scaling law of L^3.

The electrostatic force has important implications for microhandling. In robotic contact microhandling, the electrostatic force is usually regarded as a source of disturbance and techniques to reduce it have been developed. One way to achieve this is to ground the gripper tips [9].

With non-uniform electric fields, it is possible to create forces on dielectric particles even without the particles being charged. This is a result of polarization. Depending on whether the permittivity of the medium is lower or higher than that of the particle, the particle will move into stronger or weaker electric field. The effect is observable in both AC and DC fields. This is called *dielectrophoresis* and has important implications for microhandling, as it can be used to create potential traps. The term dielectrophoresis was first coined by Pohl in 1951 [10]. Its early applications were mostly in the manipulation biological cells in liquid medium [11].

This self-centering because of electrostatic forces has also been demonstrated as a gripping principle [12]. Furthermore, electrostatic force has been used as the driving force in two-dimensional self-assembly in dry media [5].

Recently, the dielectrophoretic effect was achieved using light induced electrodes [13]. With this method, the locations of the potential traps can be redefined by light only, making it very flexible for the manipulation of small particles.

Moreover, the ambient environment (temperature, humidity, medium) affects the electrostatic force [14]. Humidity can affect the leakage current and consequently the scale of electrostatic forces. In general, higher humidity will increase permittivity. The permittivity is also function temperature. Moreover, moisture level in a dielectric substrate will significantly affect the electrical properties [15].

C. Capillary force

Capillary force results from the surface tension of a meniscus. In the simplest form, the energy associated with a meniscus is $E = \gamma A$, where E is surface energy of the meniscus, γ is the *surface tension* (or *interfacial energy*) and A is area of the surface.

Not only liquid-vapor interfaces, but also solid-liquid, and vapor-liquid interfaces carry energy. These define the contact angle of the liquid-vapor interface by the Young's equation $\gamma_{sv} - \gamma_{sl} - \gamma_{lv}\cos\theta = 0$ where γ_{sv} is the interfacial energy at solid-vapor interface, γ_{sl} is the interfacial energy at the solid-liquid interface, γ_{lv} is the interfacial energy at the liquid-vapor interface and θ is the contact angle. When dealing with water, if the contact angle is larger than 90°, a surface is called *hydrophobic*, otherwise it is called *hydrophilic*.

By looking at the Young's equation, it can be seen that the contact angle changes if the surface tension is changed. Indeed, this can be done with the aid of voltage, which is called *electrowetting*. This property has many applications from fluidic lens to digital micro fluidics [16].

The scaling law of the surface energy is L^2. Thus, comparing this to gravity and electrostatics, it is expected to have a more dominant effect upon miniaturization. Indeed, the capillary forces have a role in three important areas of microhandling as shown in Fig 3: 1) Air humidity may form a liquid bridge between a tool and a micro object [17], affecting the part adhesion to the tool. 2) It has been used as the gripping force itself, in what is commonly known as capillary gripper [18]. Moreover, self-centering has been demonstrated in capillary grippers [19], which is a result of the principle of minimum energy, as applied to the surface energy. 3) The capillary forces

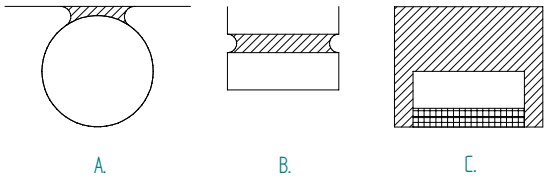

Fig. 3. Three roles of capillary forces: A. contribution to adhesion; B. capillary gripping and self-centering; C. fluidic self-assembly.

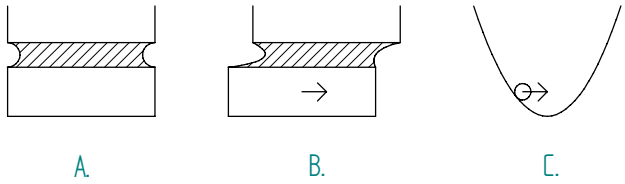

Fig. 4. Self centering of a capillary gripper. A. The part is perfectly centered to the tool B. With small displacement, the surface tension will try to bring it back to the center C. The potential well associated with the surface tension.

have been used as the driving force of fluidic self-assembly [20]. The potential well is created by hydrophobic coatings.

The self-centering property of capillary grippers is further illustrated in Fig. 4. With this property, the potential well interpretation of capillary forces becomes clearer. What makes this especially attractive is that this potential trap, unlike the electrostatic potential, affects only the objects in contact with the meniscus. In some sense, it can be regarded more local than electrostatic forces, as it does not interfere with nearby objects and/or potential well.

D. Radiation pressure

Radiation pressure is the pressure exerted by electromagnetic radiation on any matter. This is a result of light carrying momentum. When the electromagnetic radiation is absorbed to the matter, the pressure P is given by $P = I/c$, where I is the intensity of the light and c is the speed of light. If the light is reflected, the pressure is doubled, given by $P = 2I/c$.

In everyday situations, the pressure is very small: for example, assuming that the sunlight is completely absorbed to earth and the intensity of sunlight is approximately 1400 W / m^2, the pressure exerted at earth is only about 4.7μPa.

However, by using a laser and suitable optics it is possible to concentrate enough radiation on a small particle to create meaningful forces to be used as gripping forces. Optical trapping of micrometer scale particles relies on this phenomenon. Three dimensional optical traps can be formed with a single laser [21].

E. Adhesion

Adhesion forces are surface forces that result in two surfaces sticking to each other. Many different phenomena contribute to the forces, including van der Waals forces, capillary forces and hydrogen-bonding [22].

With van der Waals forces, we understand the total attractive intermolecular forces, including Keesom, Debye and London interactions. Of those three, the London interactions require quantum mechanical treatment. However, for two molecules, the intermolecular interaction have all potential functions with inverse sixth order dependence of distance, so that they can be combined into one potential function $E(r) = -C/r^6$ where r is the distance of two molecules and C is a constant. The constant C measures the strength of the van der Waals forces between the molecules.

The strength of van der Waals forces between two solids is more commonly described with the Hamaker constant, because it's easier to experimentally verify, which relates to C with $H = \pi^2 C \rho_1 \rho_2$ where ρ_1 and ρ_2 are the number of atoms per unit volume of the two solids [23].

In addition to van der Waals forces, a repulsive interaction should keep surfaces separate. The repulsive interactions are also quantum mechanical in nature and there is no general equation describing their distance dependence [23]. Empirically, it has been verified that for two molecules a good semi-empirical model for these interactions between is a potential with inverse 12th order dependence of distance, $E(r) = A/r^{12}$, positive sign reminding that the interaction is repulsive. Indeed, the total of these two potentials presented for van der Waals and repulsive interactions is called the Lennard-Jones potential, which is shown in Fig. 5. The Lennard-Jones potential alone shows the potential well and helps understanding the tool-object adhesion problem as the part getting stuck in local potential minimum. However, for two parallel flat surfaces, the potential well is only attracting them in the direction of the surface normal, so that only 1D positioning is achieved with adhesion forces. Therefore, the adhesion force is not favorable as the driving force for self-assembly.

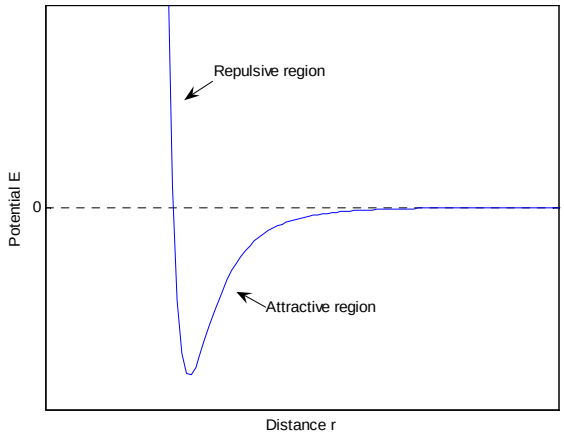

Fig. 5. Shape of the Lennard-Jones potential, which is a popular choice for modeling total intermolecular forces between two molecules. Units arbitrary.

And, as noted earlier, the van der Waals forces are not responsible for the adhesion alone, but capillary condensation plays a significant role also. The effect of capillary condensation depends on humidity and surface roughness [23]. The relationship can be quite complex; the adhesion can increase until certain amount of humidity, after it starts to decrease again.

Moreover, when two solid bodies are in contact, local deformation appears due to the elasticity of the material and the external load and intersurface forces. Such adhesion also has the hysteresis behavior. Different models such as Hertz, JKR [24], DMT [25] and Maugis [26] has been developed to describe such phenomena. In potential well point of view, this is actually very similar to a deep well. Of course, the phenomena are rather complicated and energy is not necessary conservative.

F. Friction and viscous forces

Friction and viscous forces are the forces opposing movement, former in the case of two surfaces in contact and the latter in the case of liquids. These forces are responsible for energy dissipating from kinematic energy to heat and, as such, crucial for making the principle of minimum potential energy to work. As such, they themselves cannot be described with a potential energy function.

Traditionally, friction force has been categorized into static friction, sliding friction and rolling friction. The simplest model has been the Coulomb friction $F = \mu N$, where F is the friction force, μ is friction coefficient and N is the normal force between surfaces.

Notice that N does not depend on the contact area. However, when adhesive forces dominate the Coulomb friction

approximation breaks down and the friction does depend on the contact area and load. Micro-nano tribology tries to find out these relationships and is actively researched; so far, no universal models have emerged, but applicable models depend on the geometry, scale, materials, surface roughness and environment.

IV. MICRO GRIPPERS

Microgripper is the fundamental tool for position base microhandling. In this Section, microgrippers based on different physical principles are discussed using the principle of minimum potential energy.

A. Tweezers

Tweezers are mechanical micromanipulators with two fingers and tools, also known as tips, in the ends. This type of micromanipulators has been extensively studied since early times of microrobotic research [27][28][9][29][30][31].

The simplest tweezers have only one degree-of-freedom (DOF); namely, opening and closing the tips. Such grippers can be monolithic, cheap and/or very small, because they can be fabricated with lithographic methods. The more feature-rich (e.g. multiple DOFs [31], force sensing [32], exchangeable tooltip [33]) grippers are usually assembled and are larger in size. Tweezers are rather capable, as there are many parameters, such as geometry, tip material, sensors and so on, which can be changed in the design to adapt to many different tasks. With proper design, dexterous manipulation can be achieved even using only the tweezer itself, as shown in Fig. 6. The limitation is that sometimes large gripping force is required, and damage to the object may result because the force is applied to a few contact points only.

The main forces affecting the micropart in mechanical micromanipulation are friction, adhesion and electrostatic forces. The friction keeps the part from dropping from between the tips. Adhesion is responsible for the sticking of the part to a tip upon release. Electrostatic force is the result of charge distribution in the tips and the micropart. If not properly accounted for, it can have unexpected results on the manipulation and thus reduces reliability of the manipulation.

The main problems of micrograpping can be explained with the potential well concept or mainly the lack of thereof. When picking, the part can be picked from many different contact points. There is no potential well to position the micropart accurately respective to the gripper. Thus, for accurate gripping, the location of the micropart with respect to gripper must be measured. To avoid errors accumulating, it is beneficial to do this is as late as possible – the position measurement is usually done using machine vision. Thus, in practice the accuracy of tweezers is limited by the accuracy of microscopes.

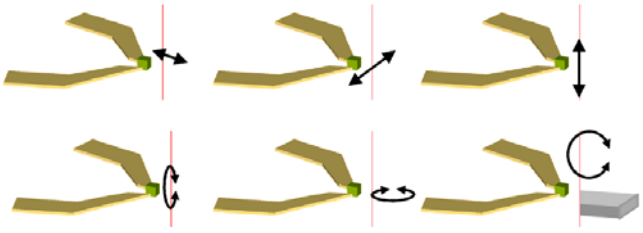

Fig. 6. Different degrees of freedom in 6 DOF microgripper [31].

Instead of relying on position measurement, form-closure type of tips can be applied. When designed properly, such gripper tips are a kind of potential well that can define the position of the part related the gripper. However, the form-closure tips are closely coupled with the shapes of the part to be manipulated. Therefore, techniques such as tool exchange are necessary to make the gripper work with parts of different geometry shapes.

Releasing microparts is even harder. Upon the release of a micropart on a non-adhesive surface, the final position is wholly ambiguous, only fixed in place by gravity and friction. Because of the adhesion to the tool, the release may not succeed at all or the object can move to wrong location before being released. Returning to the potential well concept, the adhesion of the object to the tool can be seen as the part getting stuck in a local potential minimum of the tool-part-receptor system.

Because of these two reasons, the accuracy of a gripper cannot be regarded as the same as the accuracy of its actuators. Also, the reliability of grippers is not good in releasing, due to the electrostatic and adhesion effects.

The potential view is helpful when discussing the proposed solutions to the previous problems. A common way to reduce the part-tip adhesion problem is to change the material properties or the surface roughness of the tip [34][35]. Another solution proposed is to control the humidity of the environment [36]. In effect, they both reduce the depth of the potential well, making it easier for the part to escape local minimum.

Another solution is to create a new potential well at the receptor site so that the object transfers into it. One option is to place the part on an adhesive surface [31], effectively using adhesion potential well to aid the transfer.

Yet another solution is the creation a capillary potential well. This can be employed if the release location can be shaped to match the shape of the part, or close it. By dispensing a droplet of liquid in between the part and the receptor site, the capillary potential trap aids in the release and final positioning of the part.

Fig. 7 shows a simple case of hybrid microhandling strategy combining the robotic microhandling process and the

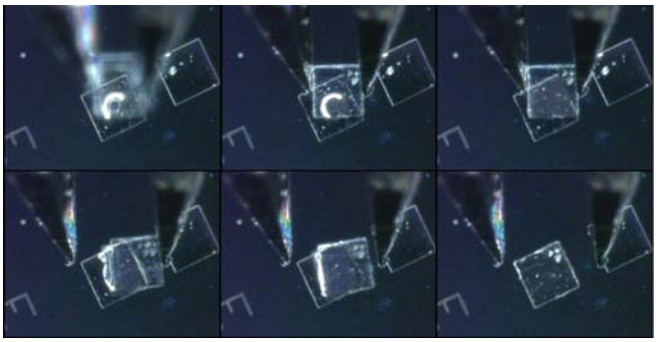

Fig. 7. Using capillary potential trap to aid tweezer release a) dispensing of droplet; b) micropart contact the droplet; c) droplet wets the gap between the micropart and the receptor; d) releasing starts, the adhesion between the micropart the gripper; e) capillary force overcome the adhesion force between the part and the gripper; f) self-alignment achieves fine-positioning.

droplet-based capillary self-assembly process [6]. In this experiment, a droplet is dispensed before the micro component (dimension about 300 μm) handled by a robotic microgripper approaching the target site. The releasing process is assisted by capillary self-alignment. In the figure, we can observe that the micro component is initially stuck with one of the tips of the micro gripper. After certain displacement of the tip, the capillary force overcomes the adhesion force between the micro component and the tip of the micro gripper. After that, the micro component automatically moves to the target site driven by capillary self-alignment. As a result, the accuracy and reliability of the handling have increased.

B. Capillary grippers

Capillary grippers employ capillary force as the gripping force [18][19]. A gripper is 'contacted' to a micropart with a liquid bridge where the gripper has to be approximately the same shape as the object gripped.

Capillary grippers have several advantages over mechanical tweezers: 1) The risk of part damage is much lower; 2) The minimization of surface energy results in automatic self-centering of the micro object with respect to the gripper; 3) The self-centering occurs even when the part and the gripper head are not exactly the same size or shape; 4) The capillary grippers grip only from one side, leaving others accessible.

Thus, the accuracy of capillary gripper when picking is good, in the sense that the part is automatically centered with regard to the gripper. Also, it has good capabilities because it can handle parts without exact shape matching and damaging them. In the mean while, it does not block view to more than one side. However, multiple DOFs handling can be harder to achieve than with tweezers.

The ease of gripping of capillary grippers comes at the price of difficulty to release accurately. Different release techniques have been proposed including gluing the object on the surface, using injecting gas, using mechanical release with needles [19], acceleration release, reducing volume of liquid, tilting gripper or changing gripper geometry [37]. The amount of liquid can also be hard to control accurately.

Since surface tension is the gripping force in capillary grippers, electrowetting has been proposed to help releasing from capillary gripper [38].

C. Electrostatic gripper

The ambiguous picking and releasing problems have also been tried to solve by using electrostatic potential trap [12]. By applying a voltage between two concentric circle shaped planar electrodes, a three dimensional potential well is formed. The object is centered in the middle of the circle.

Relatively high voltages, as high as 1200V, have been used for successful manipulation of glass spheres with diameters ranging from 100 to 800 μm. High humidity prevented successful manipulation altogether.

There are some limitations in capabilities of the electrostatic gripper, as the size of the gripper must match approximately the size of the manipulated part. Another problem is that the electrostatic potential interferes with nearby objects so that manipulation in a setup having more than one part can be hard. Because of the tool-part adhesion, the reliability of electrostatic grippers suffers similar problems as mechanical grippers.

D. Phase-changing grippers

The phase-changing grippers utilize the variation of adhesion force of a gripping intermediate to perform gripping and release operation. Early examples used the adhesive property of ice to hold a micro object [39] by freezing a thin film of water between the tip of the gripper and part. Later, other phase-changing intermediates were demonstrated, such as magneto-rheological fluids, thermoplastic polymers and thermosetting polymers, in which the phase-change is based on electromagnetic field, heating/cooling or ultraviolet light, respectively [40].

There are a few advantages in phase-changing grippers. First, the shape of the gripper and the manipulated part does not need to be similar, which greatly improve the range of objects can be manipulated by same gripper. Also, large gripping forces can be achieved, up to 1 N / mm^2 in the case of water/ice.

The gripping may take place in dry air, with the intermediate being inserted between the gripper and the micropart, or the micropart may be completely submerged in the intermediate. For example, part being completely submerged in water, with local freezing to achieve gripping, has been demonstrated [41].

Under a general framework, the effect of phase-changing gripper can be interpreted with potential wells as the phase-change making the adhesion potential well very deep (potential from the elasticity of the solids).

E. Mechanical lock

Snap-lock mechanisms have been used in both as the gripping principle and to aid the release of microparts to receptor sites. Mechanical compliant beams are required to allow snapping occur when the part is pushed in place, either to the gripper or to the receptor site. Second, there should be interlocking structure that connect the part firmly. Finally, the features should fix the position and orientation of the part, preferably in 6 DOF.

This method effectively reduces the accuracy requirements of the manipulator. The accuracy is limited by the fabrication accuracy of the structures.

The potential well interpretation of this method is that the mechanical bending creates a potential well of spring force. The properties of the well can be controlled by controlling the thickness of the beam, effectively controlling the spring constant. This manipulation principle has been employed to create three dimensional structures [42].

The problem with this method is that the gripper and/or the manipulated parts must be specifically designed for this type of manipulation, which is not always feasible.

F. Optical tweezers

Microsized spheres can be trapped by forces of laser radiation pressure [21]. The trap consists of a single strongly focused laser beam. The refraction of the laser beam from the sphere results in a force that tries to restore axial and transverse displacement from the focus. The manipulation usually happens in liquid medium [43]. From potential point of view, an optical tweezer is a 3D potential well, which is relatively local and can be created and controlled on demand (through the power and focus control of the laser).

The principle has been applied to micro-sized particles and variety of biological particles, including living cells and organelles with living cells. For biological applications, there is a risk of damaging the sample; for example, reduction of sperm motility after being manipulated with optical tweezers has been reported [44]. Because of this, light in the infrared spectrum has been employed.

G. Others

There are gripping techniques that have not been addressed in the above discussion, such as vacuum [45], magnetic [46], Bernoulli [47] and squeeze effect [48] grippers. Most of them are similar to the grippers we have discussed in the nature of potential well, e.g. vacuum gripper shares similarity with the electrostatic gripper by having a controllable potential well and tool-part adhesion problem. Of course, some grippers have their distinguished features and limitations, e.g. magnetic gripper can only handle paramagnetic material. We do not try to give an extensive review of all those grippers, because the previous discussion in this Section is sufficient to serve the purpose of the paper.

V. Self-assembly

Self-assembly is a technology that relies on the principle of minimum potential energy. Self-assembly can be carried out in dry environment or liquid medium. Often, the self-assembly process is massively parallel and stochastic in nature.

A. Dry self-assembly

The electrostatic force has been used on a two-dimensional flat surface to attract randomly located parts to predefined locations by Böhringer et al. [5]. In this work, voltage was applied between aluminium and a patterned chrome-gold layer with glass in between, effectively acting as a capacitor. When parts were placed on the topmost chrome-gold layer, the position was guided by the patterns in the layer. Vibration was used to overcome friction and adhesion forces that bound the parts to the surface or each other.

Many times gravity is regarded to have negligible effect in micro manipulations. However, even if weak, it can and has been used as the driving force for self alignment.

In one of the early examples of using gravity to position microparts, Cohn et al. [8] placed hexagonal microparts on a slightly concave diaphragm. Upon vibration, the hexagons arranged themselves into a perfect lattice.

Fang and Böhringer [49] demonstrated also using the gravity as the driving force of self-assembly. The potential traps were square shaped holes, with a peg in one corner to fix the orientation.

Self-assembly has also been carried out in generally dry environment but with local liquid existence, such as solder ball self-assembly [50], and water-steam induced capillary self-assembly [51].

B. Fluidic self-assembly

In fluidic self-assembly of microparts, fluidic transport is used because surface interactions can designed more easily in liquid environment than in gas phase [52]. The binding and receptor sites are usually prepared with photolithographic techniques. Hydrophilic and hydrophobic interactions provide the basis of many fluidic self-assembly processes.

After preparing the structures, the structures are freed from substrate to the liquid medium and random kinetic energy is used to move the parts. The random kinetic energy can be supplied with fluidic agitation or ultrasonic agitation. Both two-dimensional and three dimensional assembly have been demonstrated [53].

With this technique, micro mirrors have been assembled on a planar surface. In this example, yields of 100% and accuracy in the sub micrometer range have been reported. The binding and receptor sites were made hydrophobic using octadecanethiol self-assembled monolayers, while other parts remained hydrophilic [20].

VI. Handling strategies

In this Section, we present the general considerations for accurate positioning of micro objects, especially in the view of the principle of minimum potential energy.

A. Create a potential well

For accurate positioning, the desired position should be the minimum of a potential well. If no potential well exists, it can be created artificially. So far, a number of different techniques have been proposed (with respect to the potential wells they use): lithographic etching of holes to aid positioning of objects on surface (gravity), electrostatic driven self-assembly and gripping (electrostatic), droplet aided releasing of micro objects (capillary), surface adhesion aided release from tweezers (adhesion) etc.

Some techniques to create a potential well can be done on demand when the potential well is needed, while other potential wells must be created in advance. Even if the well is prefabricated, some properties of the potential well can be adjusted by changing local parameters. Table 1 lists different techniques to create potential well, including 1) the type of the well they create, 2) if the well can be created on demand and 3) if their shape can be controlled on demand. Global parameters (e.g. environment conditions) that affect the shape of the potential wells are excluded from the table. Those parameters are discussed in the next subsection.

B. Environment control

With environment we mean physical quantities that are quickly smoothed and thus are global all over the system. With simple manipulation schemes, the ambient environmental parameters only affect a few properties (like reducing humidity to increase the reliability of releasing from tweezers) of the system, so that they can be tuned to achieve optimal performance. In more complex schemes, the environment becomes a tradeoff.

Often, what the environment actually does is that it controls the shape of the potential wells. The adhesion depends on humidity, the electrostatic trap depends on humidity, the hydrophobic/-philic well depends on the medium and so on. Thus, this is a connection between ambient environment conditions and the accuracy of self-assembly processes.

The environmental properties are global in the sense that any local change quickly diffuses and is smoothed out, thus effectively meaning that any change in parameters affects

Table 1. Comparison of different techniques to create potential wells.

	Source of potential	Positioning on demand	Shape controlled by
surface coating	capillary	no	medium
lithographic etching	gravity	no	tilting
dielectrophoresis	electrostatic	no	AC/DC voltage, frequency (if AC)
snap-locking	spring	no	-
droplet	capillary	yes	dispensing/aspiration, voltage
laser trapping	radiation pressure	yes	power
ultrasonic	acoustic	yes	power, frequency
optically induced dielectrophoresis	electrostatic	yes	optical power
phase changing	phase change	limited or no	depending on the material

forces and potentials everywhere, which may call for compromises.

C. Surface properties

Surface properties affect forces and potentials locally. Usually, the surface properties are chosen to target the shape of specific potential well. By proper selection of materials and coatings, the potential trapping effect can be increased or reduced. In general, this selection has to be made in advance.

So far, examples of surface property effects on potential wells have been the surface roughness, material and grounding to reduce tool-part adhesion problem, surface hydrophilic property to help micropart location in liquid medium or humid air, using adhesive surfaces to aid part releasing from a microgripper.

D. Artificial disturbances

The general problem of getting stuck in local, undesired minimum can be solved by adding more kinetic energy to the system. This can be done in random or deterministic fashion. In both cases, there are few parameters to be selected in the form of disturbances.

The idea of random disturbances is employed in fluidic self-assembly, by stirring the liquid medium. The deterministic disturbances usually come in one of the two forms: sinusoidal and pulses. The sinusoidal disturbances were used in the gravity based self-assembly. In this method, the parameters of the disturbances are the amplitude and frequency of the sinusoidal signals. One of the attractive features of sinusoidal perturbations is that they may exploit the resonant frequencies of the system to enhance the effect of disturbance.

Finally, the pulse shaped disturbances have been used with capillary grippers and to solve adhesion problems. Basically, the kinetic energy given to the part should be more than then height of the local potential well to escape.

E. Coarse-fine positioning

Another commonly found method to increase the capabilities of a handling strategy is to include hierarchical levels of positioning accuracy to the strategy. This is often done with microgrippers, as they usually include motorized stages for coarse positioning and piezoelectric actuators for fine positioning. But the hybrid strategy using droplet for fine positioning and gripper for coarse positioning can be seen as a manifestation of the same principle.

In our view, the coarse positioning can be utilize robotic devices for dexterous manipulation and capability and the fine positioning should be replaced with the use of a local potential well. In this way, the automation is in two levels. The first is robotic automation of the coarse positioning system. And the second is the automation in fine positioning due to the principle of minimum potential energy. Such combination utilizes the advantage of both techniques in traditional microhandling.

VII. Conclusion

This paper reviewed relevant forces and two major branches of microhandling – deterministic microhandling and self-assembly – from the point of view of the principle of minimum of potential energy. Both branches have their benefits and limitations; typically deterministic microhandling has good capabilities and self-assembly is more efficient. Reliability and precision are design parameters which depend on the process or are tradeoffs between other parameters such as efficiency.

In our point of view, most micro handling strategies are actually trying create setup that a micropart will transfer to the desired location using potential wells. Even in tweezers, which are not so much a potential well, the configuration of the whole system can be discussed under the same framework, where the different potential well shapes are achieved through proper selection of material properties and ambient environment conditions.

Many non-tweezer type microgrippers fundamentally are also potential wells created using different physical principles. Thus, because self-assembly also relies on potential wells, deterministic microhandling and self-assembly are actually working on similar principles. This helps in bringing ideas from self-assembly to deterministic microhandling and vice versa.

As noted earlier, there are four important parameters to lead competent microhandling techniques for automation: capability, efficiency and precision and reliability. For any single technology of the two branches, it is very hard to achieve them simultaneously. We need to combine features of both branches to create hybrid techniques based on the principle of minimum potential energy to make microhandling more applicable to automation. The combination of both branches is a natural trend of future development of microhandling.

References

[1] W. S. N. Trimmer, "Microrobots and Micromechanical Systems", *Sensors and Actuators*, Vol. 19, pp. 267-287, 1989.

[2] M. Wautelet, “Scaling laws in the macro-, micro- and nanoworlds” *European Journal of Physics*. vol. 22, pp. 601-611, 2001.

[3] M. B. Cohn, K.-F. Böhringer, J. M. Novorolski, A. Singh, C. G. Keller, K.. Goldberg, R. T. Howe, "Microassembly Technologies for MEMS," Proc. SPIE Micromachining and Microfabrication, Santa Clara, CA, September 21-22, 1998.

[4] H.-J. Yeh, J.S. Smith, “Fluidic self-assembly of microstructures and its

application to the integration of GaAs on Si", Proceedings of IEEE Workshop on Micro Electro Mechanical Systems, MEMS'94, pp. 279-284, 1994.
[5] Böhringer, K.F., Goldberg, K., Cohn, M., Howe, R., Pisano, A., "Parallel microassembly with electrostatic force fields", Proceedings of 1998 IEEE International Conference on Robotics and Automation, ICRA'98, pp. 1204 -1211, 1998.
[6] Q. Zhou, B. Chang, "Microhandling using Robotic Manipulation and Capillary Self-alignment" Intelligent Robots and Systems, 2006 IEEE/RSJ International Conference on, pp. 5883-5888, October 2006.
[7] Q. Zhou, "Strategies in Automatic Microhandling", Proceedings of IEEE international conference on mechatronics and automation, IEEE-ICMA'07, Harbin, China, August 2007.
[8] M.B. Cohn, C.J. Kim, A.P. Pisano, "Self-assembling electrical networks: An application of micromachining technology", Proc. 6th Int. Conf. Solid-State Sensors and Actuators, pp. 490-493, June 1991.
[9] A. Albut, Q. Zhou, C. del Corral, H.N. Koivo, "Development of Flexible Force-Controlled Piezo-Bimorph Microgripping System", Proceedings of 2nd VDE World Microtechnologies Congress, MICRO.tec 2003, Munich, Germany, pp. 507-512, 2003.
[10] H. A. Pohl, "The Motion and Precipitation of Suspensoids in Divergent Electric Fields", J. Appl. Phys. 22(7), 869–871, 1951.
[11] H.A. Pohl, I. Hawk, "Separation of living and dead cells by dielectrophoresis," Science, vol. 152, pp. 647–649, 1966.
[12] J. Hesselbach, S. Buettgenbach, J. Wrege, S. Buetefisch, C. Graf, "Centering electrostatic microgripper and magazines for microassembly tasks", Proc. SPIE, vol. 4568, p. 270-277.
[13] P.Y. Chiou, Z. Chang, M.C. Wu, "A Novel Optoelectronic Tweezer Using Light Induced Dielectrophoresis", Proceeding of IEEE/LEOS International Conf. Optical MEMS, 2003.
[14] Q. Zhou, B. Chang, H.N. Koivo, "Temperature and Humidity Effects on Micro/nano Handling", Materials Science Forum, vols. 532-533, pp. 681-684, 2006
[15] J.M.M. Perez, C. Freyre, "A Poly(ethyleneterephthalate)-based humidity sensor", Sensors and Actuators B, Vol. 42, pp. 27-30, 1997.
[16] F. Mugele, J.-C. Baret, "Electrowetting: from basics to applications", Journal Of Physics: Condensed Matter, vol. 17, pp. 705–774, 2005.
[17] F. Arai, D. Ando, T. Fukuda, Y. Nododa, T. Oota, "Micro Manipulation Based on Micro Physics - Strategy Based on Attractive Force Reduction and Stress Measurement", IEEE/RSJ International Workshop on Intelligent Robots and Systems, IROS'95, vol. 2, pp. 263-241, 1995.
[18] H. Aoyama, S. Hiraiwa, F. Iwata, J. Fukaya, A. Sasaki, "Miniature robot with micro capillary capturing probe", Proceedings of the Sixth International Symposium on Micro Machine and Human Science, MHS'95, pp. 173 - 178, 1995.
[19] C. Bark, T. Binnenbose, G. Vogele, T. Weisener, M. Widmann, "Gripping with low viscosity fluids", Proceedings of the Eleventh Annual International Workshop on Micro Electro Mechanical Systems, MEMS'98, pp. 301 - 305, 1998.
[20] U. Srinivasan, D. Liepmann, R.T. Howe, "Microstructure to Substrate Self-Assembly Using Capillary Forces", Journal of Microelectromechanical Systems, vol. 10, pp. 17-24, 2001.
[21] A. Ashkin, J. M. Dziedzic, J. E. Bjorkholm, S. Chu, "Observation of a single-beam gradient force optical trap for dielectric particles", Optics Letters, vol. 11, pp. 288-, 1986.
[22] F. Arai, T. Fukuda, "Adhesion-type micro end effector for micromanipulation", Proceedings of the 1997 IEEE International Conference on Robotics and Automation, IEEE-ICRA'97, vol. 2, pp. 1472-1477, 1997.
[23] J. Israelachvili, Intermolecular and Surface Forces, 2 ed. London: Academic Press, 1992.
[24] K. L. Johnson, K. Kendall, A.D. Roberts, "Surface Energy and the Contact of Elastic Solids", Proc. R. Soc. Lond. A. 324, pp. 301 - 313, 1971.
[25] B.V. Derjaguin, V.M. Muller, YU.P. Toporov, "Effect of contact deformations on the adhesion of particles", Journal of Colloid and interface science, 53, No. 2, pp. 314-326, 1975.
[26] D. Maugis, "Adhesion of Spheres: The JKR-DMT Transition Using a Dugdale Model", Journal of Colloid and Interface Science, vol. 150, no. 1, pp. 243-269, 1992.
[27] I. W. Hunter, S. Lafontaine, P.M. F. Nielsen, P.J. Hunter, J.M. Hollerbach, "Manipulation and Dynamic Mechanical Testing of Microscopic Objects Using a TeIe-Micro-Robot System", Proceedings of 1989 IEEE International Conference on Robotics and Automation, ICRA'89, vol. 3, pp. 1553 – 1558, 1989.
[28] C.-J. Kim, A.P. Pisano, R.S. Muller, M.G. Lim, "Polysilicon microgripper", Proceedings of IEEE Solid-State Sensor and Actuator Workshop, pp. 48-51, 1990.
[29] J. Agnus, P. De Lit, C. Clevy, N. Chaillet, "Description and performances of a four-degrees-of-freedom piezoelectric gripper" Proceedings of the IEEE International Symposium on Assembly and Task Planning. pp. 66-71, 2003.
[30] G. Yang, J.A. Gaines, B.J. Nelson, "A Supervisory Wafer-Level 3D Microassembly System for Hybrid MEMS Fabrication", Journal of Intelligent and Robotic Systems, vol. 37, pp. 43–68, 2003.
[31] Q. Zhou, P. Korhonen, J. Laitinen, S. Sjövall, "Automatic dexterous microhandling based on a 6-DOF microgripper", Journal of Micromechatronics, vol. 3, no. 3-4, pp. 359-387, 2006.
[32] J.A. Thompson, R.S. Fearing, "Automating microassembly with ortho-tweezers and force sensing", Proceedings of 2001 IEEE/RSJ International Conference on Intelligent Robots and Systems, IROS'01, pp. 1327 - 1334, 2001.
[33] C. Clevy, A. Hubert, N. Chaillet, "A New Micro-tools Exchange Principle for Micromanipulation", Proceedings of 2004 IEEE/RSJ International Conference on Intelligent Robots and Systems, IROS'04, pp. 230-235, September 28 - October 2, 2004, Sendai, Japan, 2004.
[34] F. Arai, A. Daisuke, Y. Nonoda, T. Fukuda, H. Iwata, K. Itoigawa, "Integrated Microendeffector for Micromanipulation", IEEE/ASME Transactions on Mechatronics, vol. 3, no. 1, pp. 17-23, march 1998.
[35] E. Shimada, J.A. Thompson, J. Yan, R.J Wood, R.S. Fearing, "Prototyping Millirobots using Dextrous Microassembly and Folding", ASME Int. Mechanical Engineering Cong. and Symposium on Microrobotics, vol. 69-2, pp. 933-940, 2000.
[36] Q. Zhou, A. Albut, C. Corral, P.J. Esteban, P. Kallio, B. Chang, H. N. Koivo, "A Microassembly Station with Controlled Environment", Microrobotics and Microassembly III, Bradley J. Nelson, Jean-Marc Breguet, Editors, Proceedings of SPIE, vol. 4568, pp. 252 - 260, 2001.
[37] P. Lambert, A. Delchambre, "Design Rules for a Capillary Gripper in Microassembly", Assembly and Task Planning: From Nano to Macro Assembly and Manufacturing, 2005. (ISATP 2005). The 6th IEEE International Symposium on, pp. 67- 73, 2005.
[38] S. Chandra, C. Batur, "Manipulation of Capillary force by Electrowetting for Micromanipulation", Technical Proceedings of the 2006 NSTI Nanotechnology Conference and Trade Show, vol. 3, pp. 578 – 581, 2006.
[39] A. Kochan, "European project develops 'ice' gripper for micro-sized components", Assembly Automation, vol. 17, pp. 114-115, 1997.
[40] D. Lang, M. Tichem Marcel, BLOM Steven, "The Investigation of Intermediates for Phase Changing Micro-gripping" Proceedings of 5th International Workshop on MicroFactories, IWMF 2006, [online] Available from: http://www.mechse.uiuc.edu/portals/courses/ME598/dk/IWMF2006/ [referred: 18.9.2007].
[41] B.L. Walle, M. Gauthier, N. Chaillet, "Submerged Freeze Gripper to Manipulate Micro-objects", Proceedings of IEEE/RSJ International Conference on Intelligent Robots and Systems, pp. 784-789, 2006.
[42] N. Dechev, W. L. Cleghorn, J.K. Mills, "Microassembly of 3-D Microstructures Using a Compliant, Passive Microgripper" Journal of Microelectromechanical Systems, vol. 13, no. 2, pp. 176-189, April 2004.
[43] T.A. Nieminen, H. Rubinsztein-Dunlop, N.R. Heckenberg, "Calculation and optical measurement of laser trapping forces on non-spherical particles", Journal of Quantitative Spectroscopy & Radiative Transfer, vol. 70, pp. 627–637, 2001.
[44] W.H. Wright, G.J. Sonek, Y. Tadir, M.W. Berns, "Laser trapping in cell biology", IEEE Journal of Quantum Electronics, vol. 26, no. 12, pp. 2148-2157, 1990.
[45] W. Zesch, M. Brunner, A. Weber, "Vacuum tool for handling microobjects with a NanoRobot", Proceedings of IEEE International Conference on Robotics and Automation, ICRA'97, pp. 1761 - 1766, 1997.
[46] T. Inoue, K. Iwatani, I. Shimoyama, H. Miura, "Micromanipulation using magnetic field", Proceedings of IEEE International Conference on Robotics and Automation, ICRA'95, Vol. 1, pp. 679 - 684, 1995.
[47] H. Grutzeck, and Kiesewetter, "Downscaling of grippers for micro assembly", Microsystem Technologies, Vol. 8, pp. 27 - 31, 2002.
[48] T. Watanabe, N. Fujino, J. Zhongwei, "Micromanipulation using squeeze effect" Proceedings of 2004 IEEE/RSJ International Conference on Intelligent Robots and Systems, IROS'04, vol. 4, pp. 3357-3362, 2004.
[49] J. Fang, K. F. Böhringer, "High yield batch packaging of micro devices with uniquely orienting elf-assembly", Proceedings of IEEE International

Conference on Micro Electro Mechanical Systems, MEMS'05, pp. 12-15, 2005.
[50] K.F. Harsh, V.M. Bright, Y.C. Lee, "Solder self-assembly for three-dimensional microelectromechanical systems", Sensors and Actuators A, vol. 77, pp. 237–244, 1999.
[51] J. Fang and K. F. Böhringer, "Parallel micro component-to-substrate assembly with controlled poses and high surface coverage", Journal Of Micromechanics and Microengineering, vol. 16, pp. 721–730, 2006.
[52] U. Srinivasan, M.A. Helmbrecht, C. Rembe, R.S. Muller, R.T. Howe, "Fluidic self-assembly of micromirrors onto microactuators using capillary forces", IEEE Journal of Selected Topics in Quantum Electronics, Vol.8, Issue 1, pp. 4 - 11, 2002.
[53] C.J. Morris, S.A. Stauth, B.A. Parviz, "Self-Assembly for Microscale and Nanoscale Packaging: Steps Toward Self-Packaging" IEEE Transactions on Advanced Packaging, vol. 28, no. 4, November 2005.

Micro-assembly and modeling of the liquid microworld: the PRONOMIA project

M.Gauthier[1], S. Régnier[2], B. Lopez-Walle[1], E. Gibeau[1], P. Rougeot[1], D. Hériban[1], N. Chaillet[1].

[1]Laboratoire d'Automatique de Besançon
CNRS - ENSMM - UFC
24, rue Alain SAVARY
25000 Besançon (France)
gauthier@ens2m.fr

[2]Laboratoire de Robotique de Paris
CNRS - UPMC
BP 61
92265 Fontenay Aux Roses (France)
regnier@robot.jussieu.fr

***Abstract*— This paper presents an overview of the French research program PRONOMIA which deals with new methods for robotic micromanipulation and especially on submerged micromanipulation. During microscale object manipulation, contact (pull-off) forces and non-contact (capillary, van der Waals, and electrostatic) forces determine the behavior of the micro-objects rather than the inertial forces. This article introduces a review of the major differences between dry and submerged micromanipulations and gives an experimental analysis of the physical phenomena at a microscopic scale in dry and liquid media. New submerged microhandling strategies is necessary to perform micromanipulation in a liquid. Two solutions are proposed in this article which use a freeze gripper and a dielectrophoretic gripper. Finally, microassembly and biological applications are presented.**

***Keywords:* Microassembly, liquid medium, microforce modeling, microforce measurement, handling strategies.**

I. Introduction

The complexity of the microsystems is always higher and requires a lot of different materials and different microfabrication processes. Without micro-assembly technologies, it is more and more difficult to build microsystems and especially optical microsystems [1]. Consequently, the advent of new hybrid microsystems requires new micro-assembly technologies and methods. There are two main approaches in this domain: Self-assembly and robotic assembly. The first approach is useful for a very large production batch but the reliability stays low [2]. The second approach is more flexible and is relevant for a smaller production batch [3], [4].

Robotic micro-assembly tasks require firstly to be able to manipulate (to catch, to position, to release) microscopic objects whose typical size is included between one millimeter and one micrometer (micromanipulation).

The physical scale of micromanipulation is near to the lower limit of traditional mechanics. In general, the laws of Newtonian physics are still valid and the quantum effects neglected: The scale considered is thus at the boundary of two traditional spaces whose limits are not exactly known. The major difference with the macroscopic scale is indeed the results from the considered forces. The volume forces are negligible in respect to the surface forces for the microscopic objects [5-8]. These forces, whose effects are negligible on a macroscopic scale, modify drastically the contact mechanics and the interactions between the various media.

These surface forces may affect the micromanipulation task and especially the release of the micro-object. The frontier generating the modification of the micro-object behavior (from a behavior dominated by surface forces rather than volume based forces) is a function of the material of the micro-gripper, object, and the surrounding medium. In most cases, this frontier corresponds to the specific dimension of the micro-object near 100 micrometers, and at the present time, no repeatable and reliable micromanipulator exists under this physical limit.

Most modeling of the micro-world is done in the dry medium (air or vacuum) [7], [9]. The liquid medium is not studied even through it could have a lot of advantages in micromanipulation of artificial objects under the limit of 100 micrometers. The objective of this work is to present the potential advantages of the liquid in artificial micro-object micromanipulation by means of theoretical and experimental forces analysis and first comparative pushing micromanipulations.

This article focuses on the theoretical and experimental comparison between both types of medium. However we focus this article on the experimental and theoretical analysis on micromanipulations in water, our general approach concerns liquids and not only water. The aim of to propose an overview on the advantages and drawback of the submerged micro-assembly.

The following section focuses on the theoretical impact of the medium on distance forces (van der Waals, electrostatic, capillary forces), contact forces (pull-off forces) and hydrodynamic forces . Thereafter, the measurements of distance and contact forces are presented and compared to theoretical values. Innovative submerged handling strategies is also proposed. The last

section deals with applications in microassembly and biological application.

II. Theoretical Analysis

A lot of studies have been carried out on forces at microscopic scale. They use either classical models of forces at microscopic or nanoscopic scale (van der Waals, capillary, electrostatic forces) or theories of macroscopic contact (Hertz, JKR or DMT models). We propose a general approach by sorting out these forces considering the distinction whether there is contact or not. When there is no physical contact between two solids, the forces in action are called distance forces. According to the scientific literature in this domain [8], [10], [11], the latter are electrostatic, van der Waals and capillary forces. In case of water medium, hydrophobic forces, steric forces and double-layer forces have to be considered too. When two solids are in contact, some object deformation appear which induce adhesion forces in the contact surface. In this case, we consider contact forces (usually denoted pull-off forces). Electrostatic or capillary effects can be added, but van der Waals forces are not considered anymore, because they are already involved in the pull-off term. In liquid the hydrodynamic effects have to be considered. Thus, the third type of forces presented is the hydrodynamic forces [12].

A. Surface Forces

1) Van der Waals Forces: The van der Waals forces are a well-known interatomic interaction forces. For an interaction between a flat substrate (1) and a spherical object (2), the integrated van der Waals force is equal to:

$$F_{vdw}(D) = -\frac{A_{12}R}{6D^2} \tag{1}$$

where A_{12} is the Hamaker constant of the interaction (1-2), D is the contact distance between (1) and (2) and R is the radius of the spherical object (2).

Parameter A_{12} usually takes values included in the interval $[0.4-4]\times10^{-19}$J [12-15]. It is possible to obtain approximated values of A_{12} by using the "combination laws", derived from the expression of A_{12} introduced by Mac Lachlan in 1963 [17]: For two materials interacting in vacuum, A_{12} is computed according to the constants A_{ii} of each material:

$$A_{12} \simeq \sqrt{A_{11}A_{22}} \tag{2}$$

The Hamaker constant could be determined through the Lifshitz-van der Waals constant too [18]:

$$A_{12} = \frac{3H_{LV}}{4\pi} \tag{3}$$

where H_{LV} is the Lifshitz-van der Waals constant.

For interaction of two materials in the presence of a third medium (3), the total force F_t to considered is expressed by the extended DLVO theory (XDLVO) proposed by Xu and Yoon [19], [20]:

$$F_t = F_{vdw} + F_{dl} + F_h \tag{4}$$

The total force is the sum of the van der Waals force, the double-layer force and a third term which represents all other forces except van der Waals force and double-layer force, such as solvation, structural, hydration, hydrophobic, steric, fluctuation forces, etc.
The van der Waals force in a third medium is a function (1) of the Hamaker constant denoted A_{132} estimated by:

$$A_{132} = A_{12} + A_{33} - A_{13} - A_{23} \tag{5}$$

Consequently, from (2), A_{132} verifies:

$$A_{132} =\simeq (\sqrt{A_{11}} - \sqrt{A_{33}})(\sqrt{A_{22}} - \sqrt{A_{33}}) \tag{6}$$

The repulsive double layer force F_{dl} can be currently written as [15], [21], [22]:

$$F_{dl} \simeq 4\pi R\epsilon_3\kappa_3\Phi_1\Phi_2 e^{-\kappa_3 D} \tag{7}$$

where ϵ_3 is the dielectric constant of the medium, Φ_1 and Φ_2 are the surface potentials of the sphere and the surface and κ_3 the Debye length of the medium. The repulsive double layer force F_{dl} is typically greater than the van der Waals force between $D = 1\,nm$ to $D = 10 - 20\,nm$ [15]. This repulsive force is able to reduce the impact of the van der Waals force in this range.
The third term represents notably the solvation forces which have typically significant impact at very small range lower than $10\,nm$. In water, these forces are repulsive for hydrophilic surface and attractive for hydrophobic surface [15]. In case of hydrophilic surface these forces are able to reduce the impact of the van der Waals force.

Table I gives the values of Hamaker constant for some materials in vacuum and in water. The immersion is then able to reduce the value of the van der Waals force. However, this force has a short range (typically $< 100\,nm$) compared to the size of the object (greater than $1\,\mu m$). The impact of this force on the micro-objects behavior is thus limited compared to the very long range of electrostatic interaction and contact forces.

Materials	**Vacuum**	**Water**
Gold	40	30
Silver	50	40
Al_2O_3	16.8	4.4
Copper	40	30

TABLE I
Values of Hamaker constant for some materials
$A \times 10^{-20} J$ [23]

2) Electrostatic Forces: The force applied by an electrostatic surface (σ surface charge density) on an electric charged particle (q) is given by:

$$F_e = \frac{q\sigma}{2\varepsilon_0\varepsilon} \tag{8}$$

where ε and ε_0 are respectively the relative dielectric constant of the medium and the dielectric constant of the vacuum.

Comparison of dielectric constants between the water and the air is presented in Table II. The water dielectric constant is more important than the air dielectric constant. So, in the same electrical charges configuration (q, σ) electrostatic force is significantly reduced in water.

Moreover electrostatic perturbations observed in micromanipulation are caused by tribo-electrification. During a micro-assembly task, friction between manipulated objects induces electric charges on surface of the objects. The charge density depends on the tribo-electrification and conductivity of the medium. Effectively, a higher electric conductivity medium is able to discharge objects surfaces. The water, especially ionic water, has better electric conductivity than the air (Table II). Consequently, charge density in water is reduced. The electrostatic force directly proportional to the charge density σ is therefore reduced.

Electric parameters	**Air**	**Water**
Dielectric constant ε	~ 1	80.4
Conductivity	$10^{-7}\, S.m^{-1}$	$> 10^{-4}\, S.m^{-1}$

TABLE II
RELATIVE DIELECTRIC CONSTANT AND ELECTRICAL CONDUCTIVITY OF AIR AND WATER

Both impacts of the immersion on electric properties of the medium (dielectric constant and conductivity) induce a reduction of electrostatic forces. In conclusion, electrostatic perturbations are highly reduced in water compared to the air.

3) Capillary Forces: Basically, the capillary forces arise in two ways: Either a liquid drop is put between two solids (e.g. a gripper and a component) that turns itself towards a meniscus (a liquid bridge), or a capillary bridge appears by condensation of the ambient humidity in the small cracks and pores made by two rough profiles brought together in contact.

In both cases, the situation can be described by a liquid bridge presented in Figure 1 characterised by a volume V, a liquid surface tension γ and wettability properties defined by the contact angles θ_1 and θ_2. Most often the capillary forces are approximated by several formulations. With the assumptions that the contact angles are equal $\theta_1 = \theta_2 = \theta$, a constant volume and immersion height (D) is small, capillary force between a plan and sphere (radius R) is equal to [15]:

$$F_c = \frac{4\pi R\gamma\cos\theta}{1 + (D/d)} \tag{9}$$

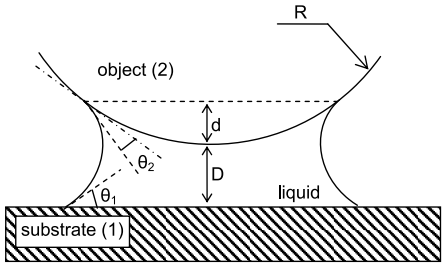

Fig. 1. Liquid meniscus formation between a spherical object and a substrate.

This capillary force is induced by the surface between the liquid and the air near to the object. In liquid this surface disappears, so this force is canceled in liquid medium. However, capillary force appears in the interface between the liquid and the air. This force is able to perturb end-effectors behavior and micro-object immersion. A complete study of the impact of capillary force on submerged micromanipulations is proposed in [24].

B. Contact Forces

The pull-off force represents the force necessary to break the contact surface between two objects. In case of a sphere (radius R) on a planar surface, pull-off force P is approximately given by JKR[1] (for the lower boundary) or DMT[2] (for the higher boundary) contact models [25], [26]:

$$\frac{3}{2}\pi R W_{12} \leq P \leq 2\pi R W_{12} \tag{10}$$

where W_{12} is the work of adhesion between both objects (1) and (2).

In the air, the work of adhesion is expressed by [27]:

$$W_{12} = \gamma_1 + \gamma_2 - \gamma_{12} \simeq 2\sqrt{\gamma_1\gamma_2} \tag{11}$$

where γ_{12} is the interfacial energy and γ_1, γ_2 are the surface energy of both objects.

According to [28], the Maugis elasticity parameter λ can be used to choose the most appropriate contact model for a given case. This parameter is expressed for an interface between two bodies (1) and (2) with:

$$\lambda = 2\sigma_0 \left(\frac{R}{\pi W_{12} K^2}\right)^{\frac{1}{3}} \tag{12}$$

$$\tag{13}$$

where K is the equivalent elastic modulus, calculated using the both Poisson's ratios μ_1, μ_2 and both Young's modulus E_1, E_2:

$$K = \frac{4}{3}\left(\frac{1-\mu_1^2}{E_1} + \frac{1-\mu_2^2}{E_2}\right)$$

[1] Johnson, Kendall and Roberts [25]
[2] Derjaguin, Muller and Toporov [26]

The parameter σ_O is defined by:

$$\sigma_0 = \frac{W_{12}}{h} \tag{14}$$

where $h \simeq 10^{-10} m$.

Using λ, the pull-off force can be estimated with:

$$\begin{array}{rl} \lambda < 0.1 & \Longrightarrow \text{DMT model: } P = 2\pi R W_{12} \\ \lambda > 5 & \Longrightarrow \text{JKR model: } P = \frac{3}{2}\pi R W_{12} \\ 0.1 < \lambda < 5 & \Longrightarrow \text{Dugdale model:} \\ & P = \left(\frac{7}{4} - \frac{1}{4}\frac{4.04\lambda^{\frac{1}{4}}-1}{4.04\lambda^{\frac{1}{4}}+1}\right)\pi R W_{12} \end{array} \tag{15}$$

Moreover, in case the objects are submerged in medium (3), the surface energy, denoted W_{132}, required to separate two objects (1) and (2) submerged in a medium 3 is given by:

$$W_{132} = W_{12} + W_{33} - W_{13} - W_{23} \simeq \gamma_{13} + \gamma_{23} - \gamma_{12} \tag{16}$$

For example, in case of a SiO_2-SiO_2 contact ($\gamma_{SiO_2} = 290\ mJ.m^{-1}$ [23]), the theoretical surface energies in air and in water are (from (11), (16)):

$$W_{12} = 580\ mJ.m^{-1} \quad W_{132} = 146\ mJ.m^{-1} \tag{17}$$

In this example, the pull-off force is reduced in water compared to the air. Usually, solid state surface energies are around $1000\, mJ.m^{-1}$ and the theoretical pull-off reduction is around 50% to 80%.

C. Impact of the Hydrodynamic Forces on the Micro-objects Behavior

In this section the impact of the hydrodynamic forces on the behavior of micro-objects is described. In the micro-world, the Reynolds number which characterizes the liquid flow is usually very low (< 1). The flow is thus highly laminar. In case of a micro-object placed in an uniform liquid flow, the Stokes law directly gives the hydrodynamic force applied on the object. This law is valid when the flow Reynolds number is lower than 1 and can be extrapolated to Reynolds number lower than 10 with a good approximation.
The Stokes law defines the force applied on an object in a uniform flow of fluid defined by a dynamic viscosity μ and a velocity V:

$$\overrightarrow{F}_{hydro} = -k.\mu.\overrightarrow{V} \tag{18}$$

where k is a function of the geometry. In case of a sphere with a radius R, k is defined by

$$k = 6\pi R$$

Table III gives the values of dynamic viscosity μ of both water and air. Then the hydrodynamic force proportional to the dynamic viscosity highly increases in a submerged medium.

Dynamic viscosity	**Water**	**Air**
$\mu\ [kg.m^{-1}.s^{-1}]$	10^{-3}	$18.5\,10^{-6}$

TABLE III
DYNAMIC VISCOSITY OF WATER AND AIR, $T^{\circ} = 20^{\circ}C$

As inertial effects are very small in the micro-world, micro-objects accelerations are usually very high. In this way, micro-object velocity is able to increase in a very short time. Consequently, micro-objects can reach high velocity, and object trajectory could be difficult to control especially in case of a visual feedback. In fact, the object can jump rapidly out of the field of view and this induces its loss. So, in most cases, velocity limitation in the submerged micro-world does not depend on inertial physical limitation but on hydrodynamic physical limitation. From this, a liquid medium is able to reduce maximal micro-objects velocity [29]. Consequently, the increasing of hydrodynamic force is able to limit the maximal velocity of the objects and thus significantly reduces the loss of micro-objects.

However, movements of liquid induced by the movement of the effector are able to lead to significant hydrodynamic force on micro-objects. Consequently the hydrodynamic force induces a limitation of the maximum velocity of the effector to avoid disturbance on the micro-object position. Nevertheless, experimentally the maximum velocity of the effector can stay high (eg. $1\, mm.s^{-1}$) compared to the typical size of the object manipulated ($50\, \mu m$).

In conclusion, contact, non contact and hydrodynamic force were presented in both liquid and dry media. This analysis shows the reduction of contact and non contact forces in liquid compared to the air. As these effects are able to perturb the micromanipulation tasks, the use of a liquid could improve the efficiency of micromanipulation. Moreover, the increase of the hydrodynamic effects are beneficial on the micro-objects behavior during their micromanipulation. Thus, the theoretical study shows the interest of submerged media for such tasks.

III. Forces Measurement

To analyse the validity of the micro-force modeling, some experimental force measurements are necessary. This part deals with the presentation of the micro-force measurement device and the comparison between theoretical and experimental values.

A. AMIS System

The micro-forces are measured by a specifically developed system called *AMIS* (AFM based MIcromanipulation System). This system is based on a standard Atomic Force Microscope (AFM) and a 3D micromanipulation system which allows large displacement (which is not usually the case in a standard AFM). In particular, AMIS is used to study the pull-off force. Experiments were carried out with polystyrene (PS) and glass substrates.

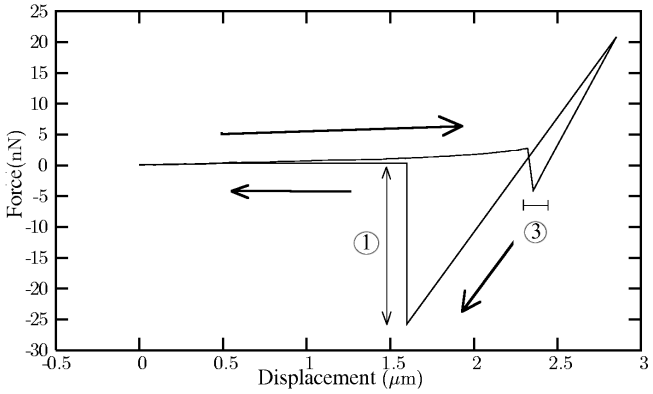

(a) Interactions between AFM tip and a PS substrate.

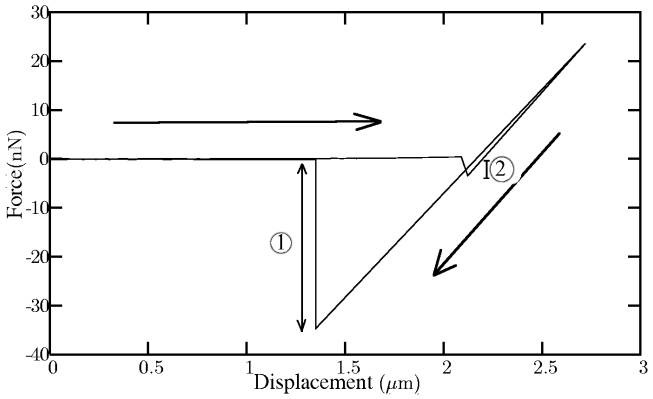

(b) Interactions between AFM tip and a glass substrate.

Fig. 2. Force-distance curves in air.

The pull-off force is measurable on the experimental force-distance curves when the breaking load between the AFM tip and the substrate appears (mark (1) in the Figure 2). From these curves (Figure 2), an experimental value of the pull-off forces for both interactions is measured. These values are estimated as:

$$P^{\text{measured}}_{\text{silicon-PS}} = 26\ nN \tag{19}$$

$$P^{\text{measured}}_{\text{silicon-glass}} = 35\ nN \tag{20}$$

From equation (11), (12), (15) and physical properties described Table IV, theoretical pull-off forces can be calculated:

$$P_{\text{silicon-PS}} = 28\ nN \quad (\lambda = 0.33\ ) \tag{21}$$

$$P_{\text{silicon-glass}} = 49\ nN \quad (\lambda = 0.54\ ) \tag{22}$$

These values (21)-(22) fit very closely to the measurements (19)-(20). Hence, theoretical estimation of pull-off forces can generally be trusted when no direct measurements are possible.

In order to analyse the influence of the environment, pull-off force measurement was done in aqueous medium. Figure 3 describes the force-distance curve of a silicon-glass interface in water. The experimental pull-off force is thus estimated as:

$$P^{\text{measured}}_{\text{silicon-water-glass}} = 5.5\ nN \tag{23}$$

From equation (16), (12), (15) and physical properties described Table IV, theoretically calculated pull-off force is then:

$$P_{\text{silicon-water-glass}} = 16.0\ nN \tag{24}$$

Pull-off force induces adhesion effects in a micromanipulation task. Consequently the significant reduction of the pull-off force in liquid is able to reduce adhesion perturbations in submerged micromanipulations.

Material	γ	A	ν	E
Unity	mJ.m^{-2}	$\times 10^{-20}$ J	-	GPa
Silicon	1400	26	0.17	140
Polystyrene (PS)	36	7.9	0.35	3.2
Glass	170	6.5	0.25	69

TABLE IV

Physical properties of the materials used in the experiments.

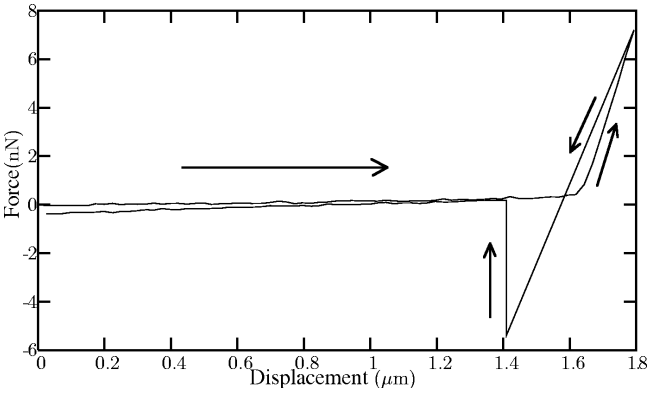

Fig. 3. Force-distance curve for an interaction between the cantilever and a glass substrate in an aqueous medium.

1) Electrostatic Forces: This part deals with the electrostatic forces in case of contact with conductors and insulators. AFM tip is made of silicon and is grounded. The first experiment describes a contact with a gold substrate (Figure 4). Comparative electrostatic force measurements were done on grounded and non grounded gold surface. These experimentations clearly show that the electrostatic force (marks 2 in Figure 4) is reduced when the substrate is grounded. On a non grounded substrate, the electrostatic forces appears at a very significant separation distance (mark 1 in Figure 4a) compared to the other forces (ten micrometers).

The second study is led on an insulator, PS substrate. The results are done in Figure 5. In the same way, to avoid this force, the substrate is cleaned with distilled water. The curve obtained is then represented on the Figure 5b. The electrostatic force is clearly reduced after charge cleaning (marks 2 in figure 5). In the first case, the interaction distance of the

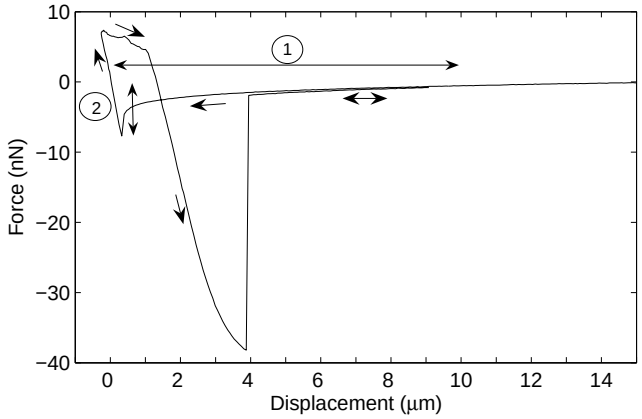

(a) Non grounded substrate.

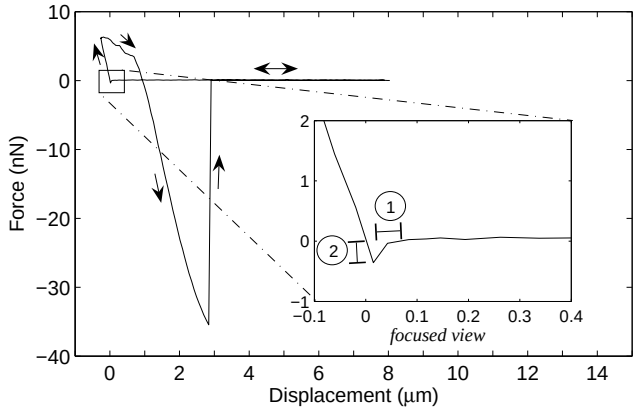

(b) Grounded substrate.

Fig. 4. Force-distance curves in air with a gold substrate.

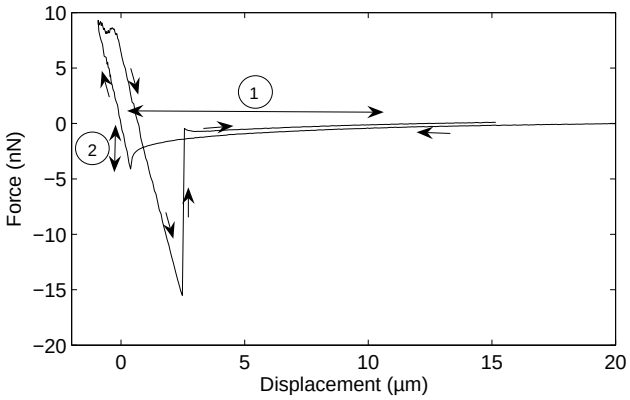

(a) Substrate without charges cleaning.

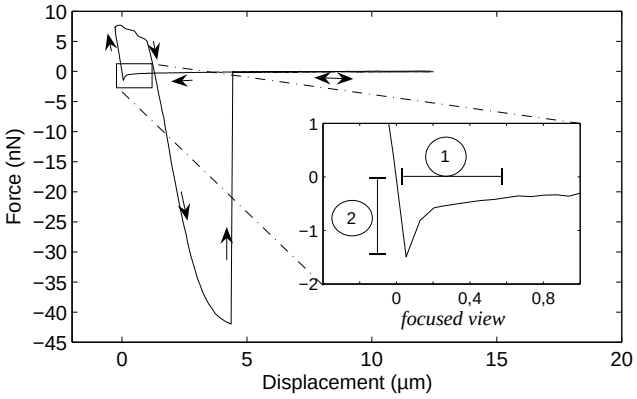

(b) Substrate after cleaning the substrate with distilled water.

Fig. 5. Force-distance curves with a polystyrene substrate.

electrostatic (marks 1 in figure 5a) which is about ten micrometers is larger than the interaction distance of the other forces again. The modification of the pull-off force between both cases presented figure 5 has not been studied. It could be explained by capillary forces induced by residual water after cleaning.

To illustrate electrostatic perturbations, a third experimental study was done: The approach of the AFM cantilever with a copper substrate initially charged with a 2 V voltage. The approach curve of the AFM cantilever is then drastically modified (see Figure 6). The cantilever is periodically attracted by the substrate and release due to electrostatic effects. The attraction is induced by the long range of the electrostatic forces while the release is obtained by a local discharge of the substrate induced by the contact with the micro-tip. Moreover, tip effects can be observed, making difficult any identification. In the same way, this phenomenon disappears as soon as the substrate is grounded.

Electrostatic forces are efficient in long range, starting at 10 μm and have the highest modules of the distance forces. As the charge density of a micro-object is not exactly known, the values of the electrostatic forces in a real system are hard to model. The reduction of the electrostatic perturbations is thus a key point to perform repeatable and precise micromanipulations. In dry medium, the cancellation of electrostatic effects can be obtained by grounding for conductor or by using distilled water for insulator. In liquid, i.e water, the electrostatic effects are highly reduced (section II-A.2). In fact, no electrostatic forces were measured in water.

The force measurements performed with the AMIS device prove a relatively good correlation between the micro-force models and the experimental forces. Moreover, the advantages of the liquid presented in section II, is confirmed by the experimental forces measurement.

In conclusion, the measurements of the non contact and contact forces generally show a good correlation between the theoretical models and the experiments. The correlation between the theoretical forces and the measured forces is better than 40% (except for pull-off in water). The measurement of the reduction of the pull force in water, and the cancellation of the electrostatic perturbations confirm the theoretical analysis. The interest of the submerged micromanipulation is thus

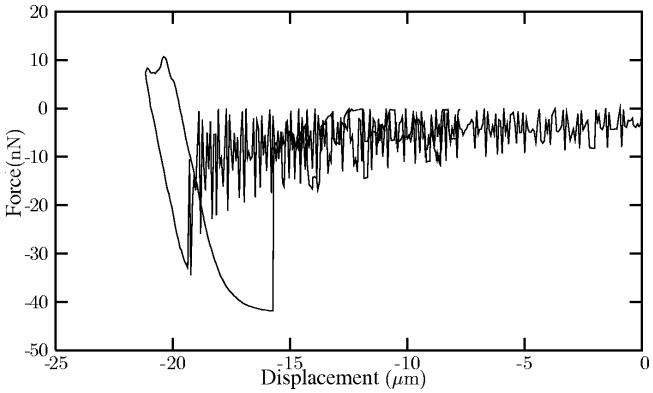

Fig. 6. Electrostatic perturbations measured by AMIS.

confirmed by the force measurements.

IV. Submerged Microhandling Strategies

Though the adhesion forces are reduced in liquid, sticking effects are not totally canceled[12] and the release task stays a critical problem. Thus the study of new release strategies of artificial micro-objects in liquid is a key-point to perform submerged micro-assembly. As current microhandling strategies of artificial objects are performed in the air (or vacuum), new micromanipulation strategies are required to manipulate in the liquid. Two ways can be explored:

- strategies based on principles used in biomicromanipulation. In this case, principles can be improved or modified to be able to handle artificial objects in spite of biological objects (no more biocompatibility, more degree of freedom required...);
- new strategies, currently not use in liquid because of biological constraints.

One example of each ways is presented in the following : a dielectrophoretic gripper and a freeze gripper.

A. Dielectrophoretic Gripper

In the current micromanipulations, usual approaches consist in control of a repulsive physical force to overcome the pull-off force (eg. acceleration in air [30]). We propose to use repulsive dielectrophoretic force to overcome pull-off force to control the release of the micro-objects. This principle usually used in biological cell manipulations is easily controllable by an electric field and is particularly efficient in liquid.

1) Principle of Dielectrophoresis: The time averaged dielectrophoretic force F_{DEP} and torque T_{DEP} applied by a particle in an inhomogeneous electric field $\vec{E}(t)$ is expressed by [31]:

$$\vec{F}_{DEP} = K_g.K_{DEP}.\epsilon_3.\vec{\nabla}E(rms)^2 \quad (25)$$

$$\vec{T}_{DEP} = K_g.K'_{DEP}.\epsilon_3.(E_x^2 \bigtriangledown \phi_x + E_y^2 \bigtriangledown \phi_y + E_z^2 \bigtriangledown \phi_z) \quad (26)$$

where $E(rms)$ is the rms value of the electric field strength, E_i and ϕ_i are the magnitude and phase of the field components in the axis i and K_g is a function of the geometry of the particle. For example in case of a spherical micro-object with a diameter r_2, K_g is expressed by:

$$K_g = 2\pi r_2^3 \quad (27)$$

The parameters K_{DEP} and K'_{DEP} is the real part and the imaginary part of the complex Clausius-Mosotti parameter. These parameters characterise the electric behavior of the particle and the medium and are expressed by:

$$K_{DEP} = Re\left(\frac{\kappa_2 - \kappa_3}{\kappa_2 + 2.\kappa_3}\right) \quad (28)$$

$$K'_{DEP} = Im\left(\frac{\kappa_2 - \kappa_3}{\kappa_2 + 2.\kappa_3}\right) \quad (29)$$

where
$\kappa_2 = \epsilon_2 - j\sigma_2/\omega$
$\kappa_3 = \epsilon_3 - j\sigma_3/\omega$
ϵ_2 : dielectric constant of the particle
ϵ_3 : dielectric constant of the medium
σ_2 : conductivity of the particle
σ_3 : conductivity of the medium
ω : angular freq. of the electric field

If the K_{DEP} parameter is positive, microparticle tends to move to the highest electric field gradient (near to the electrode). The dielectrophoretic force is attractive and is called 'positive-DEP'. In case of a negative K_{DEP}, microparticle tends to move to the lowest electric field (far from the electrode). The dielectrophoresis force is repulsive and is called 'negative-DEP'.

The dielectrophoresis (DEP) is usually used in cell micromanipulation to perform direct cell sorting [32][33] or field-flow-fractionation (FFF-DEP) [34][35]. In specific configurations, it allows to catch individual cells too [36]. Moreover dielectrophoresis is used to manipulate Carbon Nano Tubes (CNT) in the field of nanomanipulation [37]. Although this principle is not really effective in air, recently Subramanian presents first tests on the use of DEP in artificial objects manipulation in air [37]. In this medium, this kind of physical principle requires high voltage (eg. 200V).

Considering the submerged micro-objects manipulation is relevant and the DEP is particularly effective in liquid, we propose to apply this principle to submerged artificial micro-objects manipulation.

2) Robotic Micro-manipulation using Dielectrophoresis: The principle proposed is an original way to perform artificial micro-objects positioning. As the grasping by a gripper with two fingers allows to induce complex 3D trajectories and complex microassembly task (ie. insertion), we choose to manipulate micro-objects with a two fingers gripper. Consequently the

release task is perturbed by the adhesion force (pull-off force). We propose to use negative dielectrophoresis to control the micro-object release. Electric field could be produced by electrodes placed on the gripper or by using a conductive micro-gripper. After opening the gripper, an alternative electric field is applied on the gripper electrodes and induces a repulsive force on the micro-object whose objective is to release the object.

The behavior of the micro-object is composed of two phases:

- The micro-object is in contact with the gripper and is immobile (Fig 7(a)) .
- The micro-object is in motion in the liquid (Fig 7(b)) .

Before the release, forces applied to the micro-object is the adhesion force and the dielectrophoresis force. The release appears if the dielectrophoresis is greater than the pull-off force:

$$F_{DEP} > F_{PO} \tag{30}$$

After the release, in a very short time the micro-object reaches its maximum velocity. The micro-object trajectory is then defined by the equilibrium of the dielectrophoretic force and the hydrodynamic force F_{drag} induced by the liquid.

$$\overrightarrow{F}_{DEP} = -\overrightarrow{F}_{drag} \tag{31}$$

Consequently from (18) the trajectory of the particle is defined by its velocity $\overrightarrow{V}$:

$$\overrightarrow{V} = \frac{1}{k.\mu}\overrightarrow{F}_{DEP} \tag{32}$$

The transition (acceleration of the micro-object) between both cases is made in a very short time (ie. $50\mu s$) because of the small inertia of the micro-object. As the precise description of this acceleration phase has no specific interest in micromanipulation, the complete behavior of the micro-object is described by the equations (30-32).

3) Experimentations: To valid our approach, experimentations were performed on glass microsphere with a diameter $20\,\mu m$. The gripper is a four Degree Of Freedom (DOF) piezoelectric microgripper described in [38]. Specific end-effectors in Silicon were build with microfabrication technologies (D-RIE) and glued on the microgripper as presented in [38]. The silicon end-effectors and micro-gripper is presented in Figure 8. Thickness of the end-effectors is $12\,\mu m$ and the shape is presented in Figure 9. Gold electrodes are sputtered on the silicon end-effectors to applied alternating electric field.

An example of glass micro-sphere release is presented in Figure 9. The electric voltage used was a sinusoidal signal $\pm 20V$ peak-to-peak. The release and the trajectory of the micro-object is visible in Figure 9.

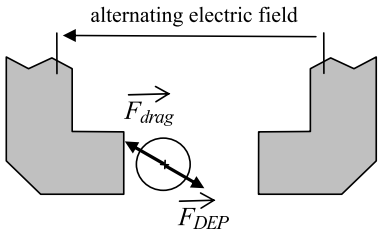

(a) First step: the dielectrophoretic force F_{DEP} overcome the pull-off force F_{PO}

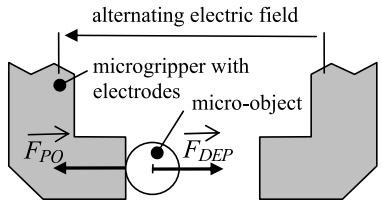

(b) Second step: the dielectrophoretic force F_{DEP} is opposed to drag force F_{drag}

Fig. 7. Principle of the dielectrophoretic release

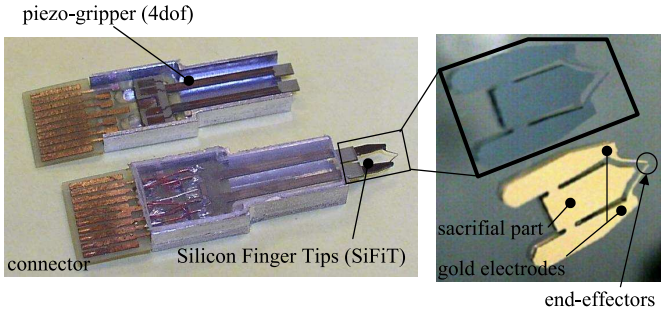

Fig. 8. Piezo-microgripper and Silicon Finger Tips (SiFiT)

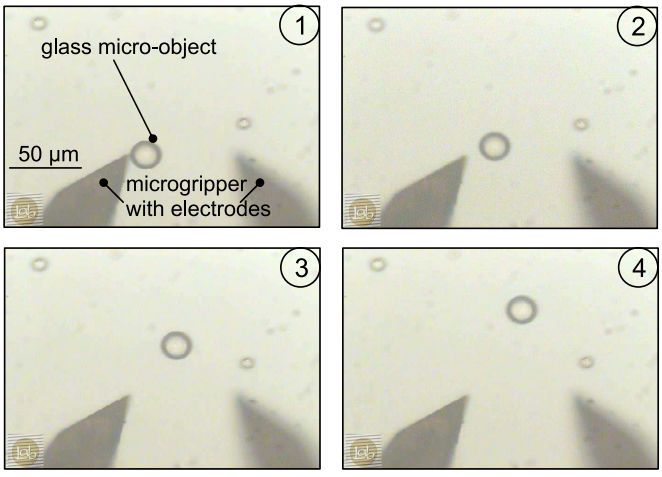

Fig. 9. Experimental DEP release

Experimentations show a high reliability on glass micro-object releases. The control of the release is easy to perform via the tension of electrodes. This first result demonstrates the interest in using dielectrophoresis release in submerged micromanipulations.

However at present, the final position of the released micro-object is not controlled. Further works will be done to purchase the modeling of the micro-object behavior after the release to control its final position. The shape, number, and architecture of electrodes will be studied and tested to optimize and control this release principle.

B. Submerged freeze gripper

This section is focused on the study of a submerged freeze microgripper. Its handling strategy is shown in Fig. 10. Firstly, the gripper comes close to the object without touching it. Secondly, an ice droplet is generated holding just a small part of the object. The object can be then picked and positioned. Finally, the ice droplet thaws mixing with the water and the object is released without any influence of capillary force.

As described below, the submerged freeze gripper utilizes the water environment to create an ice droplet. The cooling energy for freezing water is provided by two Peltier thermoelectric components.

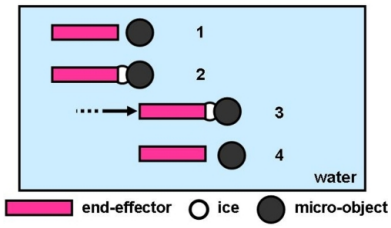

Fig. 10. Handling Strategy: (1) the micro-gripper approaches, (2) an ice droplet is generated and catches the object, (3) the object is manipulated, (4) the ice thaws and the object is liberated.

A Peltier module provides an electrical current-proportional generation or absorption of heat when direct current flows through it. The direction of the heat flow depends on the direction of the current, and the difference of temperatures caused by the heat transfer imposes two faces: a cold one and a hot one. The hot face must be associated to a heat sink in order to dissipate the heat flux.

As illustrated in Fig. 11, the submerged freeze system consists on two Peltier module stages, and a forced convection system. The first stage contains a Peltier micromodule named MicroPelt (μP). The end-effector is directly attached to its cold side. By this way, the MicroPelt can cool it and consequently generates the ice droplet on its acting part. The freezing process increases the temperature of the MicroPelt's hot face. Convection heat flow in water is thus so important than the whole system (liquid, gripper and Peltier micromodule) could warm up. To actively decrease the temperature at the MicroPelt's heat sink, a second Peltier element is connected. We called it MiniPeltier (mP). The temperature of its hot face must be constant to optimize its performance: it is maintained at the ambient temperature by forced convection using a liquid cooling system [39]. As MicroPelt's maximal cooling capacity is not sufficient to freeze the end-effector from ambient temperature, the liquid cooling system can not be used directly on its hot face.

The end-effector and the MicroPelt are completely submerged and electrically insulated. The MiniPeltier and the cooling liquid system stay in air to dissipate heat outside water.

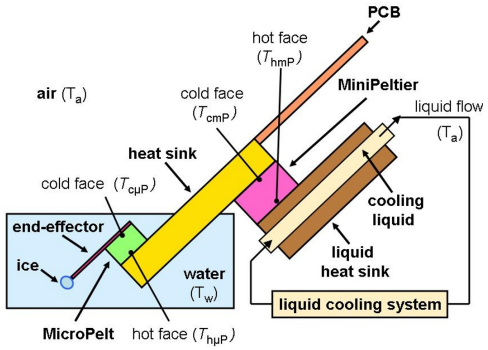

Fig. 11. Submerged Freeze System Principle.

1) Physical and Technical Characteristics: The first prototype of the submerged freeze gripper (without the end-effector) is shown in Fig. 12.

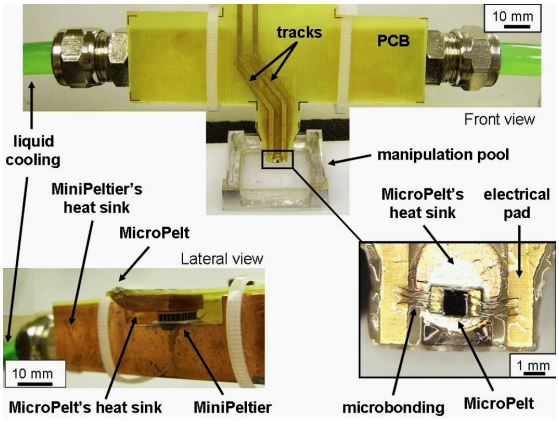

Fig. 12. Experimental freeze gripper.

The MicroPelt (Infineon Technologies AG) has as dimensions $720 \times 720 \times 428\ \mu m^3$. Its hot face is fastened to a copper heat sink (MicroPelt's heat sink). The MiniPeltier (Melcor FC0.6-18-05), which dimensions are $6.2 \times 6.2 \times 2.4\ mm^3$, is fixed on its cold face to the MicroPelt's heat sink; and on its hot face to the copper liquid heat sink of the cooling liquid system.

A specific PCB has been fabricated to establish the electrical connections of both Peltier modules. Because of the very small dimensions of the MicroPelt, microbonding technology were used for its connections.

2) First Experimentations: The first experimentations using the prototype described above were performed in distilled water at 2 ^{o}C. The objectives were to validate the good working of the system and its reliability. For these first tests, the end-effector was not included.

Fig. 13 describes the tele-manipulation of a silicon object whose dimensions are: 600 × 600 × 100 μm^3. A pre-cooling phase is necessary to decrease the temperature of the MicroPelt's heat sink. During this phase, only the current in the MiniPeltier (i_{mP}) is applied and set constant at 0.9 A (Fig. 13a). When the temperature is about 0.5 ^{o}C (this temperature is sufficiently close to 0 ^{o}C but it prevents the heat sink to freeze), the MicroPelt is approached to the micro-object and its current ($i_{\mu P}$) is turned on at 0.5 A. The cooling energy generates the ice droplet (4 μl) which involves a part of the object in 3 s (Fig. 13b). The freeze gripper can thus displace it towards a new position (Fig. 13c). To release it, the MicroPelt's current is inverted at -0.3 A. The ice droplet thaws in 7 s and melts with the aqueous medium, liberating the micro-object without adhesion perturbations (Fig. 13d). The micromanipulation has been performed in 30 s. As previously mentioned, the cycle time for pick and release, obtained for optimal working conditions of the Peltier modules, is 3 + 7 = 10 s. The rest of the time, i.e. 20 s of transportation time in this case, depends principally on operator's ability, or microgripper speed in case of full automation. Contrary to the cryogenic grippers in air, capillary force does not perturb the release because the object and the MicroPelt are submerged. The Peltier currents choice is based on the thermal simulation presented in [40].

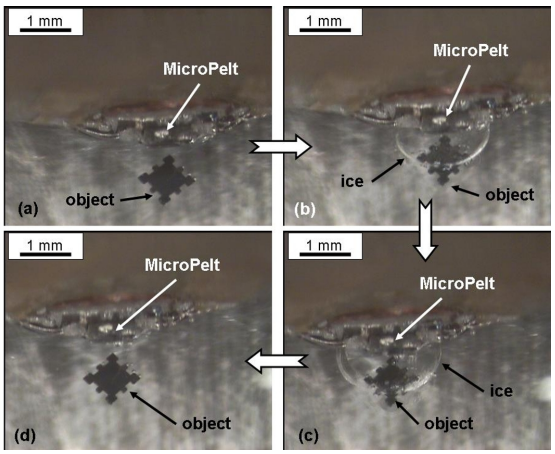

Fig. 13. Micromanipulation of a 600 × 600 × 100 μm^3 silicon object with the submerged freeze gripper.

The same experiment was successfully repeated several times. The submerged freeze principle seems thus a promising approach to manipulate micro-objects. Further manipulations will be dedicated to objects sized under 100 μm.

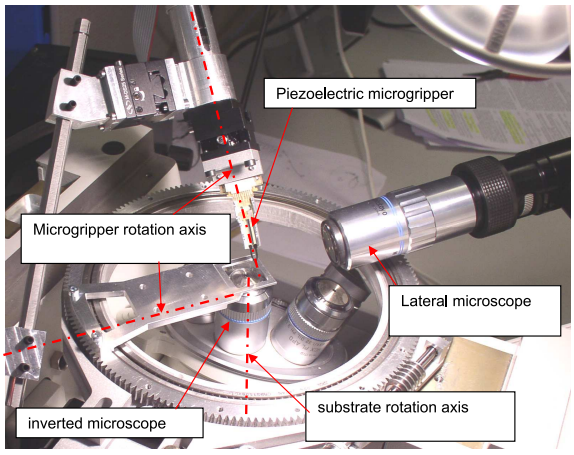

Fig. 14. 6 DOF robotic devices for micro-assembly

The thermal management becomes a crucial part of the microsystem design. However, thermal processes of the submerged freeze gripper involves combined heat conduction and convection leading to a complex system. The definition of a control strategy requires a model of the thermal exchanges in the whole system. The thermal modeling by electrical analogy is described in [39], [41].

V. Micro-assembly Platform

A. Platform Architecture

A 6 DOF (Degree Of Freedom) robotic platform has been build to perform complete microassembly tasks. An inverted microscope is used to visualized the micro-objects placed in a small pool (3cm square). The pool can be moved in the focus plane (2 translations and 1 rotation, see in figure 14). Thus each submerged objects can be positioned up to the microscope. A piezoelectric microgripper is placed on a 3 DOF robots which contains 2 rotations and 1 vertical translation (see in figure 14). A lateral microscope is used to visualize the vertical position. This view is only accessible in the air and not in liquid.

Only 4 DOF is currently used in teleoperation mode. Future works will focus on the geometrical modeling and the control of this structure to be able to use easily the 6 DOF.

B. Microassembly Application

The robotic platform is used to manipulate and to assembly micro-objects. Some silicon objects were build to produce microassembly benchmark. Objects is currently planar micro-objects as presented in figure 15. The silicon objects is build by using DIE etching in SOI wafers. After microfabrication, objects are linked to a millimetric silicon part through a breakable link.

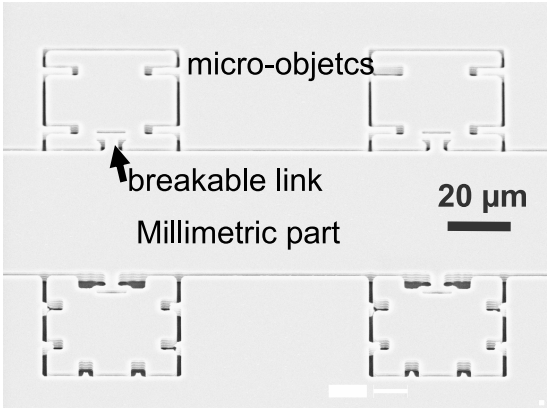

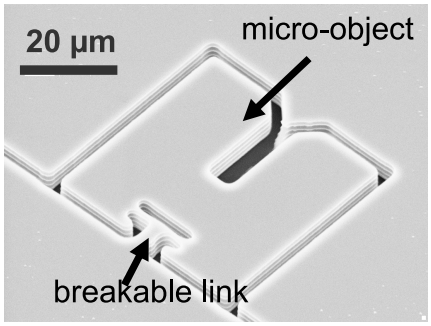

Fig. 15. Silicon Micro-objects to be assembled

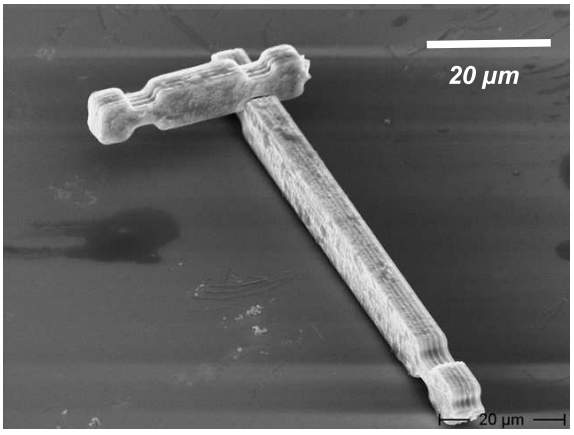

Fig. 16. Example of microassembly between to silicon tip

A first tool is used to break the link. During the release viscous forces are able to limit the micro-object velocity and avoid to loss the micro-object. The microgripper is then used to handle micro-object.

As the lateral view is not accessible for liquid micromanipulation, teleoperation in liquid is quite difficult and the current tests are performed in the air. The lack of vision access in liquid seems to be the major drawback to perform submerged microassembly. An example of microassembly of silicon parts is presented in figure 16.

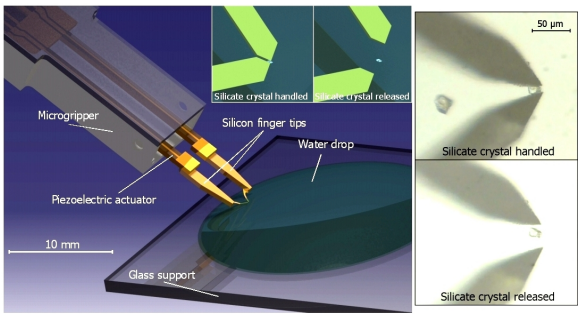

Fig. 17. Silicate crystal micromanipulation

C. Biological Application

Micromanipulation of artificial objects in a liquid has also applications in biological word. In particular, studying specific cells behavior in interaction with artificial objects could be used to determine their biocompatibility. In collaboration with the LST (Laboratoire de Sciences de la Terre, Lyon, France) a biological application has been chosen as a framework for the micro-manipulation station. Micro-sized particles of silicate have to be inserted in a liquid medium where E-Coli bacteria are living. Bacteria behavior around silicate particles will be studied with an inverted microscope. The applicative objective is to drop one silicate microcrystal near E-Coli bacteria in their liquid medium. Thus the micro-gripper was required to grasp one micro-crystal outside the liquid, bring it into and release it close to the biocells (see in figure 17) [42].

Conclusion

Development of new robotic micro-assembly methods and technologies is a keypoint to fabricate hybrid micro-systems as well as numerous micromechatronic products and requires reliable micromanipulation principles. At present, the release task is the most critical and unreliable phase because of the impact of the surface forces and adhesion forces. A complete modeling of the micro-forces in dry and liquid media was presented. These experiments exhibit a correlation better than 40% between the theoretical forces and the measured forces (except for pull-off in water). This theoretical and experimental comparative analysis between both types of medium shows the potential interest of the liquid in micromanipulation applications. In fact, contact and very large distance force are reduced in liquid while the hydrodynamic force significantly increases. Both phenomena are able to reduce respectively the electrostatic and adhesion perturbations and the loss of micro-objects. Furthermore, some submerged micromanipulation strategies (freeze gripper and dielectrophoretic gripper) are proposed. A 6 DOF robotic structure were build to perform complex trajectories for microassembly tasks. First results have demonstrate the microassembly capabilities of this platform. Further works will focus on the modeling of microforces in

function of the environment and on the automation of microassembly tasks.

References

[1] H. Van Brussel, J. Peirs, D. Reynaerts, A. Delchambre, G. Reinhart, N. Roth, M. Weck, and E. Zussman. Assembly of microsystems. *Annals of the CIRP*, 49(2):451–472, 2000.

[2] George M. Whitesides and Mila Boncheva. Beyond molecules: Self-assembly of mesoscopic and macroscopic components. *Proceedings of the National Academy of Sciences of the United States of America*, 99(8):4769–4774, 2002.

[3] T. Udeshi and K. Tsui. Assembly sequence planning for automated micro assembly. In *International Symposium on Assembly and Task Planning*, 2005.

[4] N. Dechev, W. L. Cleghorn, and J. K. Mills. Microassembly of 3d microstructures using a compliant, passive microgripper. *Journal of Microelectromechanical Systems*, 13(2), April 2004.

[5] R. Feynman. Infinitesimal machinery. *Journal of Microelectromechanical Systems*, 2, No 1:4–14, 1993.

[6] Y. Rollot, S. Regnier, and J-C. Guinot. Micro-robotics : A dynamical model of micro-manipulation by adhesion. In *Proc. of the Twelfth CISM-IFToMM Symposium, Theory and Practice of robots and manipulators, Paris, France , july*, pages 111–118, 1998.

[7] D.S. Haliyo and S. Régnier. Manipulation of micro-objects using adhesion forces and dynamical effects. In *Proceedings of ICRA/IEEE Internation Conferenace on Robotics and Automation*, May 2002.

[8] R.S. Fearing. A planar milli-robot system on air bearing. In *7th International Symp. Robotics Research*, HerrschingGermany, Oct. 1995.

[9] Q. Zhou, B. Chang, and H. N. Koivo. Ambient environment effects in micro/nano handling. In *Proc. of the Int. Workshop on Microfactories*, pages 146–51, Shangai, China, October 2004.

[10] R. Allen Bowling. A theoretical review of particle adhesion. In *Proc. of Symposium on particles on surfaces 1: Detection, Adhesion and Removal*, pages 129–142, San Francisco, 1986.

[11] J. Peirs. *Design of micromechatronic systems: scale laws, technologies, and medical applications*. PhD thesis, KUL, Belgium, 2001.

[12] M. Gauthier, S. Régnier, P. Rougeot, and N. Chaillet. Forces analysis for micromanipulations in dry and liquid media. *Journal of Micromechatronics*, 3(3-4):389–413, Sept. 2006.

[13] L.-H. Lee. The chemistry and physics of solid adhesion. In L.-H. Lee, editor, *Fundamentals of Adhesion*. Plenum Press, 1991.

[14] Y. Rollot. *Micro-manipulations par adhésion: Modélisations dynamiques et expérimentation*. PhD thesis, Université Pierre et Marie Curie, Paris, France, 2000.

[15] J. Israelachvili. *Intermolecular and Surface Forces*. Academic Press, 1991.

[16] Arthur W. Adamson and Alice P. Gast. *Physical Chemistry of Surfaces*. John Wiley and Sons, 6^{th} edition, 1997.

[17] A. McLachlan. Three-body dispersion forces. *Mol. Phys.*, 7:423–427, 1964.

[18] R. Allen Bowling. A theoretical review of particle adhesion. *ParticlesonSurfaces I*, 1988.

[19] Z. Xu and R. H. Yoon. The role of hydrophobic interactions in coagulation,. *J. Colloid Interface Sci.*, 44(132):532–541, 1989.

[20] Z. Xu and R.H. Yoon. A study of hydrophobic coagulation. *J. Colloid Interface Sci.*, 45(134):427–434, 1990.

[21] X-Y Lin, F. Creuset, and H. Arribart. Atomic force microscopy for local characterzation of surface acid-base properties. *J. Phys. Chem.*, 97:7272–76, 1993.

[22] Nehal I. Abu-Lail and Terri A. Camesano. Role of ionic strength on the relationship of biopolymer conformation, dlvo contributions, and steric interactions to bioadhesion of pseudomonas putida kt2442. *Biomacromolecules*, 4:1000–12, 2003.

[23] D. S. Rimai and D. J. Quesnel. *Fundamentals of Particle Adhesion*. Adhesion Society, 2001.

[24] M. Gauthier and M. Nourine. Capillary force disturbances on a partially submerged cylindrical micromanipulator. *IEEE Transactions on Robotics*, 23(3):600–604, Juin 2007.

[25] J.A. Greenwood K.L. Johnson. An adhesion map for the contact of elastic spheres. *J. Colloid Interface Sci.*, 192(2):326–333, 1997.

[26] B. V. Derjaguin, V.M. Muller, and YU. P. Toporov. effect of contact deformations on the adhesion of particles. *Journal of Colloid and interface science*, 53(2):314–326, 1975.

[27] Metin Sitti and Hideki Hashimoto. Teleoperated touch feedback from the surfaces at the nanoscale: Modelling and experiments. *IEEE-ASME Trans. Mechatron.*, 8(1):1–12, 2003.

[28] D. Maugis. Adhesion of spheres: the j.k.r-d.m.t transition using a dugdale model. *Journal of Colloid and Interface Science*, 150(1):243–269, 1992.

[29] M. Gauthier, B. Lopez-Walle, and C. Clévy. Comparison between micro-objects manipulations in dry and liquid mediums. In *proc. of CIRA'05*, June 2005.

[30] D. S. Haliyo and S. Régnier. Advanced applications using ţmad, the adhesion based dynamic micro-manipulator. In *Proceedings of the 2003 IEEE/ASME Int. Conf. on Advanced Intelligent Mechatronics (AIM 2003)*, pages 880–85, Port Island, Kobe, Japan, July 2003.

[31] P. Gascoyne, X. Wang, Y. Huang, and F. Becker. Dielectrophoretic separation of cancer cells from blood. In *IEEE Proc.*, pages 1366–1373, 1995.

[32] Frederick F. Becker, Peter R.C. Gascoyne, Ying Huang, and Xiao-Bo Wang. *Method and appartus for manipulation using spiral electrodes*. United States Patent, Patent Number US 5 858 192, 12 janv 1999.

[33] N. Tsukada, K. Kudoh, A. Yamamoto, T. Higuchi, M. Kobayashi, K. Sato, K. Oishi, and K. Iida. Development of oocyte rotation system for biological cell manipulation. In *Proc of the 32nd International Symposium on Robotics - ISR2001*, Seoul - Korea, 19-21 April 2001.

[34] P. Gascoyne and J. Vikoukal. Dielectrophoresis-based sample handling in general-purpose programmable diagnostic instruments. *IEEE Proceedings*, (1):22 – 42, 2004.

[35] M. Frenea, S. P. Faure, B. Le Pioufle, Ph. Coquet, and H. Fujita. Positioning living cells on a high-density electrode array by negative dielectrophoresis. *Materials Science and Engineering*, 23:597–603, 2003.

[36] A. Rosenthal and J. Voldman. Dielectrophoretic traps for single-particle patterning. *Biophysical Journal*, 88, march 2005.

[37] A Subramanian, B Vikramaditya, B J Nelson, D J Bell, and L Dong. Dielectrophoretic micro/nanoassembly with microtweezers and nanoelectrodes. In *Proc. of the 12th Int. Conf. on Advanced Robotics, Seattle*, July 2005.

[38] David Heriban, Joel Agnus, Jean-René Coudevylle, Michael Gauthier, and Nicolas Chaillet. Design of silicon finger tips for a moc (microrobot on chip) microgripper. In *Proc. of the Int. Workshop on Topica Meeting on Microfactories (TMMF05)*, Tsukuba, Japan, October 2005.

[39] B. Lopez Walle, M. Gauthier, and N. Chaillet. Dynamic modelling of a submerged freeze microgripper using a thermal network. In *proceedings of the 2007 IEEE/ASME International Conference on Advanced Intelligent Mechatronics*, sept. 2007.

[40] B.Lopez-Walle, M. Gauthier, and N. Chaillet. Submerged freeze gripper to manipulate micro-objects. In *proc. of the IEEE Int. Conf. on Intelligent Robots and Systems - IROS'06*, pages 784–789, Beijing, Chine,, oct. 2006.

[41] B. Lopez Walle, M. Gauthier, and N. Chaillet. A submerged freeze microgripper for micromanipulations. In *proc. of the 2007 IEEE International Conference on Robotics and Automation*, pages 10–14, Roma, Italy, April 2007.

[42] D Hériban, J Agnus, and M Gauthier. Micromanipulation of silicate micro-sized particles for biological applications. In *Proc. on the Int. Workshop on Microfactories*, Besancon, France, oct. 2006.